STRESS WAVES IN LAMINATED MATERIALS

by

Ray Kinslow

Tennessee Technological University

A Report of the Research

Conducted Under Grant NGR-43-003-007

September 1, 1967 - August 30, 1968

For the

National Aeronautics & Space Administrat

Manned Spacecraft Center

Houston, Texas

CONTENTS

SECTION I

INTRODUCTION

Meteoroids and other debris in outer space pose potential hazards to astronautics, spacecraft, and missiles. Although the impacted structure may have sufficient strength and thickness to resist actual puncture, damage may be caused by strong shock waves resulting from the impact. When such a stress wave encounters a free surface, it is reflected, generally as a tensile wave. If the amplitude of this reflected wave is equal to or greater than the strength of the "target" material, fracture will occur. Such fractures may appear as cracks near the surface, weakening the structure; as rear surface bulges which could jam mechanisms or block flow in pipes; or as a complete detachment of target material, creating a shrapnel effect, endangering equipment or personnel.

It has been demonstrated that damage caused by stress waves produced by hypervelocity impact can, in many cases, be reduced by employing laminated targets (Reference 1). The results of such experiments have served to alert the design engineer to the possibility of reducing the probability of damage or of using a thinner or lighter material as the outer skin or hull of spacecraft. It is perhaps more important to realize that the use of laminates does not necessarily reduce the probability of damage, but may, in some cases, actually result in increased damage to the structure (Reference 2).

It is realized that it is impossible to test all, or even a small percentage of possible laminates. This study is an attempt to

formulate a mathematical model that can be utilized to predict the action of laminates in affecting the stress wave induced by impact. Such a model must include all parameters that may affect the ability of structures to resist fracture induced by hypervelocity collisions before it can be used with confidence.

The following is an outline of this report and the approach to the problem:

(1) A theoretical study of the propagation and reflection of stress waves in solid and laminated targets was made. This included an analysis of the material properties (such as Poisson's ratio, density, modulus of elasticity), target geometry (target thickness, lamination thickness, lamination location), and the stress wave characteristics (such as amplitude, wave pulse length, decay rate, wave form).

(2) The next phase of the research consisted of an experimental investigation of stresses developed by the stress waves in both solid and laminated targets. This was limited, for the present, to sandwich plates or targets of only three layers, the two bounding layers being of one material and the center layer, or core, being of a different material. The outer layers were of a transparent material that could be studied by photoelastic methods. Stresses were determined only in the third layer of the target, this being the region of maximum tensile stress.

(3) After an analysis of the experimental results for a solid target, a theoretical model was formulated that would duplicate these results as closely as possible. This has been called a "quasi-theoretical" method (Reference 3).

(4) By using the theoretical model, the effects of laminations

were calculated. These results were then compared with those determined experimentally for identical targets.

(5) Problems encountered in this research are discussed and future studies are recommended.

SECTION II

THEORETICAL ANALYSIS

Spherical dilational wave propagation in homogeneous, isotropic material can be specified by the equation

$$\frac{\partial^2 \phi}{\partial t^2} = c^2 \left(\frac{\partial^2 \phi}{\partial r^2} + \frac{2}{r} \frac{\partial \phi}{\partial r} \right)$$

where ϕ is a scalar displacement potential, c is the wave velocity, and t is time. Particle displacement (u) and velocity (v) are specified by the relations

$$u = \frac{\partial \phi}{\partial r} \qquad \text{and} \qquad v = \frac{\partial u}{\partial t}$$

where r denotes the radius vector from the point of projectile impact. The radial and tangential stresses are given by the relations

$$\sigma_r = (\lambda + 2\mu) \frac{\partial u}{\partial r} + 2\lambda \left(\frac{u}{r} \right)$$

and

$$\sigma_\theta = \lambda \left(\frac{\partial u}{\partial r} \right) + 2(\lambda + \mu) \left(\frac{u}{r} \right)$$

where λ and μ are the Lamé constants and are related to Young's modulus (E) and Poisson's ratio (ν) as follows

$$\lambda = \frac{\nu E}{(1 + \nu)(1 - 2\nu)}$$

$$\mu = \frac{E}{2(1 + \nu)}$$

The mathematical model used in this investigation for generating spherical elastic waves is that described in References 4 and 5. It is assumed that there is a hollow hemispherical cavity in the target with its center at the point of impact, and that a time-varying pressure or forcing function is applied to the cavity surface, generating stress waves in the target. The pressure (p_o) applied to the cavity surface is an impulse that may be described by the relation

$$p_o = k_1 e^{-\alpha_1 t} + k_2 e^{-\alpha_2 t} + k_3 e^{-\alpha_3 t} + \ldots$$

where α_1, α_2, ... are decay constants, t is elapsed time, and k_1, k_2, ... are constants. By the proper choice of values of k and α, various wave forms can be generated.

The solution of the wave equation based upon Blake's work and described in Reference 5 is employed in this study.

Reflected stress waves are created in so-called "image cavities." The velocity of both the incident wave and the reflected spherical wave is given by the relation

$$c = \left[\frac{E(1 - \nu)}{\rho(1 + \nu)(1 - 2\nu)}\right]^{1/2}$$

Solid Homogeneous Targets

Figure 1 shows the target being considered. Its thickness

is denoted by $\underline{a}$ and the distance of a point, P, from the rear surface is given by $\underline{y}$. Only stresses developed along the axis normal to the target's rear surface have been considered.

Nondimensional units of stress and time are used in this theoretical part of the study as follows:

$$\bar{\sigma} = \sigma/E \qquad \text{and} \qquad \bar{t} = tc/a$$

Unless otherwise specified, the following values are also used:

$$r_o = 0.2a, \qquad \nu = 0.333, \qquad c = 1.000$$

The first case to be investigated is that of the application of a constant and continuous pressure to the cavity surface in a solid target. The tangential stress ($\bar{\sigma}_\theta$) and radial stress ($\bar{\sigma}_r$) were computed at points 0.1a, 0.2a, 0.3a, and 0.4a distance from the free surface. Results are shown in Figure 2. The stress indicated by a-a is developed as the wave front reaches the point under consideration. As this wave is reflected from the free surface as a tensile wave, it produces a sudden change in stress denoted by a'-a'. The curves of radial stress at the four points are compared in Figure 3. It is seen that the maximum tensile stress resulting from this wave has a value of approximately 20 at a point about 0.23a distance from the free surface.

The effect of the wave or pulse length upon the developed stress was next investigated. Figure 4 shows the stress-time relation at the four points for a square wave input having a length of 0.75. In this case, there will not only be discontinuities caused by the passage and reflection of the wave front, but also by the trailing edge of the pulse. Figures 5 and 6 show the resulting stress for

pulse lengths of 0.50 and 0.25, respectively. It is obvious that not only the pulse amplitude, but also its length, contributes to the developed stress. These are summarized in Figure 7. The top curve shows the maximum compressive stress developed as the pulse moves toward the free surface. The second curve (indicated by $\lambda = \infty$) shows the tensile stresses developed by the reflection of the wave generated by a constant and continuous forcing function. The various points show the maximum tensile stresses produced at the four points being considered by impulses of various lengths. It can be seen that in either case, the maximum tensile stress will occur when the reflected wave front coincides with the forward moving trailing edge. The lower curve is for these cases. It can be concluded that in any analysis of the developed stresses, the pulse length will be an important factor. For example, in the case of a very long pulse, the maximum tensile stress has been shown to have a value of about 20 at a distance of 0.23a from the free surface, but a short pulse having a length of 0.25 will develop a tensile stress of about 35 at y = 0.1a, and one having a length of 0.75 will produce a stress of approximately 50 about 0.35a from the free surface.

Forcing functions more nearly simulating impact or explosives may be formulated. One described by the series

$$p_o = 1 - (1 - e^{-\alpha t})^n$$

is described in References 4 and 5 and will not be repeated here. Figures 8 and 9 show waves formed by forcing functions that closely represent explosive inputs. The small sketch of the load-time curve

for an electrical primer is from Reference 6, page 347. Stress-time curves showing the effect of the decay constant, α, for decaying inputs are given in Figure 10. The results from an input that increases from zero and approaches a maximum value are shown in Figure 11. In these analyses, the cavity radius has arbitarily been assumed to have a value of 0.20a. The effect of using a value of 0.10a is shown in Figure 12.

Laminated Targets

An abrupt change in the physical properties of a material will result in the modification of a pressure pulse as it encounters this change. In general, a portion of the pulse will be transmitted, and a portion will be reflected. The relations which describe the modification of a pulse are based upon the boundary conditions of continuity of pressure and continuity of particle velocity across the interface between two materials. These relations depend upon the value of ρc, called the "characteristic impedance," of the two materials. If $\rho_o c_o$ is for the first, and $\rho_t c_t$ is for the second laminate and P_o is the pulse amplitude in the first, the amplitude of the transmitted component is

$$P_t = \left[\frac{2\rho_t c_t}{\rho_t c_t + \rho_o c_o}\right] P_o$$

and the reflected component is

$$P_r = \left[\frac{\rho_t c_t - \rho_o c_o}{\rho_t c_t + \rho_o c_o}\right] P_o$$

These relations are somewhat simplified by letting

$$K = \frac{\rho_t c_t}{\rho_o c_o}$$

giving

$$P_t = \left[\frac{2K}{K+1}\right] P_o$$

and

$$P_r = \left[\frac{K-1}{K+1}\right] P_o$$

The sandwich structure under consideration is shown in Figure 13. Its total thickness is a, the thickness of the first and last layers of material are t_o and t_2, respectively. The characteristic impedance of both is $\rho_o c_o$. The middle lamination has a thickness of t_1 and a characteristic impedance of $\rho_1 c_1$. This figure shows also the distance-time relation of the wave fronts. Starting at time zero at point r_o, the wave moves with a velocity of c_o through the first layer. Upon reaching the first interface, the amplitude of the transmitted component is $\left[\frac{2K}{K+1}\right] P_o$ which moves through the core at a velocity of c_1. As this pulse reaches the second interface, a portion will again be transmitted, and a part will be reflected. However, the value of the impedance mismatch at this interface is not K, but has a value of 1/K. The amplitude of the pulse transmitted is, therefore,

$$\left[\frac{2K}{K+1}\right]\left[\frac{2/K}{(1/K)+1}\right] P_o = \left[\frac{2K}{K+1}\right]\left[\frac{2}{K+1}\right] P_o = \left[\frac{4K}{(K+1)^2}\right] P_o$$

and is denoted by $P_{1\text{-}0\text{-}0}$. As only the stress developed in the last layer of the target is under consideration, it can be assumed that the target is composed of this material only, and that the initial

pulse has an amplitude of $\left[\frac{4K}{(K+1)^2}\right]P_o$ instead of P_o. The time required, however, for this pulse to reach any point is not the same as for a homogeneous target due to the change in velocity through the core. It must be adjusted by the amount

$$T_{1\text{-}0\text{-}0} = \left[\frac{c_o - c_1}{c_o c_1}\right]t_1$$

The component of the pulse reflected from the second interface is $\left[\frac{K-1}{K+1}\right]P_o$, which, upon again reaching the first interface, will again be reflected with an amplitude of $\left[\frac{K-1}{K+1}\right]^2 P_o$. A portion of this will then be transmitted through the second interface, this being

$$P_{2\text{-}0\text{-}0} = \left[\frac{K-1}{K+1}\right]^2 \left[\frac{4K}{(K+1)^2}\right]P_o = \left[\frac{4K(1-K)^2}{(1+K)^4}\right]P_o$$

If the transmitted pulse amplitudes in this layer are denoted by $P_{A\text{-}B\text{-}C}$, the other pulses $P_{A\text{-}0\text{-}0}$ may be specified as

$$P_{A\text{-}0\text{-}0} = \frac{4K(1-K)^{2(A-1)}}{(1+K)^{2A}}$$

These pulse amplitudes, $P_{1\text{-}0\text{-}0}$, $P_{2\text{-}0\text{-}0}$, $P_{3\text{-}0\text{-}0}$. . . form a rapidly converging series, the sum of which approaches the value of P_o. This is to be expected, because pulse attenuation and energy losses have been neglected up to this time. The time adjustments for these waves are given by the relation

$$T_{A\text{-}0\text{-}0} = \left[\frac{(2A-1)c_o - c_1}{c_o c_1}\right]t_1$$

This series of transmitted waves, as well as others that will be discussed, can be seen more clearly in the second page of Figure 13. Figure 14 gives these amplitudes as functions of the impedance mismatch, K.

Returning to the pulse $P_{1-0-0,}$ it is seen that this will be totally reflected from the free surface as a tensile wave. When this reflected pulse reaches the second lamination, a portion will be transmitted back into the core and a part will be reflected back into the third layer as $P_{1-1-0,}$ which, in turn, will be reflected from the free surface as was $P_{1-0-0,}$ resulting in P_{1-2-0}, and then in P_{1-3-0}, etc. Pulse P_{2-0-0}, P_{3-0-0}, . . . will likewise result in multiple reflections, the amplitudes of which are given by the relation

$$P_{A-B-0} = \frac{4K(1 - K)^{(2A+B-2)}}{(1 + K)^{(2A+B)}}$$

The corresponding time delays are given by

$$T_{A-B-0} = T_{A-0-0} + \frac{2Bt_2}{c_o}$$

These amplitudes are given in Figure 15 for various values of K. The values of P_{A-B-0} are given as percentages of P_o. Consider the case of K having a value of 0.5.

$P_{1-0-0} = 0.889$, $P_{1-1-0} = 0.296$, $P_{1-2-0} = 0.099$,

$P_{1-3-0} = 0.033$, $P_{1-4-0} = 0.011$, $P_{2-0-0} = 0.099$,

$P_{2-1-0} = 0.033$, $P_{2-2-0} = 0.011$, $P_{3-0-0} = 0.011$.

Values of P less than $0.01P_o$ are not shown.

As previously stated, $P_{1-0-0} + P_{2-0-0} + P_{3-0-0} + \cdots = P_o$. This may be illustrated for this instance of K = 0.5,

$$0.889 + 0.099 + 0.011 = 0.999.$$

It can be also shown that the sum of all the transmitted pulse amplitudes,

$$\Sigma P_{A-B-0} = \frac{1 + K}{2K}$$

In this case of K = 0.5, the sum would be 1.5. The values given above have a total of 1.482. Where K has a small value, say 0.1, the sum of these pulse amplitudes is 5.5. This means that, although the magnitudes decrease very rapidly as they undergo multiple reflections, their sum may be several times that of the transmitted pulse in a homogeneous target. The conditions under which this may occur will be shown later.

Magnitudes of P_{A-B-0} given in Figure 15 for values of K ranging from 0.1 to 0.9, also apply for values of 1/K except that for odd values of B, P_{A-B-0} will be negative. This explains why the sum of all the transmitted waves for K = 2.0, for example, is only 0.75. One should not come to the conclusion at this point in the study that the center core should always have a characteristic impedance greater than the boundary layers in order that the total stress developed in the last layer will be reduced. Under some conditions this would result in an increase in stress as the reflected tensile waves from P_{1-0-0}, P_{2-0-0}, etc. may meet the transmitted tensile waves, P_{1-1-0}, P_{2-1-0}, P_{1-3-0}, etc. and combine to increase the total tensile stress.

Referring again to Figure 13, it will be seen that there are additional transmitted waves not yet discussed. These are P_{1-0-1},

$P_{1\text{-}0\text{-}2}$, $P_{1\text{-}1\text{-}1}$, etc. These amplitudes are given by the relation

$$P_{A\text{-}B\text{-}C} = - \frac{16K^2(1 - K)^{(2A+B+2C-3)}}{(1 + K)^{(2A+B+2C+1)}}$$

and the time differential by

$$T_{A\text{-}B\text{-}C} = T_{A\text{-}B\text{-}0} + \frac{2t_2}{c_o} + \frac{2Ct_1}{c_1}$$

These waves may have significant magnitudes; however, they usually occur at such a late time and have been attenuated by traveling through great distances by their succesive reflections, that no instance has been found where they contribute significantly to the maximum tensile stress developed. Therefore, they have not been included in the example given.

The thickness of the lamination t_1 and its distance from the free surface, t_2, are significant factors in determining the resulting stress. From Figure 13 it can be seen that if the thickness of t_1 is very small, the time between the wave fronts of $P_{A\text{-}0\text{-}0}$ will also be small. The relation given for $T_{A\text{-}0\text{-}0}$ also indicates that the time intervals are directly proportional to the thickness t_1. This may have little effect upon the total developed stress if the pulses are very short. If they are long, however, and t_1 is small, the transmitted components will overlap, and the total amplitude may be as great as if there were no lamination. The time intervals of the other pulses, $P_{A\text{-}B\text{-}0}$, depend upon the thickness t_2. These effects will be noted in the examples that follow. In Figures 16 through 22, the forcing function is a constant, that is, the waves should be relatively long. Figure 16 shows the effect of the core thickness upon the stress developed at a point 0.10a distance from the free

surface and an impedance mismatch value, K, of 0.25. It is seen that both the compressive stress produced by the transmitted wave and the tensile stress resulting from the reflected wave occured at this point when t_1 was only 0.01a. The superposition and overlaping of the wave fronts are clearly seen. This did not occur in the case of thicker cores, and the stress magnitude depended very little upon the core thickness in these cases. At other distances from the free surface, the maximum stress was also developed in the case of the thinner core, but it will also be noted that at y = 0.30a the tensile stress resulting from the core thickness of 0.20a is greater than in the case of the intermediate thickness of 0.05t and 0.10t.

For K = 0.50, Figure 20 and 21, there was not as much dependence upon the core thickness. In this case, a smaller number of transmitted waves had significant values, and a still smaller number when K = 0.75, Figure 22.

The effect of the pulse length is shown in Figures 23 and 24. Comparing with Figures 20 and 21, it is seen that the tensile stress was more than twice as great in the case of shorter pulse.

In these examples of the effects of laminations, the amplitudes of the transmitted waves were not as given in Figure 15, but were smaller because of attenuation due to distance. It has been assumed that the wave amplitude attenuates at a rate inversely proportional to the distanc e traveled.

The effect of lamination thickness upon stress in the case of a wave that more nearly represents the conditions of impact is shown in Figure 25.

SECTION III

EXPERIMENTAL INVESTIGATION

This phase of the research consisted of photoelastic analyses of stress waves in both homogeneous solids and laminated targets. To photograph these waves an extremely fast camera or a short-duration light pulse is required. Both methods were employed in this study.

For single photographs, a polariscope utilizing an E.G. & G. Model 549 Microflash unit was used. This flash is rated at fifty-million-beam-candlepower with a duration of one-half microsecond. The flash was triggered by the magnetic field from the exploding wire that was used to initiate the stress wave. Photographs were 4 X 5 - inch in size. This equipment was utilized to make preliminary studies to determine the type of polariscope (light or dark field, plane or circular polaroids, etc.), kind of film, filters, model material, and energy sources to be used.

In the experimental investigation described in this report, a Beckman and Whitley Model 201 synchronous framing camera was used to record the dynamic fringe pattern generated in the model. The camera is a rotating mirror type, making twelve 0.7 X 0.9-inch photographs on a 4 X 5 - inch film at speeds up to one million frames per second. Exposure time for each photograph at this speed is approximately 0.6 microseconds. Figure 26 is a diagram of the camera and related equipment.

The two pulse generators deliver 100 Joules each at 5 KV. One was used to provide energy for the light source. Various spark

gaps, wires, and foils were tried. Spark gaps provided sufficient illumination for fast film but was very irregular and not uniform during exposure. Wires exploded with sufficient illumination and were much more satisfactory than spark gaps, but the duration was so short that it was difficult to synchronize with the camera so as to give satisfactory exposure for all twelve photographs. Exploding foils were not as satisfactory as either wire or gap. The most satisfactory light source was found to be Buss type AGC-1 safety fuses. A comparison of light intensities and duration for a spark gap, exploding wire, and fuse is shown in Figure 27.

The other pulse generator was used as the energy source for generating stress waves in the model as a simulation of hypervelocity impact. After experimenting with many kinds of model materials, PSM-1, a clear polyester sheet manufactured by Photoelastic, Inc., was selected as the basic material to be used in this study. Its manufacturer claims that it has the highest photoelastic sensitivity of any model material available and has a wave velocity of about 60,000 inches per second, sufficiently low to be photographed without apparent wave movement during exposure. Another important factor was that it is practically free of creep and edge effects. This plastic can be easily machined, polished, and cemented to other materials. The most consistent stress waves were generated by exploding a fine wire in contact with one edge of the model. The amplitudes of these waves, however, were not sufficiently great for accurate comparison of waves having only slight differences in amplitude. A stronger shock, giving a greater number of fringes, resulted when a small amount of explosive was added. Figure 28 shows a comparison of the fringe

patterns resulting from an exploding wire and a wire plus a small amount of picric acid. The gases produced by this explosive were very toxic so its use was discontinued. Urea nitrate, although not producing as strong a shock, was less discomforting and corrosive. This was used in the experimental studies being reported.

The method used for the experimental analysis of stress waves is essentially the same as that described by Dally and Riley in Reference 7.

Stresses are developed both in the direction of, and perpendicular to, the direction of wave propagation as described in Section II of this report. Deformation occurs, however, only in the direction of wave motion. The displacements are specified by

$$u_r = f(r), \qquad u_\theta = 0$$

The strain-displacement relations are

$$\varepsilon_r = \frac{du_r}{dr}, \qquad \varepsilon_\theta = \frac{u_r}{r}$$

and the stress-strain equations are

$$\sigma_r = \frac{E}{1 - \nu^2}\left[\varepsilon_r + \nu\varepsilon_\theta\right]$$

$$\sigma_\theta = \frac{E}{1 - \nu^2}\left[\varepsilon_\theta + \nu\varepsilon_r\right]$$

The shear stress, τ, has the value

$$\tau = \pm\,(\sigma_\theta - \sigma_r)/2$$

From these relations

$$2\tau = \sigma_\theta - \sigma_r = \frac{E}{1 - \nu}\left[\varepsilon_\theta - \varepsilon_r\right] = \frac{E}{1 - \nu}\left[\frac{u_r}{r} - \frac{du_r}{dr}\right]$$

But $$\frac{d}{dr}\left(\frac{u_r}{r}\right) = \frac{1}{r}\left[\frac{du_r}{dr} - \frac{u_r}{r}\right]$$

So $$\sigma_\theta - \sigma_r = -\frac{E}{1+\nu}\left[r\,\frac{d}{dr}\left(\frac{u_r}{r}\right)\right]$$

$$\frac{d}{dr}\left(\frac{u_r}{r}\right) = -\frac{1+\nu}{E}\left(\frac{\sigma_\theta - \sigma_r}{r}\right)$$

$$\frac{u_r}{r} = -\frac{1+\nu}{E}\int_r \frac{\sigma_\theta - \sigma_r}{r}\,dr$$

$$\varepsilon_\theta = \frac{u_r}{r} = \frac{-2(1+\nu)}{E}\int\frac{\tau}{r}\,dr$$

$$\varepsilon_r = \varepsilon_\theta - \frac{2(1+\nu)}{E}\tau = -\frac{2(1+\nu)}{E}\left[\tau + \int\frac{\tau}{r}dr\right]$$

The radial and tangential stresses are, therefore,

$$\sigma_r = -\left(\frac{2}{1-\nu}\right)\left[\tau + (1+\nu)\int\frac{\tau}{r}\,dr\right]$$

$$\sigma_\theta = -\left(\frac{2}{1-\nu}\right)\left[\nu\tau + (1+\nu)\int\frac{\tau}{r}\,dr\right]$$

The stress-optic relation is

$$\tau = \left(\frac{N}{2}\right)\frac{f}{h}$$

where N is the fringe order, f is the photoelastic constant of the material, and h is the model thickness.

The stress relations may be stated in terms of the model material properties and fringe order

$$\sigma_r = -\frac{f}{h(1-\nu)}\left[N + (1+\nu)\int\frac{N}{r}\,dr\right]$$

$$\sigma_\theta = -\frac{f}{h(1-\nu)}\left[\nu N + (1+\nu)\int\frac{N}{r}\,dr\right]$$

Values of displacements, strain, and stress may now be determined by numerical integration.

As the objective of the present research is to compare the stresses developed in a laminated target with those produced in a homogeneous target under the same dynamic impulse, the properties of the material, such as the dynamic modulus of elasticity and photoelastic constant, have not been determined. Resulting stresses, strains, and displacements are, therefore, relative values only and are designated by $k\sigma$, $k\varepsilon$, or ku. Values of other properties for the target material, PSM-1, are: Poisson's ratio (ν) = 0.38, density (ρ) = 20 grams per cubic inch, and wave velocity (c) = 60,500 inches per second. The characteristic impedance values of this and some other materials are given in Table I.

It was found that a light field polariscope utilizing circular polaroids, and a dark red filter gave the most satisfactory photographs of the stress pattern. Figure 29 is a typical photograph showing the fringe order values. These values, together with their locations, were then plotted. Figure 30 was prepared from three sets of photographs, shots 175, 176, and 177, and show fringe locations for each frame. Frame 12 of shot 175 is identical with frame 1 of shot 176, but there was a slight gap between the last frame of shot 176 and the first frame of shot 177. In the last frame of 176 the wave front is approaching the rear edge of the model and in 177 the wave is being reflected. The zero fringe (wave front) cannot be seen in these photographs because of the light field being used, so this fringe was determined by extrapalation from the other fringes. The broken line shows the approximate location of the reflected wave front.

Values of R and N from this figure were read into a digital computer that had been programmed to compute the displacements, strains, and stresses. Figure 31 shows the photographs and computer results. Shots 175 and 176 were considered continuous with the frame numbers indicated as being from 1 to 23.

A plot of fringe order versus distance for various times are shown in Figure 32. Computed displacements are shown in Figure 33; strains in Figure 34; and stresses in Figure 35. The different scales for the radial stress and tangential stress should be noted.

Photographs and computer results for the reflected wave are given in Figure 36. Plots of the fringe order and stress are shown in Figures 37 and 38, respectively. Separate curves were plotted for each frame in the case of reflected waves in order to avoid confusion. It will be noted that the amplitude of the reflected tensile wave in frame 12 is about the same as that of the compression wave in frame 2.

Stresses in laminated models were next determined. First, however, photographs were made of stress waves in a model of two pieces of PSM-1 cemented together in order to determine the effect, if any, of a cemented joint on the passage of the waves. Figure 39 shows waves in such a model and it is seen that the joint had practically no effect on the transmitted waves. Several models were prepared with laminates of various materials such as Lucite and CR-39. Photographs of some of these are shown in Figure 40 but as the impedance mismatch was so near unity, very little change in the wave amplitude could be detected.

Two targets were next prepared having laminates of aluminum. As the impedance mismatch between PSM-1 and aluminum is 8.9, there should be considerable differences in the developed stress, especially in the case of a thicker lamination.

In the first target, the lamination thickness was only 1/8 inch. Figure 41 shows the twelve frames of this shot (No. 240) and an enlargement of Frame 3 at a time of approximately 68 microseconds. The second target had a lamination thickness of 1.0 inch. Figure 42 is a photograph of this shot (No. 226) and an enlargement of Frame 6, also at a time of about 68 microseconds. Plots of the fringe order of these two frames and the computed stresses are shown in Figure 43. Although only fringes 0.5 and 1.5 were developed in the latter, fringe number 1.5 was barely distinguishable,so it was the maximum point on this curve.

The time of 68 microseconds corresponded to Frame 3 of Shot 176. A comparison of the three waves in the case of a homogeneous target, a 1/8 - inch lamination, and a 1.0 - inch lamination is made in Figure 44. The distances traveled are, of course, not the same, as the wave velocity in the aluminum was about three and one-half times as great as in the plastic.

A comparison of the maximum radial stresses indicates that the stress after passage through the 1/8 - inch aluminum was about 71% of that in the solid plastic model, and that the stress after passing through the 1.0 - inch aluminum was only 40% as great, indicating reductions of stress of 29% and 60%.

SECTION IV

A QUASI-THEORETICAL SOLUTION

It was shown in a previous section of this report that forcing functions could be selected that would closely simulate explosive impulses or hypervelocity impact. Figure 45 shows several such inputs and the resulting waves in PSM - 1 at a time of 55.5 microseconds. In this case a radius cavity of 0.50 inches was selected. Figure 46 gives the same information when a cavity of 0.25 inches was used. These wave profiles were compared with those of Figure 35 which were experimentally determined. It seems that forcing function number two ($p_o = 1 - e^{-t}$) and a radius cavity of 0.25 inches matches the wave at this time more closely. This function was multiplied by a constant that would give a wave amplitude as determined experimentally. Using the method described in the theoretical section of this report, values of radial and tangential stresses were computed. The results are shown in Figure 47. When the curves of Figure 35 and 47 are compared, several differences in shape and attenuation are observed. These are to be expected. In addition to the fact that the wave profiles were not matched exactly, those of Figure 47 are computed spherical waves in a three-dimensional target and those of Figure 35 were experimentally determined cylindrical waves in a two-dimensional plate. There are still greater differences in the reflected waves. Those theoretically computed are shown in Figure 48 and those experimentally determined were shown in Figure 39. Although the wave forms were not the same, there is very good agreement in the magnitude of the reflected tensile wave. Both the experimental

and theoretical computations indicated that the maximum tnesile stress would have a magnitude of about 18 at 93 microseconds.

The same forcing function was also applied to laminated targets having 1/8 and 1.0 inch aluminum cores. The stress-time relations at a point 3.5 inches from the orgin are shown in Figure 49. The stress-distance relations at a time of 68 microseconds were also computed. These curves (Figure 50) indicate that the theoretical stress wave amplitude in the 1/8 - inch laminated target is 79% of that in a solid homogeneous target, and the stress in the 1.0 - inch laminated target is 36.5% of that in the solid target. In the case of the 1.0 - inch aluminum core, the wave front has reached the free boundary and has started to reflect. If the boundary had not been there, the wave would have been of the form shown by the dotted line, but the maximum value of stress would have been the same. In comparing Figures 44 and 50, it is seen that the waves in the theoretical analysis are at a greater distance than those experimentally determined. The reason for this is that the time was determined from the time of the explosion in the experiments but in the theoretical study the forcing function was applied to a 0.25 - inch cavity and time was counted from that time. In other words, the waves in Figure 50 should be 0.25 inch ahead of those of Figure 44. If this had been taken into consideration, the comparisons would have been somewhat better. This is shown in Figure 51.

SECTION V

CONCLUSIONS

It seems that the so-called quasi-theoretical method described here can be utilized to determine the effects of laminations in targets impacted by hypervelocity projectiles. In spite of the approximations used in this first attempt to apply the method, the results were better than had been expected. A comparison of the two methods shows the following:

Method Used	Percent Reduction in Stress	
	1/8" Laminate	1.0" Laminate
Experimental	29	60
Theoretical	21	64

Many improvements can be made that should improve the accuracy of the results. It is believed that a method can be developed that will provide a forcing function that will almost exactly simulate the stress waves. A program will be written for cylindrical stress waves in plates which should more accurately agree with the experimental results. Also, three dimensional experimental methods can be developed. A more powerful energy source is needed in order to generate stress waves without the use of chemical explosives. This would give more consistent results with greater accuracy. Parts for a 800 Joule power supply are now on hand for the construction of such a unit. Hypervelocity impacts should be made in transparent targets so that wave forms due to actual collisions can be determined. This information can be obtained in the case of non-transparent targets

by attaching transparent sheets to their rear surfaces and analyzing the transmitted waves.

Two other methods of obtaining stress wave characteristics have been investigated and show promise of giving accurate results.

One of these gives a record of photoelastic fringes as they pass any given point of the model. Presently, this consists of a fiber optic light tube that passes a very small pencil of light through the model in the polariscope onto a photomultiplier tube, the response of which is recorded by an oscilloscope. A laser has been purchased and will replace the fiber optics.

The other technique gives the material velocity at a point as the stress wave passes. This consists of imbedding a short wire in the target which is placed in a strong magnetic field. As the stress waves pass the wire, the slight motion generates an electrical current proportional to its velocity. The signal is the input to an analog computer that has been programmed to compute and plot the resulting stresses.

SECTION VI

REFERENCES

1. Kinslow, Ray: Stress Waves in Composite Laminates. AEDC-TR-65-69, June 1965.

2. Kinslow, Ray: Observations of Hypervelocity Impact of Transparent Plastic Targets. AEDC-TDR-64-69 (AD438947), May 1964.

3. Cosby, William A.; and Lyle, Robert G.: The Meteoroid Environment and Its Effects on Materials and Equipment. NASA SP-78, 1965.

4. Kinslow, Ray: Properties of Reflected Stress Waves. AEDC-TR-67-112 (AD818630), August 1967.

5. Kinslow, Ray: Properties of Spherical Stress Waves Produced by Hypervelocity Impact. AEDC-TDR-63-197 (AD421578), October 1963.

6. Durelli, A. J.; and Riley, W. F.: Introduction to Photomechanics. Prentice-Hall, Inc., 1965.

7. Dally, J. W.; and Riley, W. F.: Stress Wave Propogation in a Half Plane due to a Transit Point Load. Vol. III of Developments in Theoretical and Applied Mechanics, W. A. Shaw, ed., Pergamon Press, 1967, pp. 357-396.

TABLE I

MATERIAL PROPERTIES

	DENSITY (ρ) $LB \cdot SEC^2 \cdot FT^{-4}$	WAVE VELOCITY (c) $FT \cdot SEC^{-1}$	CHARACTERISTIC IMPEDANCE (ρc) $LB \cdot SEC \cdot FT^{-3}$
Steel	15.2	19,500	29.6×10^4
Silver	20.4	13,400	27.3×10^4
Copper	17.2	14,000	24.1×10^4
Lead	22.0	7,100	15.6×10^4
Mercury	26.3	4,500	11.8×10^4
Glass	5.0	22,300	11.15×10^4
Aluminum	5.22	20,900	10.9×10^4
Lucite	2.3	8,700	2.0×10^4
PSM-1	2.36	5,100	1.20×10^4
Water	1.94	5,200	1.01×10^4

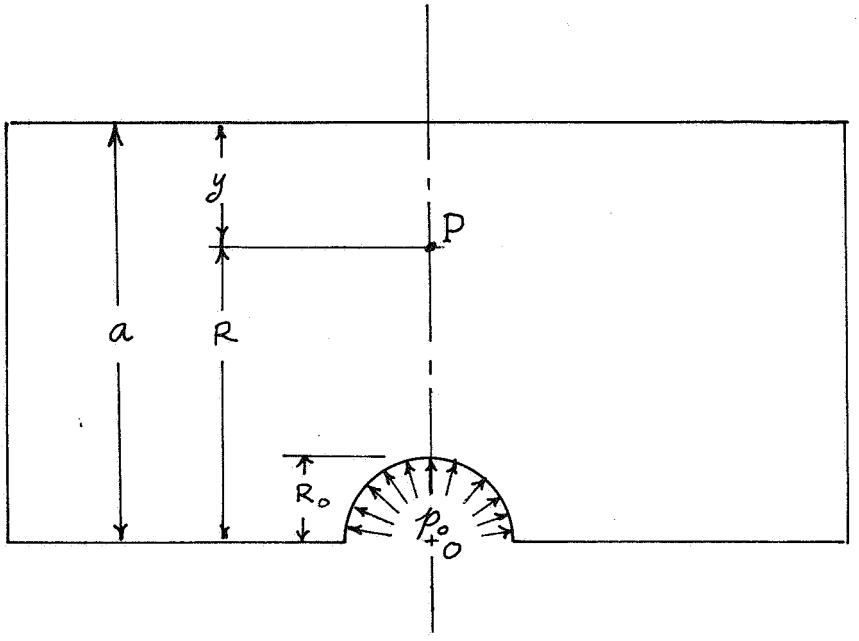

Figure 1. TARGET DIMENSIONS AND COORDINATES

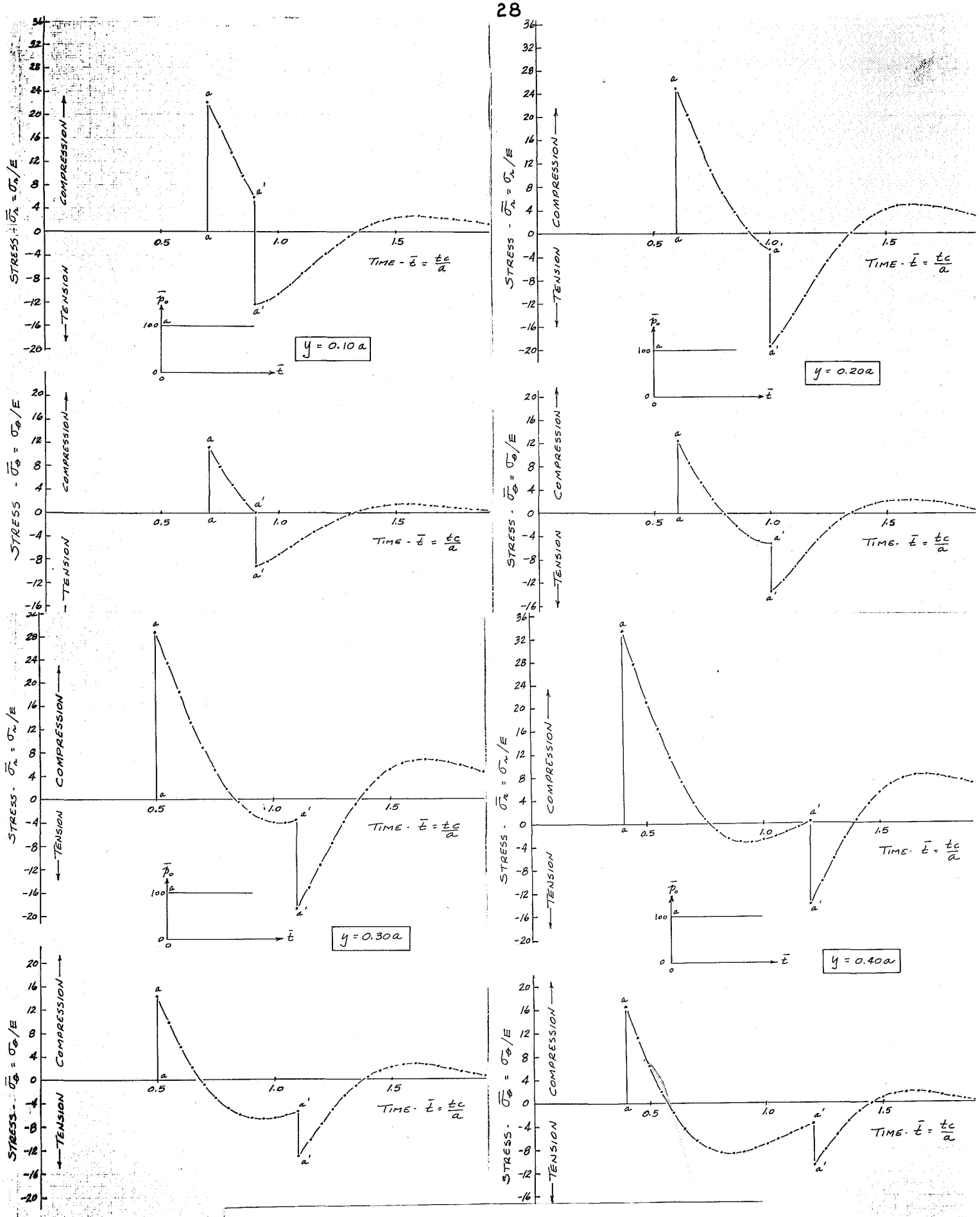

Figure 2. STRESS-TIME RELATIONS (p_0= constant)

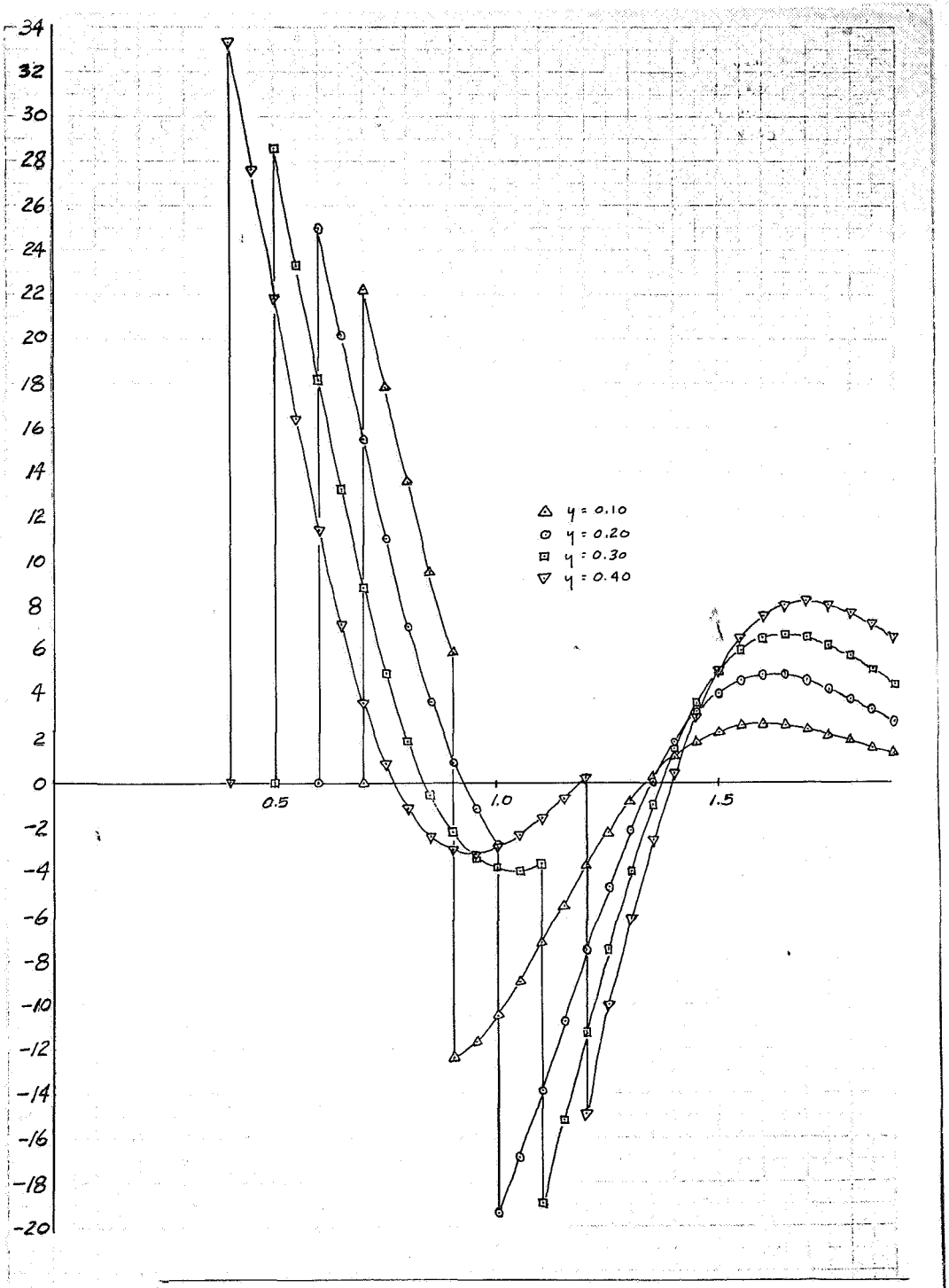

Figure 3. COMPARISON OF RADIAL STRESSES

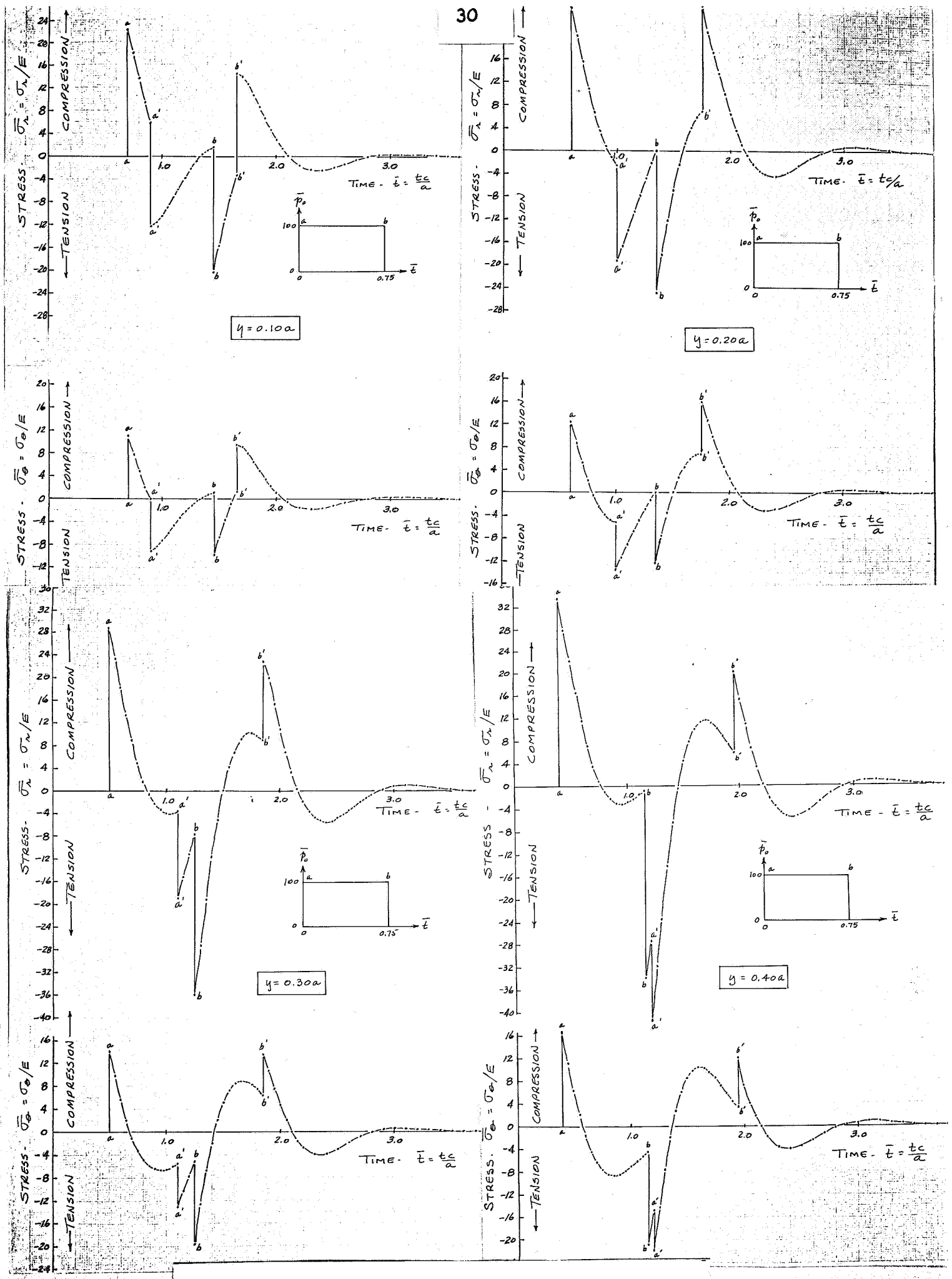

Figure 4. STRESS-TIME RELATIONS (p_o= impulse, L=0.75)

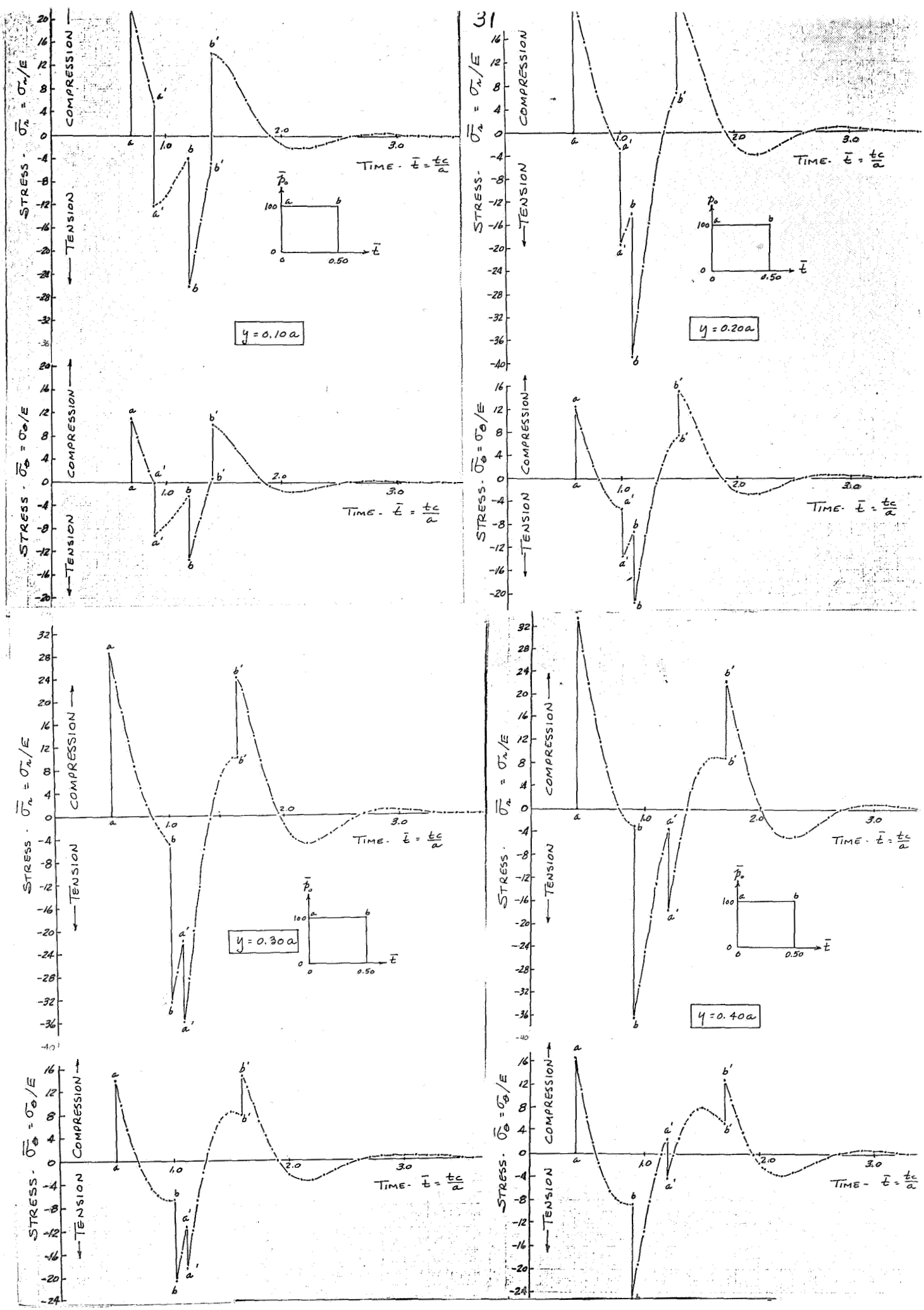

Figure 5. STRESS-TIME RELATIONS (p_o= impulse, L=0.50)

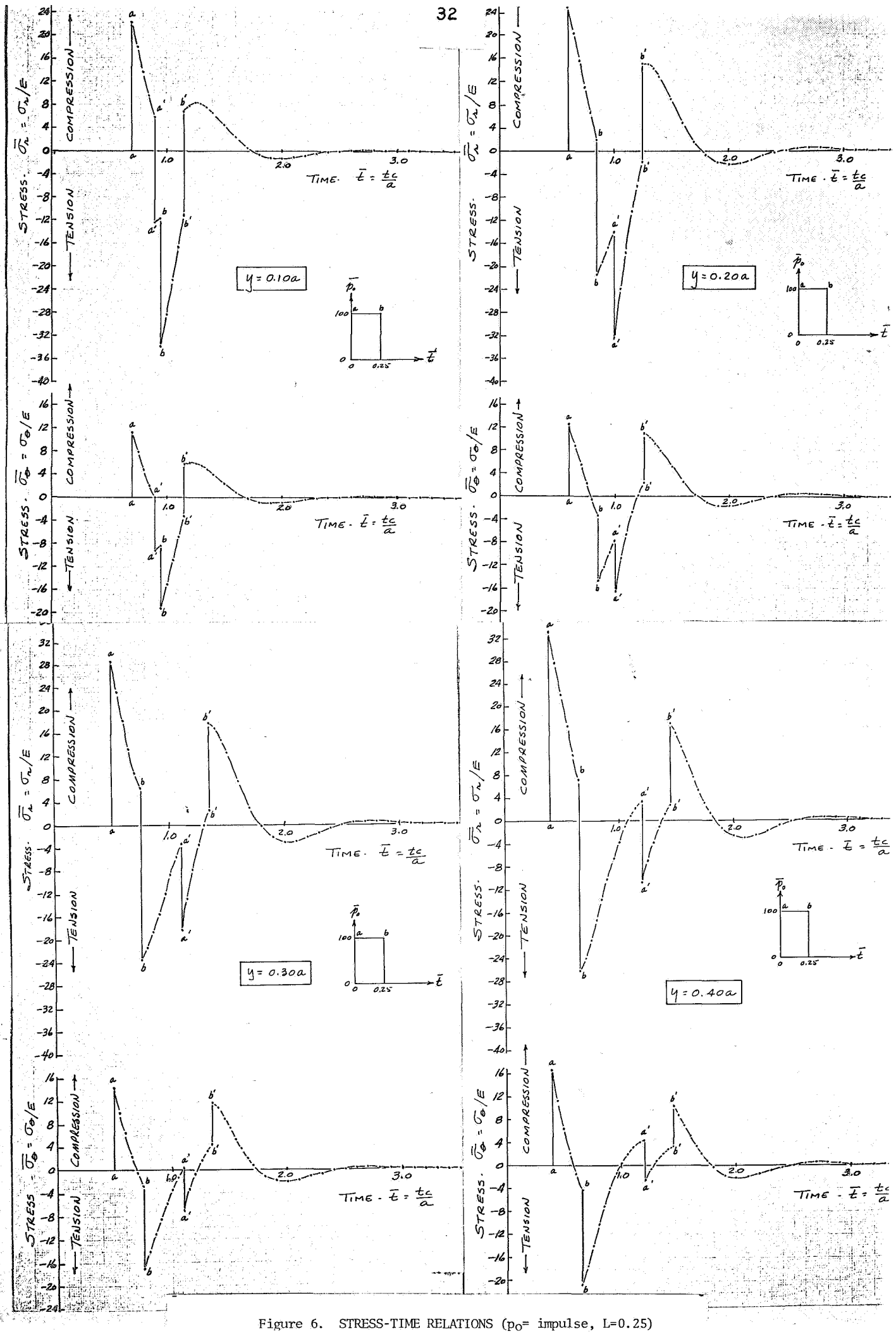

Figure 6. STRESS-TIME RELATIONS (p_o= impulse, L=0.25)

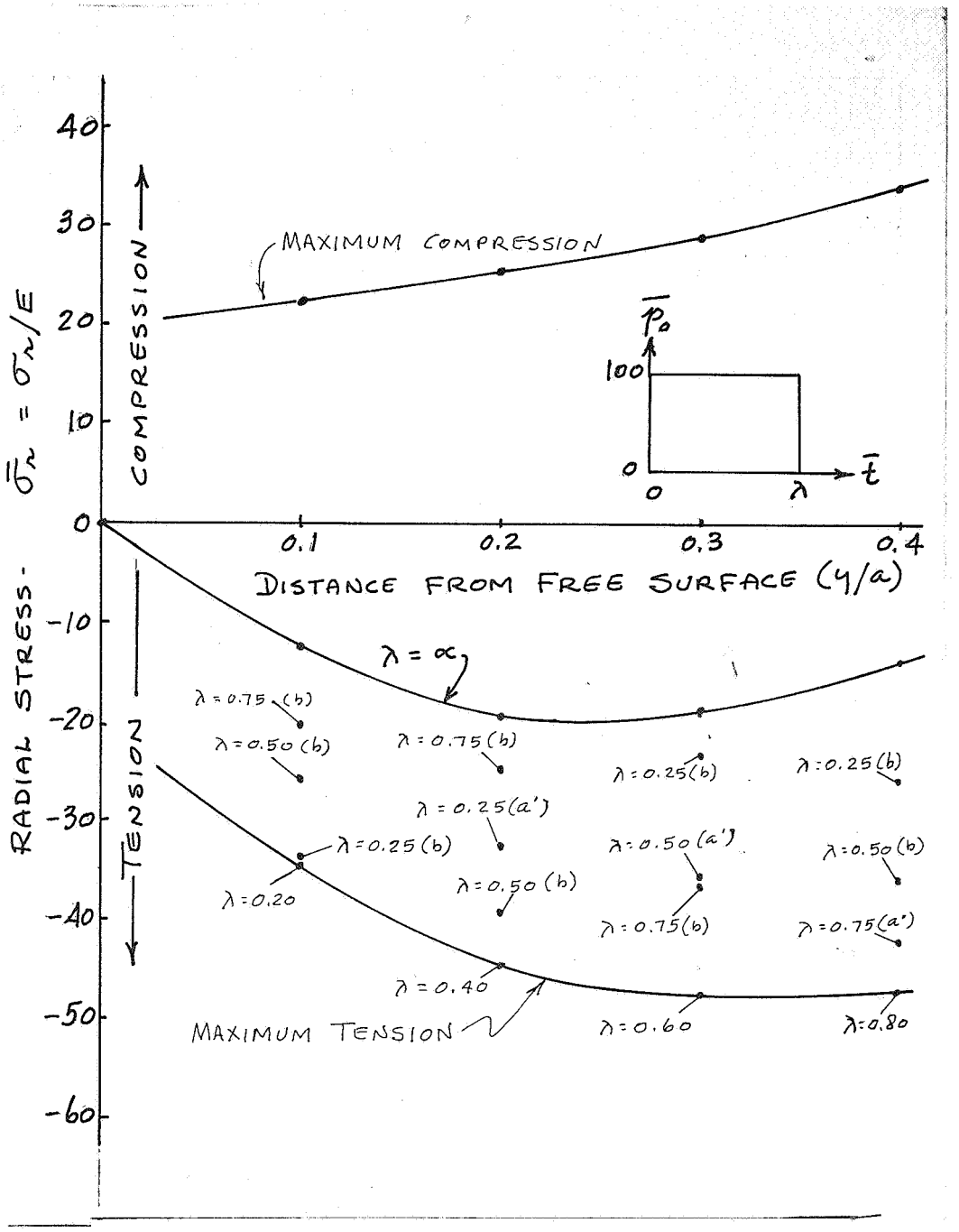

Figure 7. MAXIMUM STRESS NEAR FREE SURFACE
(step inputs)

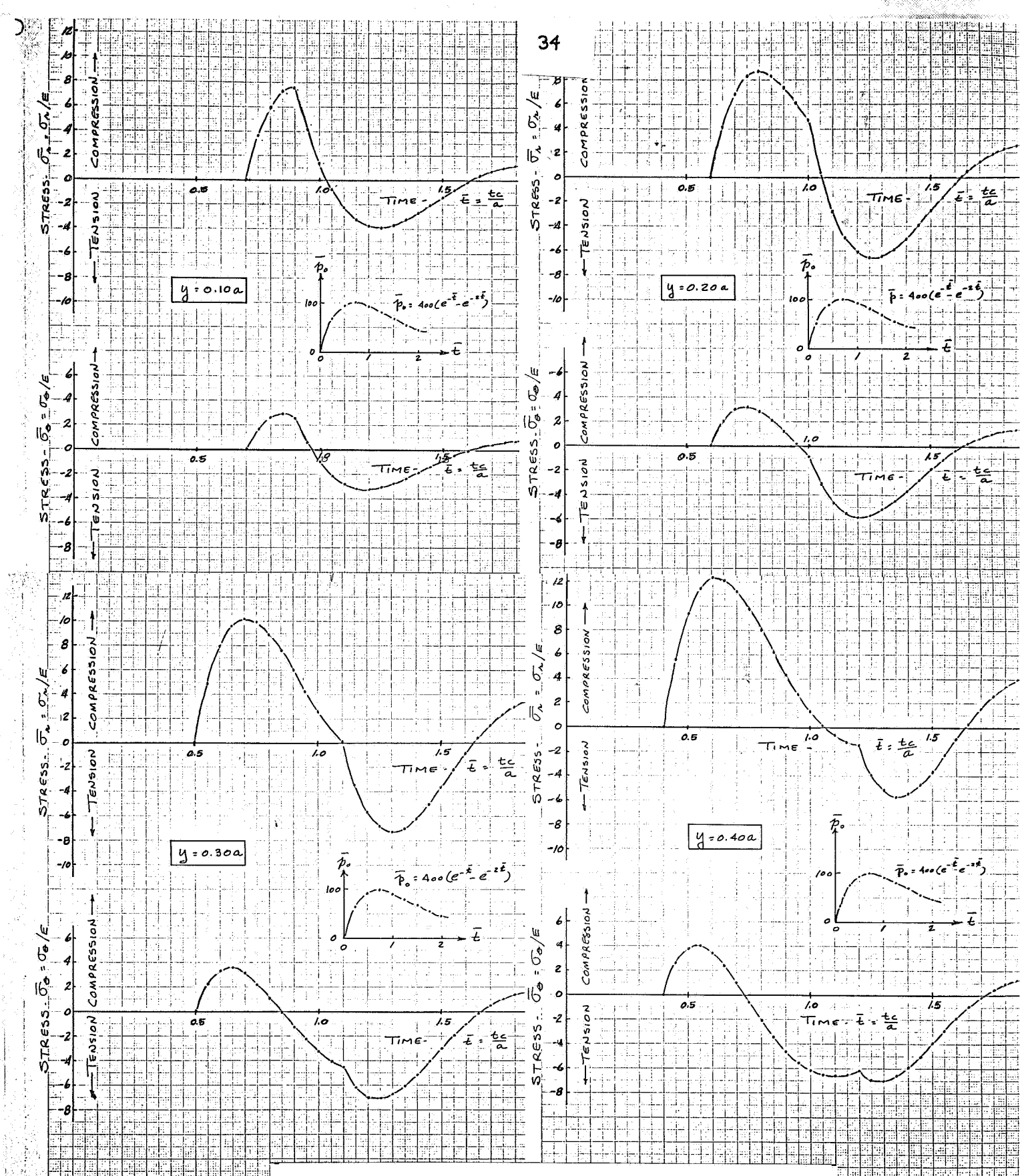

Figure 8. STRESS-TIME RELATIONS

$[\bar{p} = 400(e^{-t} - e^{-2t})]$

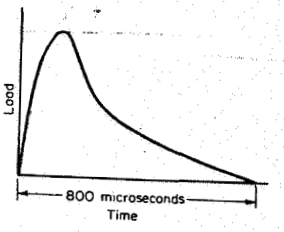

Fig. 12.9. Estimated load-time curve for the M52-A3 electrical primer

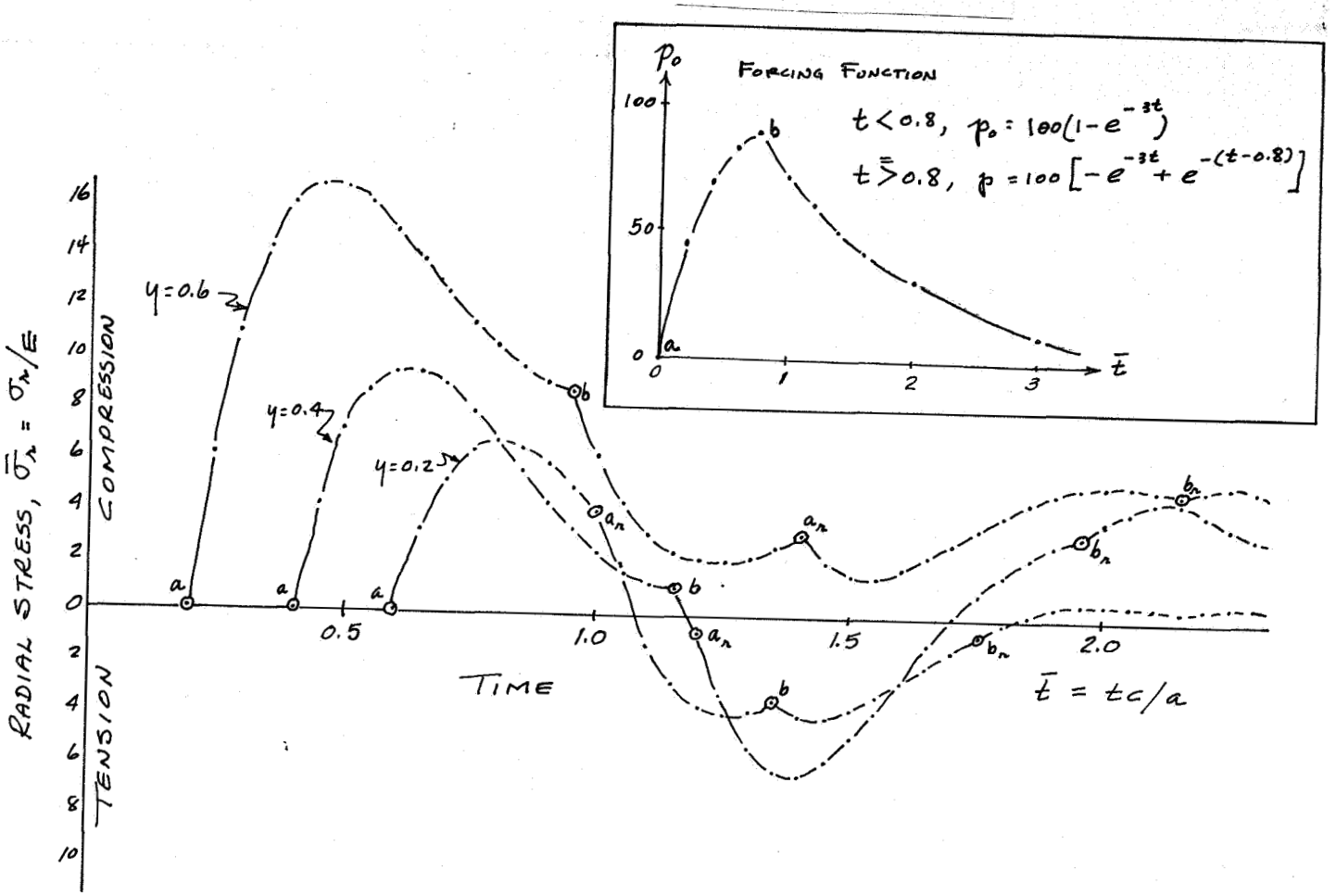

Figure 9. STRESS-TIME RELATIONS
(Explosive input)

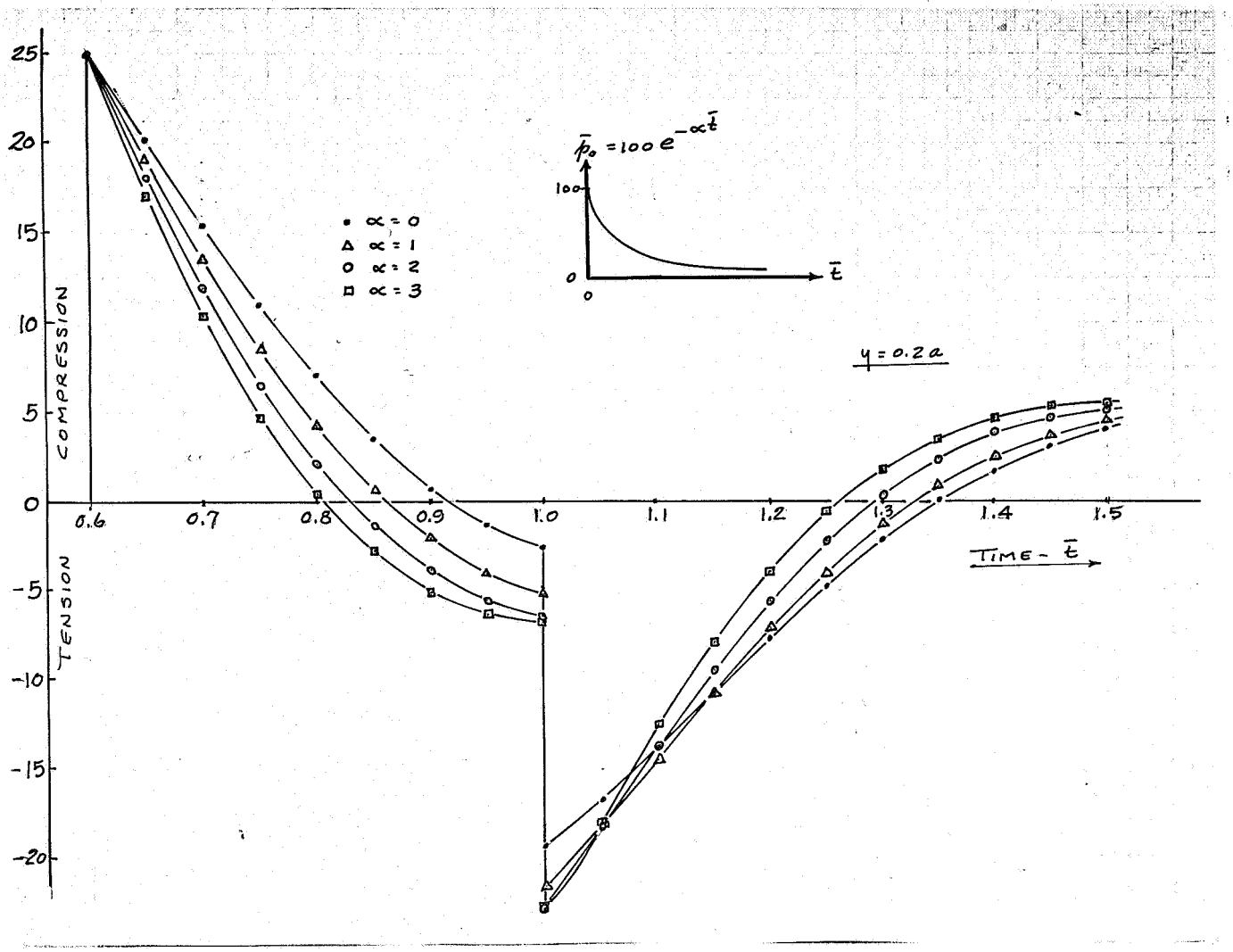

Figure 10. STRESS-TIME RELATIONS
(Decaying input)

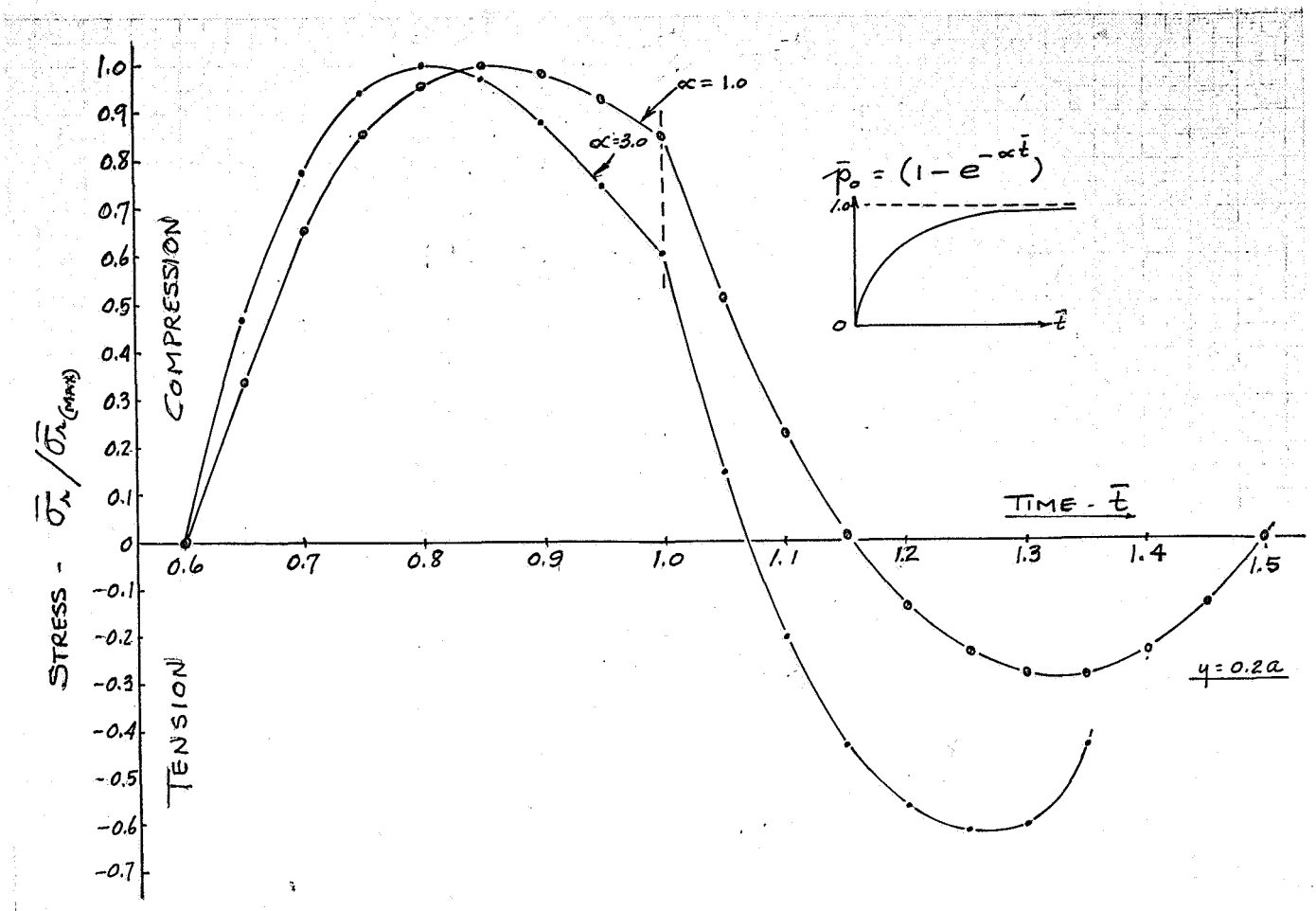

Figure 11. STRESS-TIME RELATIONS

$\bar{p} = (1 - e^{-\alpha t})$

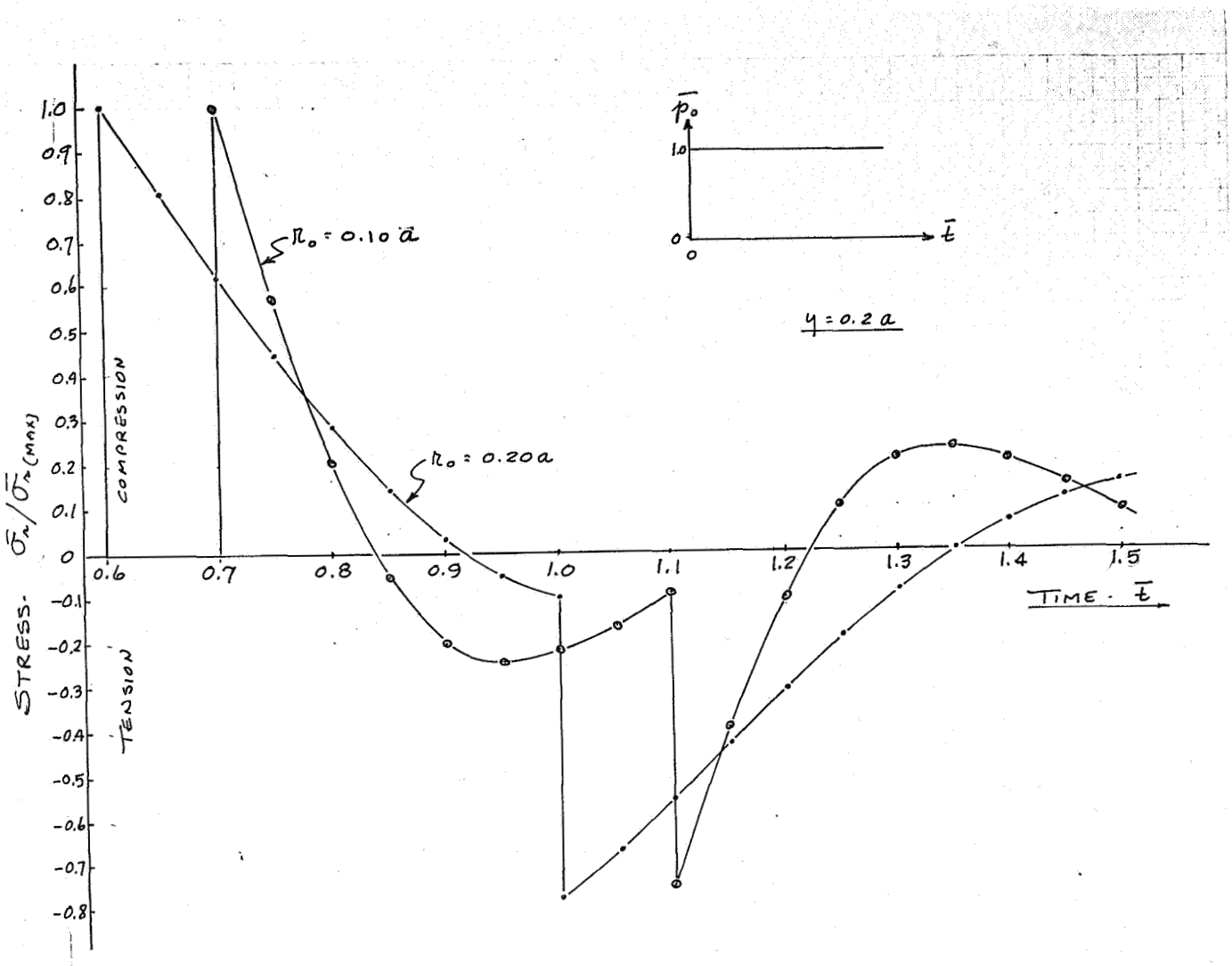

Figure 12. EFFECT OF CAVITY RADIUS

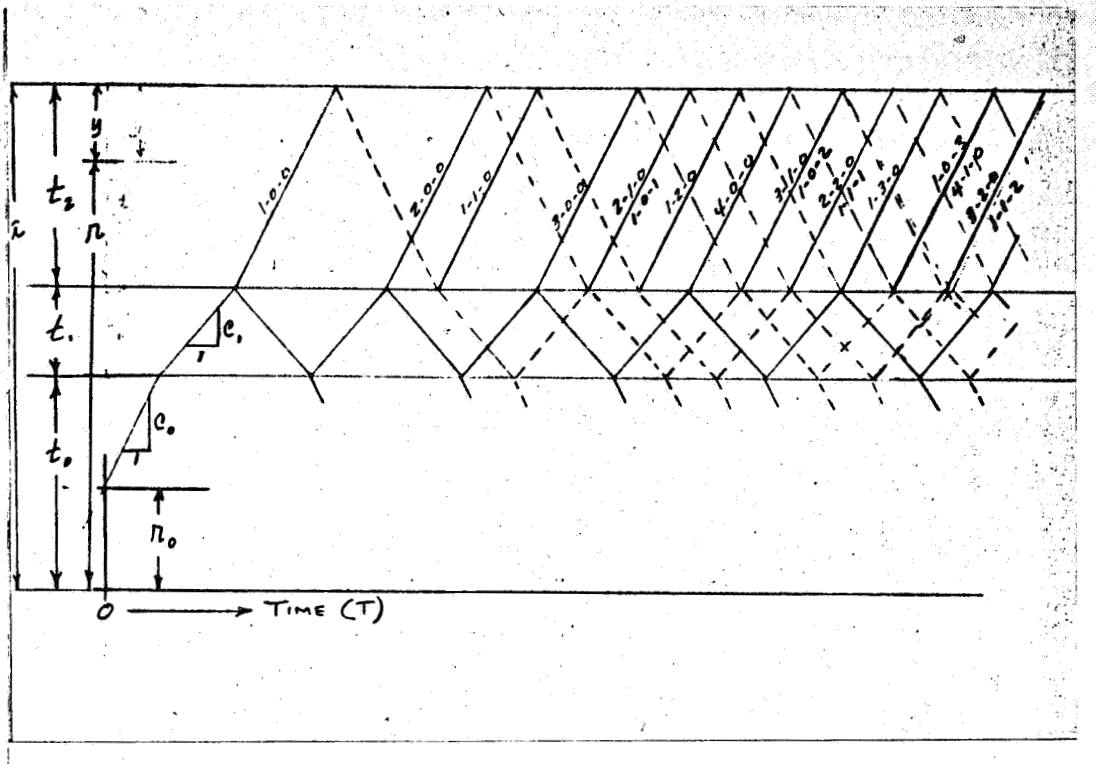

$$T_{A\text{-}0\text{-}0} = \left[\frac{(zA-1)C_0-(C_1)}{C_0C_1}\right] t_1$$

$$T_{A\text{-}B\text{-}0} = T_{A\text{-}0\text{-}0} + \frac{zBt_2}{C_0}$$

$$T_{A\text{-}B\text{-}C} = T_{A\text{-}B\text{-}0} + \frac{zt_2}{C_0} + \frac{zCt_1}{C_1}$$

Figure 13. REFLECTED AND TRANSMITTED STRESS WAVES IN LAMINATED TARGETS

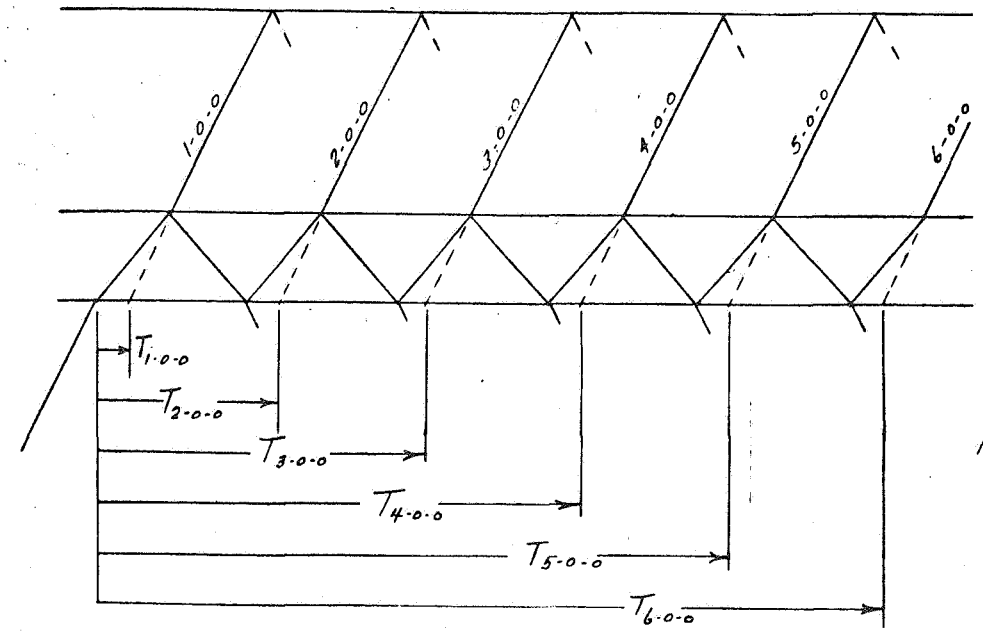

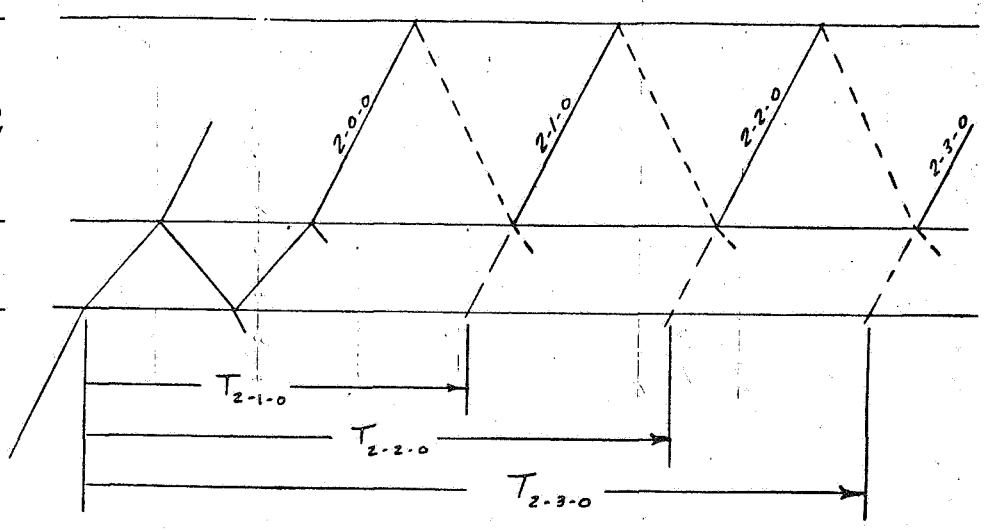

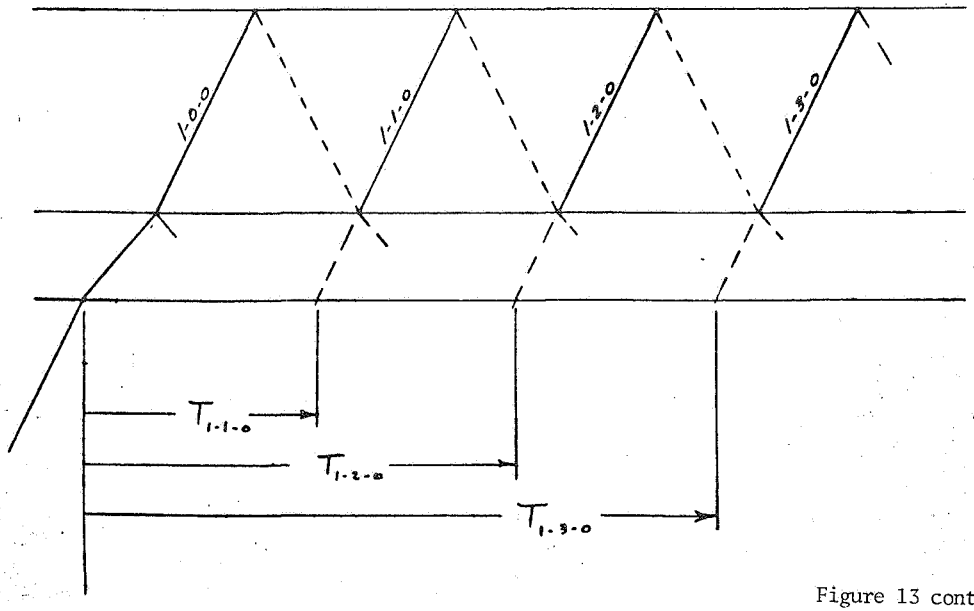

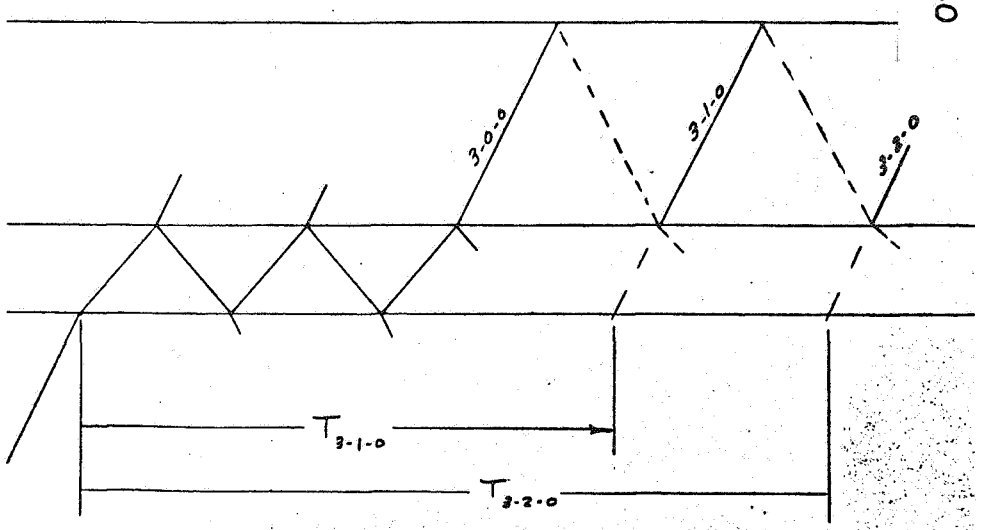

Figure 13 continued.

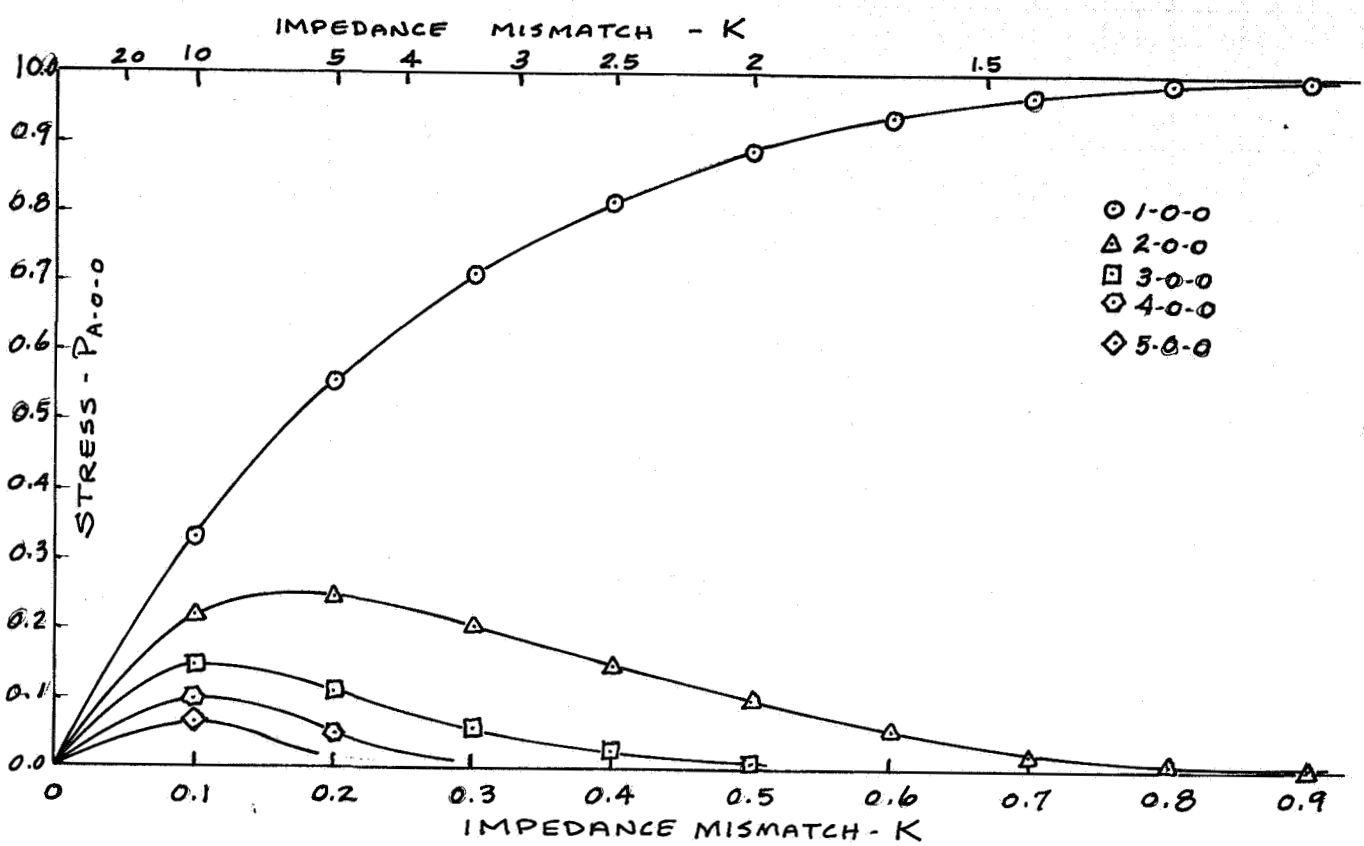

Figure 14. STRESS AMPLITUDES - IMPEDANCE MISMATCH RELATIONS

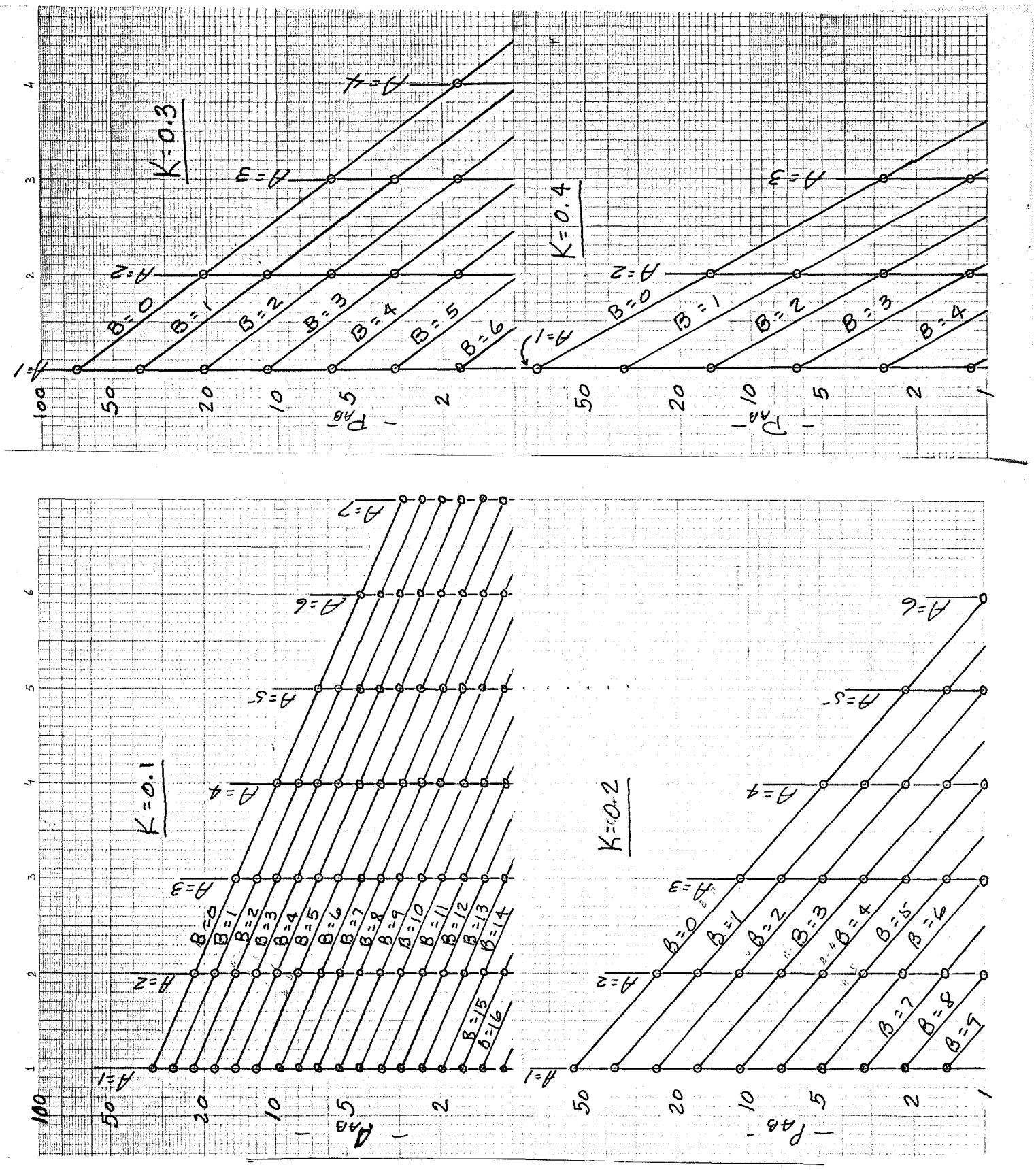

Figure 15. AMPLITUDES OF THE VARIOUS TRANSMITTED WAVES

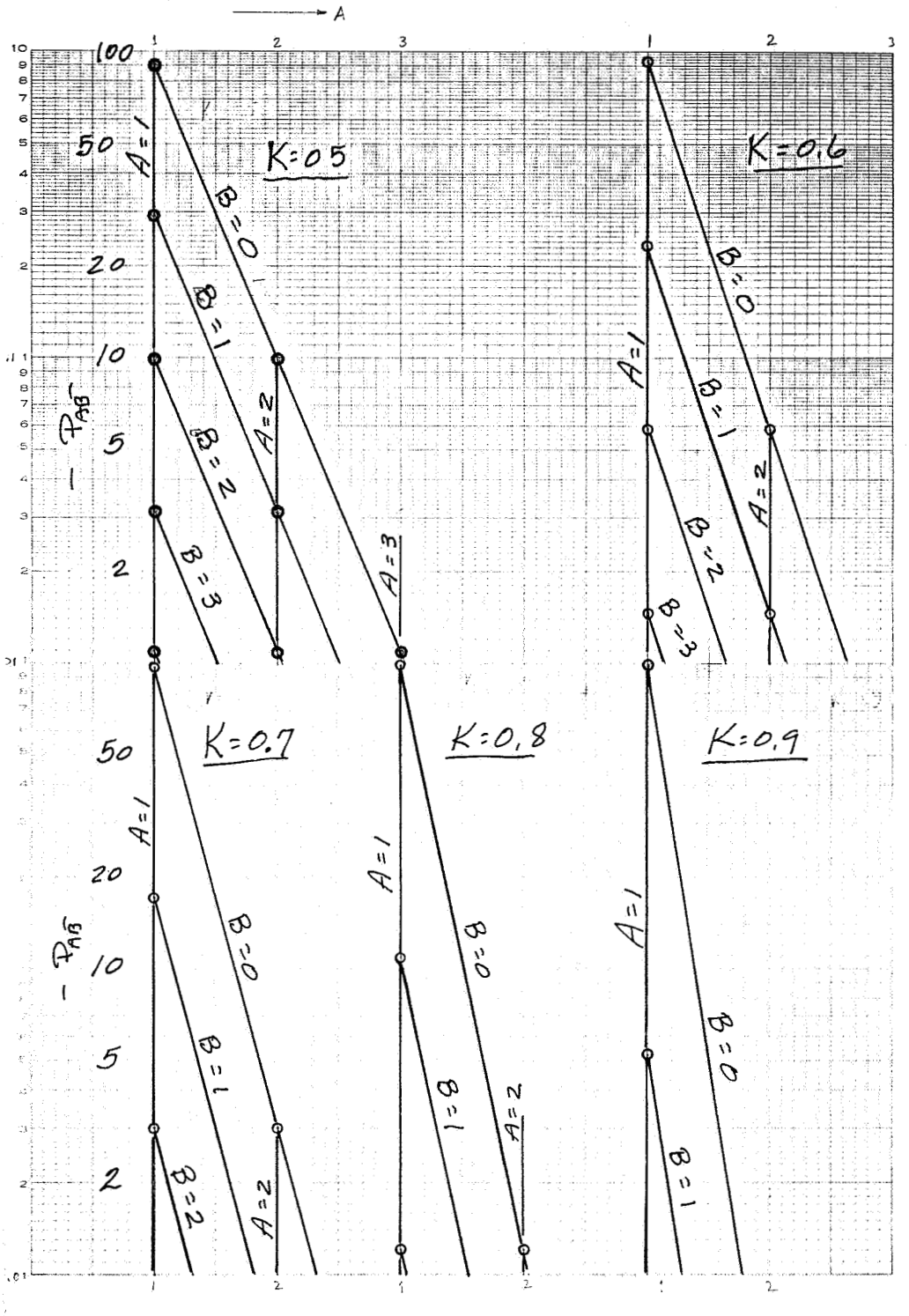

Figure 15 continued.

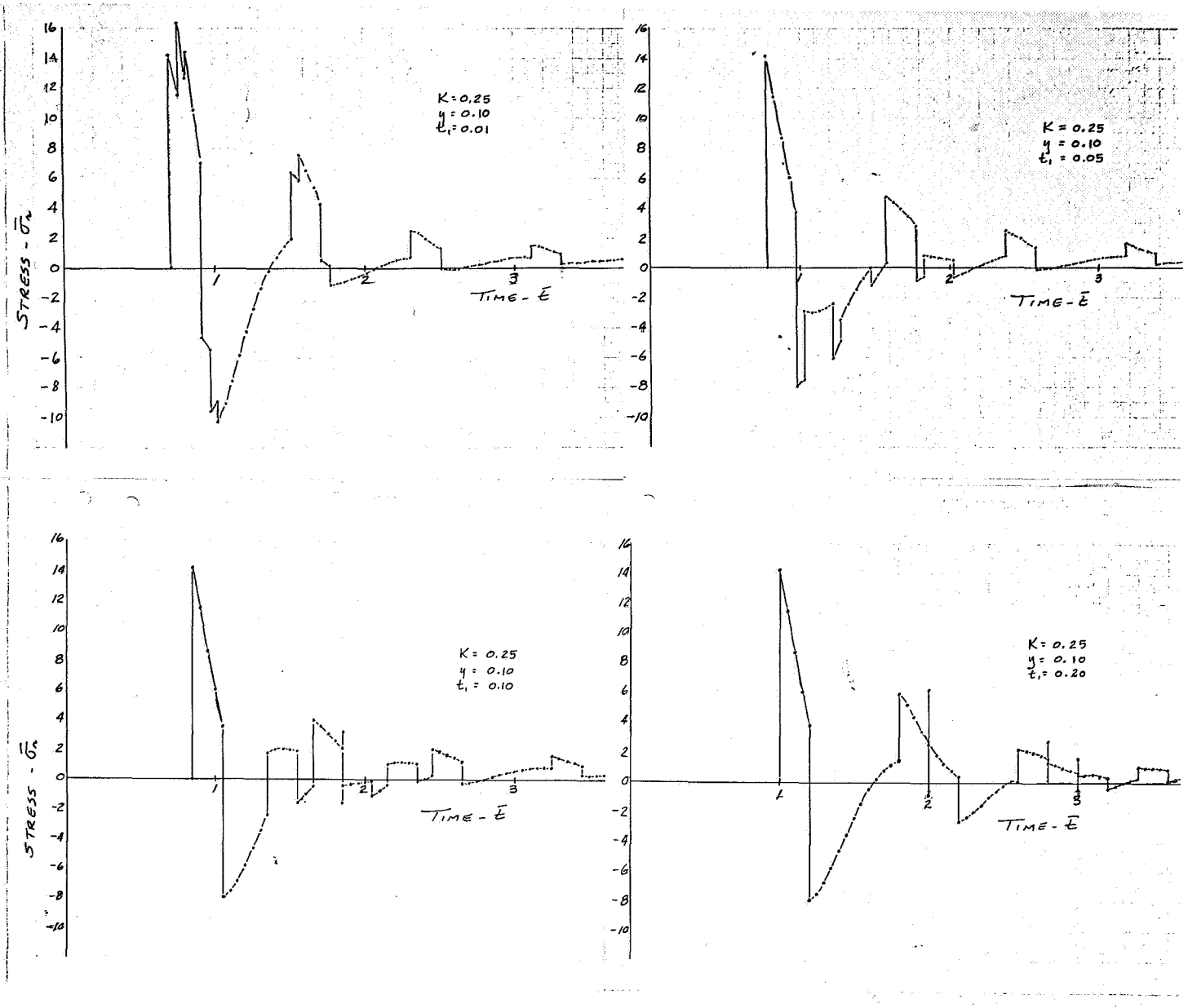

Figure 16. STRESS-TIME - LAMINATION THICKNESS RELATIONS
(p_o = constant, K = 0.25, y = 0.10a)

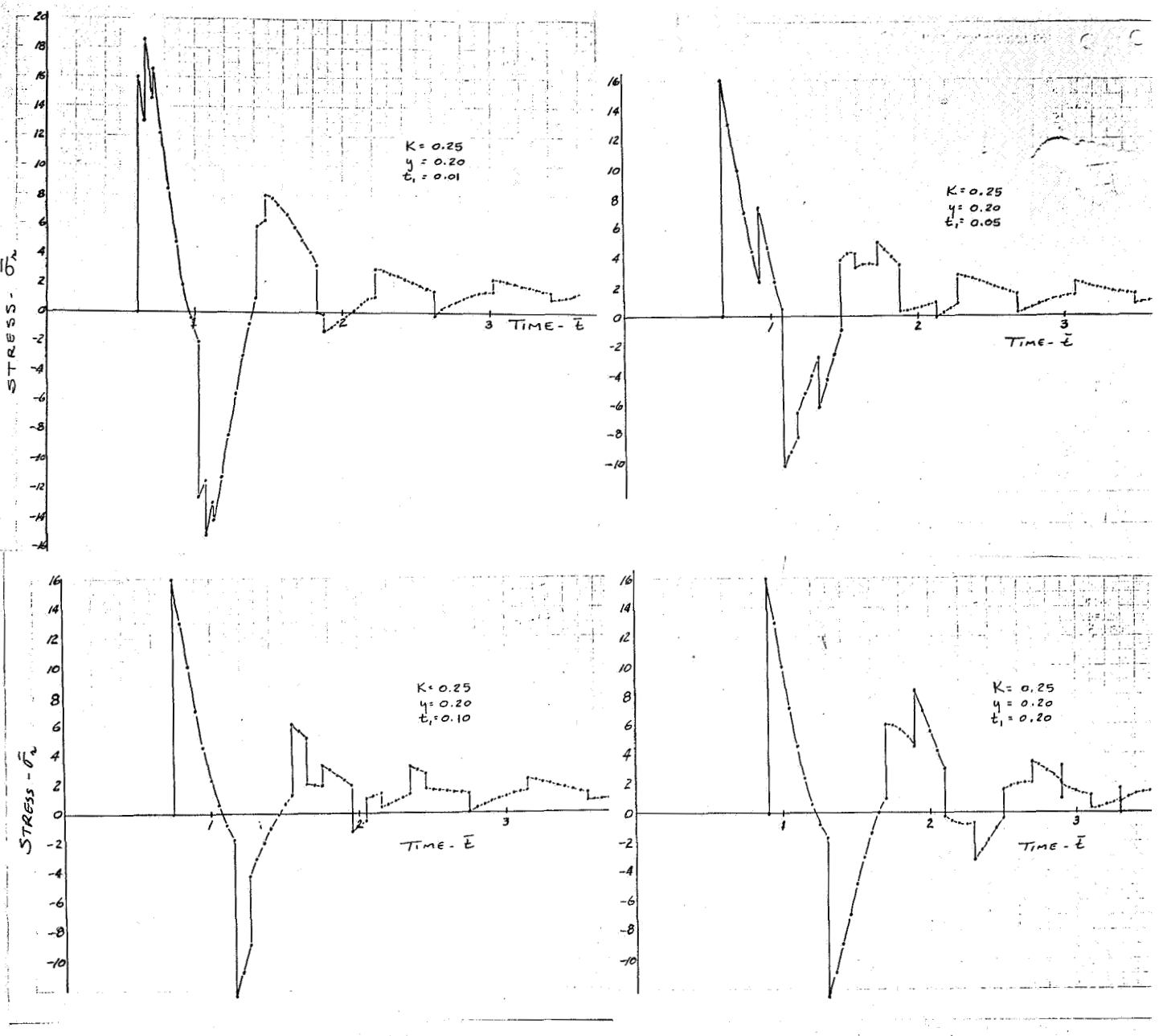

Figure 17. STRESS-TIME - LAMINATION THICKNESS RELATIONS
(p_o = constant, K = 0.25, y = 0.20a)

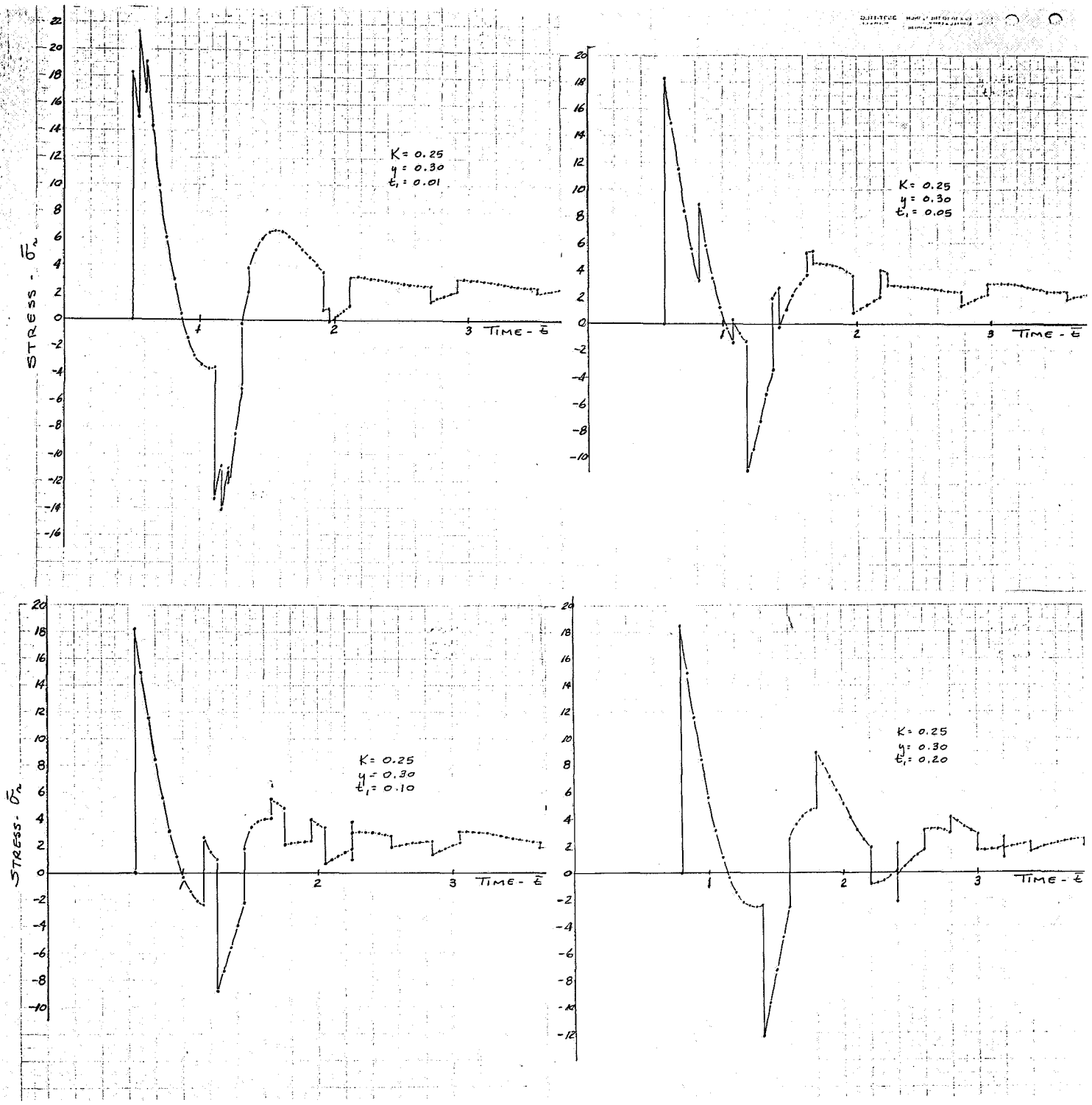

Figure 18. STRESS-TIME - LAMINATION THICKNESS RELATIONS
(p_o = constant, K = 0.25, y = 0.30a)

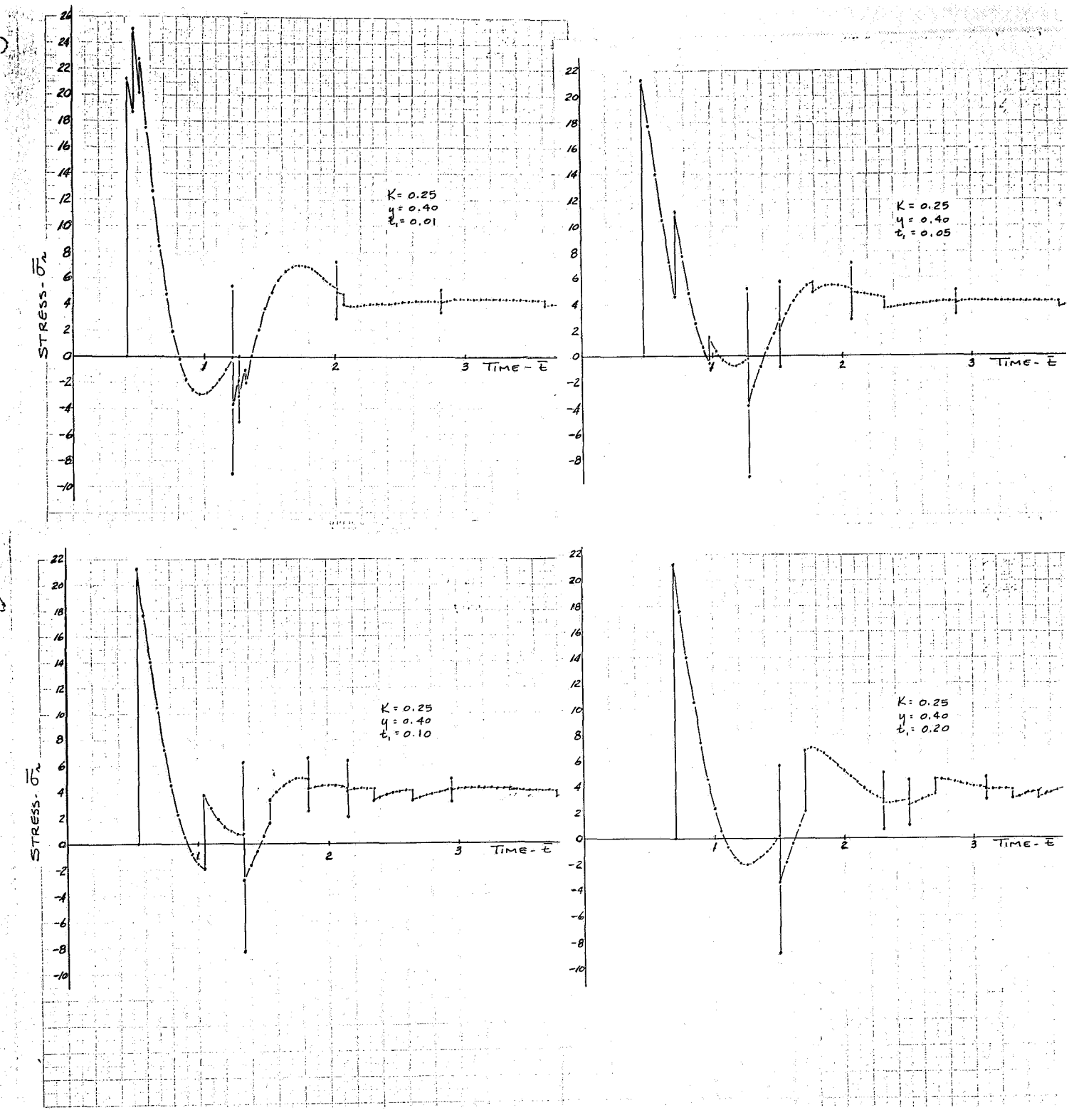

Figure 19. STRESS-TIME - LAMINATION THICKNESS RELATIONS
(p_0 = constant, K = 0.25, y = 0.40a)

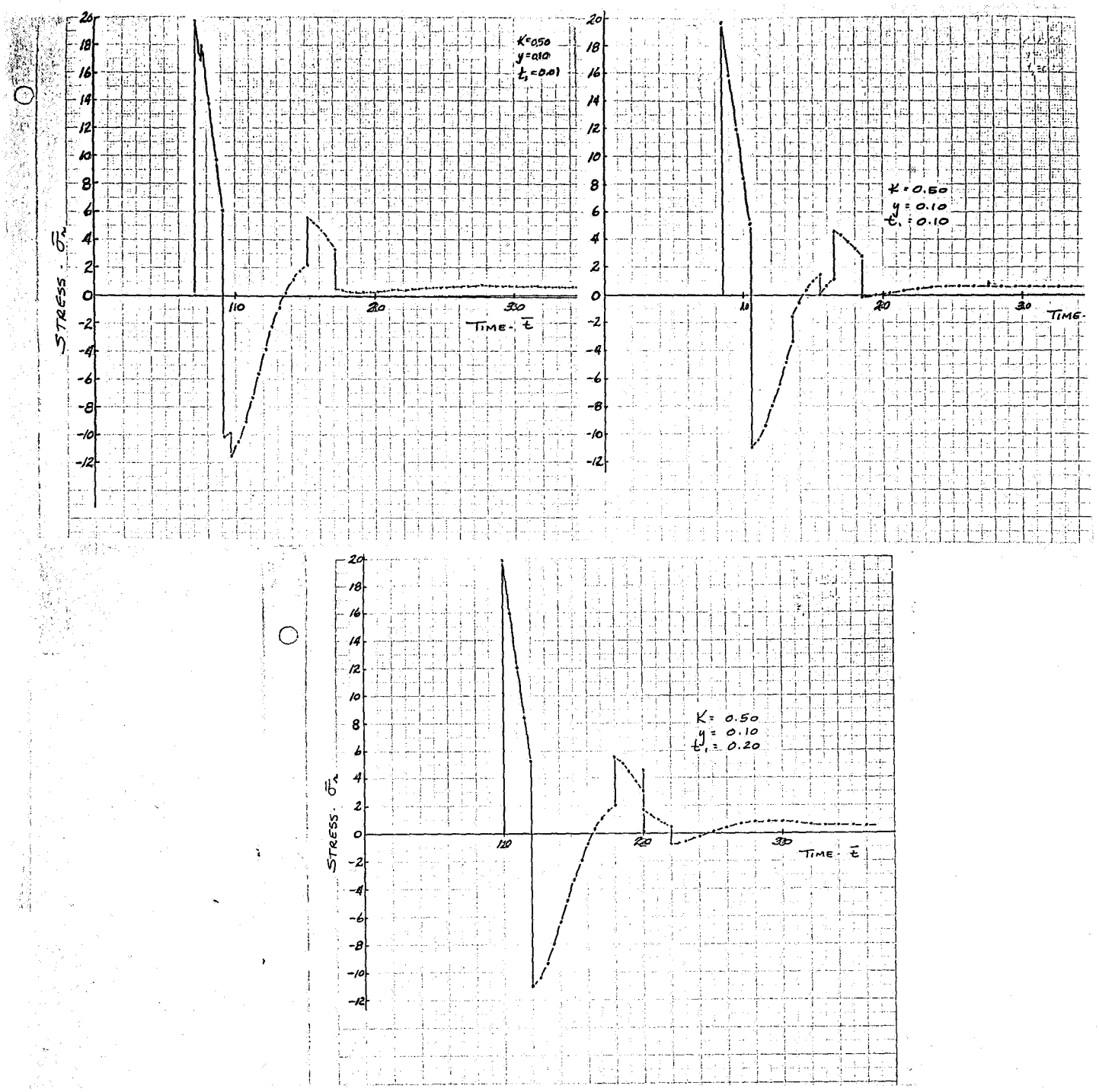

Figure 20. STRESS-TIME - LAMINATION THICKNESS RELATIONS
(p_o = constant, K = 0.50, y = 0.10a)

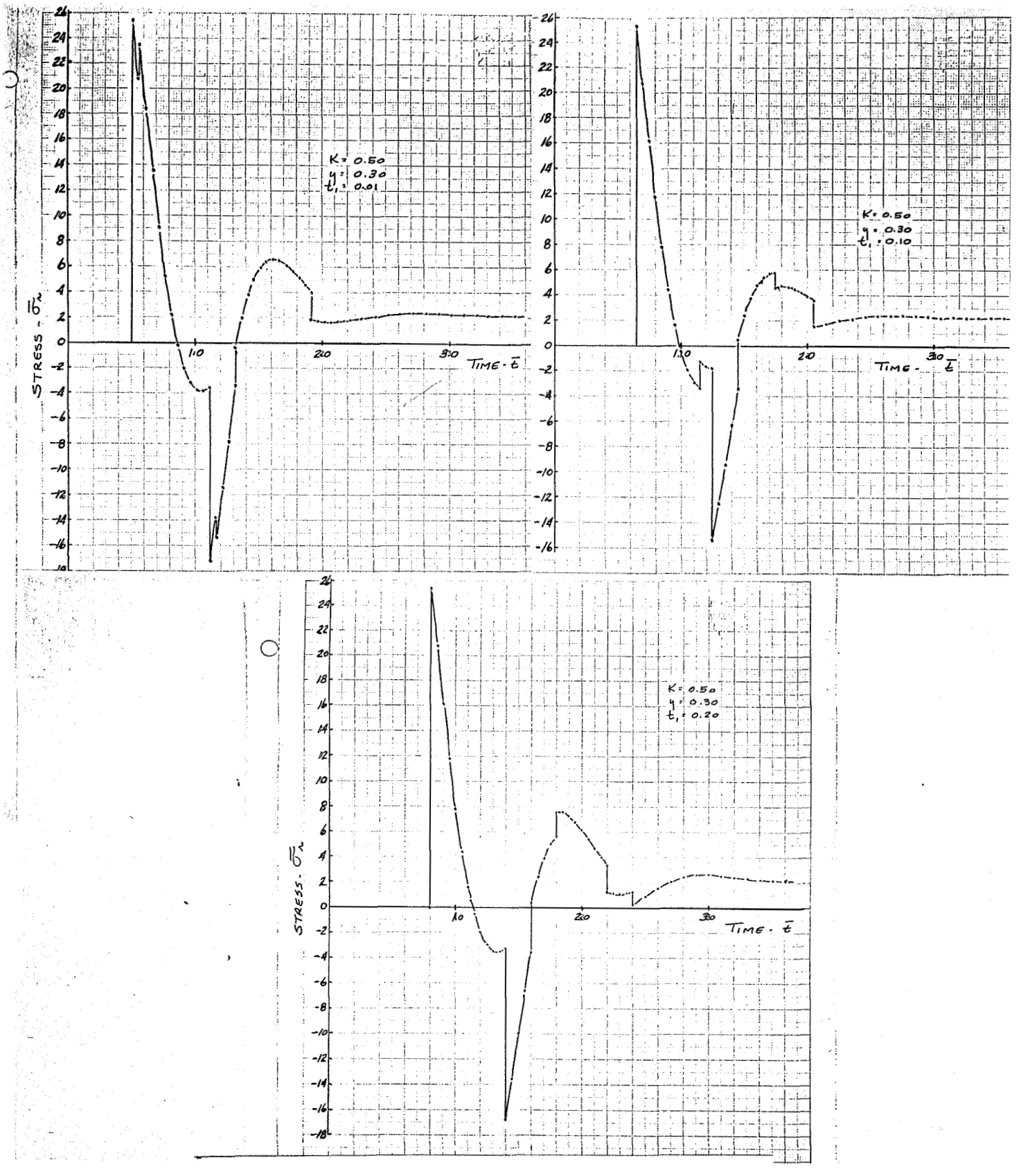

Figure 21. STRESS-TIME - LAMINATION THICKNESS RELATIONS
(p_o = constant, K = 0.50, y = 0.30a)

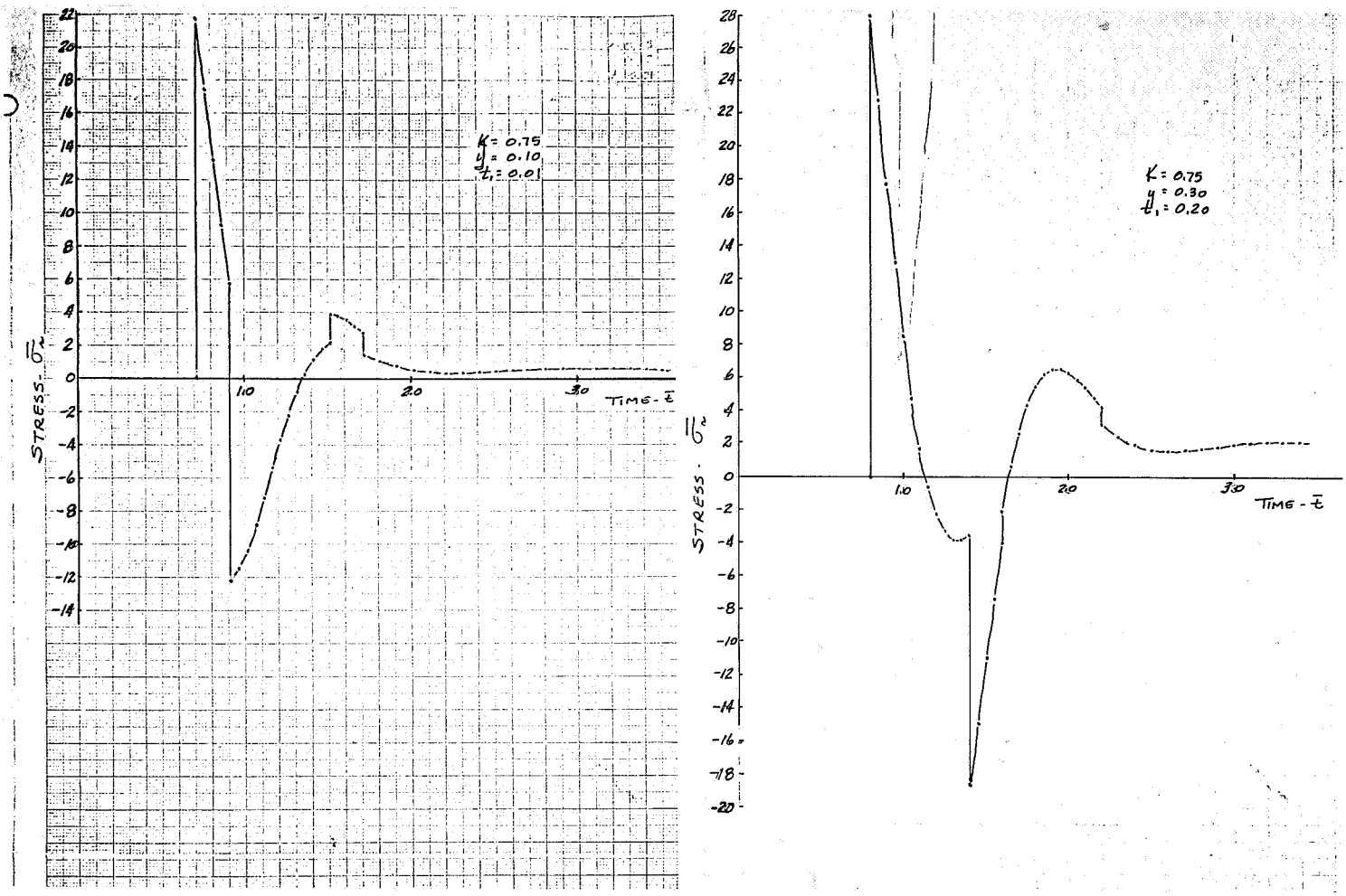

Figure 22. STRESS - TIME RELATIONS
(p_o = constant, K = 0.75)

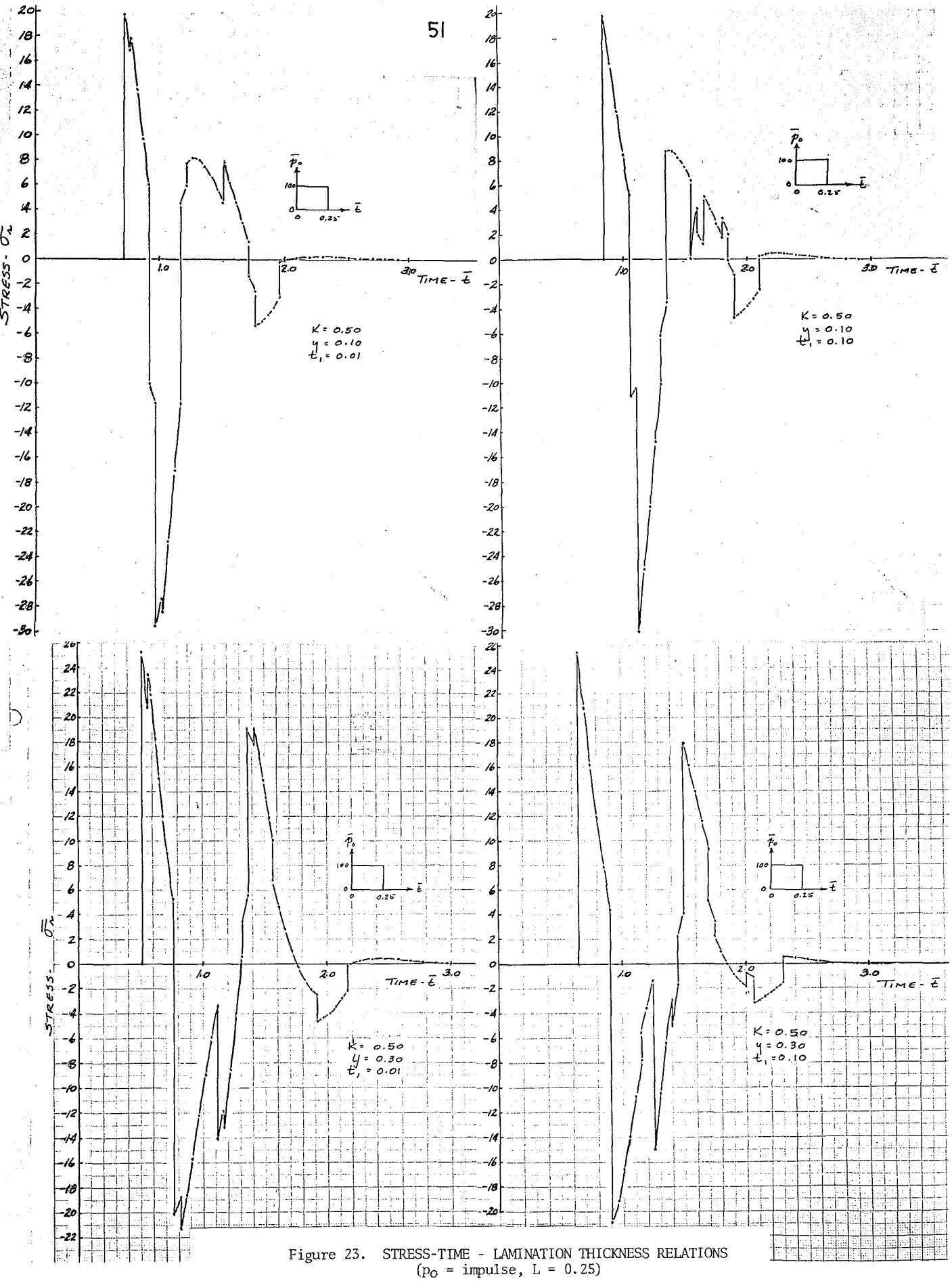

Figure 23. STRESS-TIME - LAMINATION THICKNESS RELATIONS
(p_o = impulse, L = 0.25)

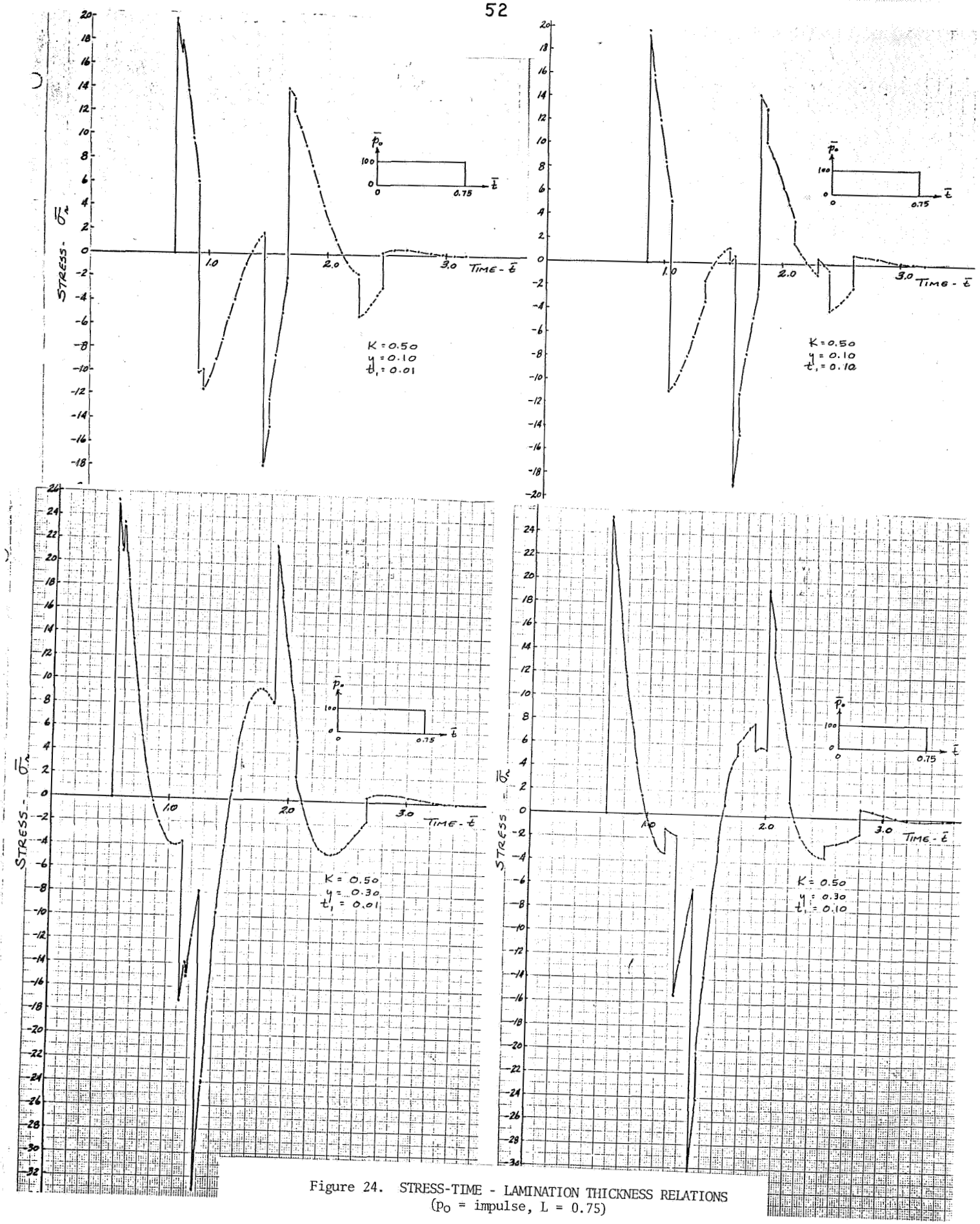

Figure 24. STRESS-TIME - LAMINATION THICKNESS RELATIONS
(P_O = impulse, L = 0.75)

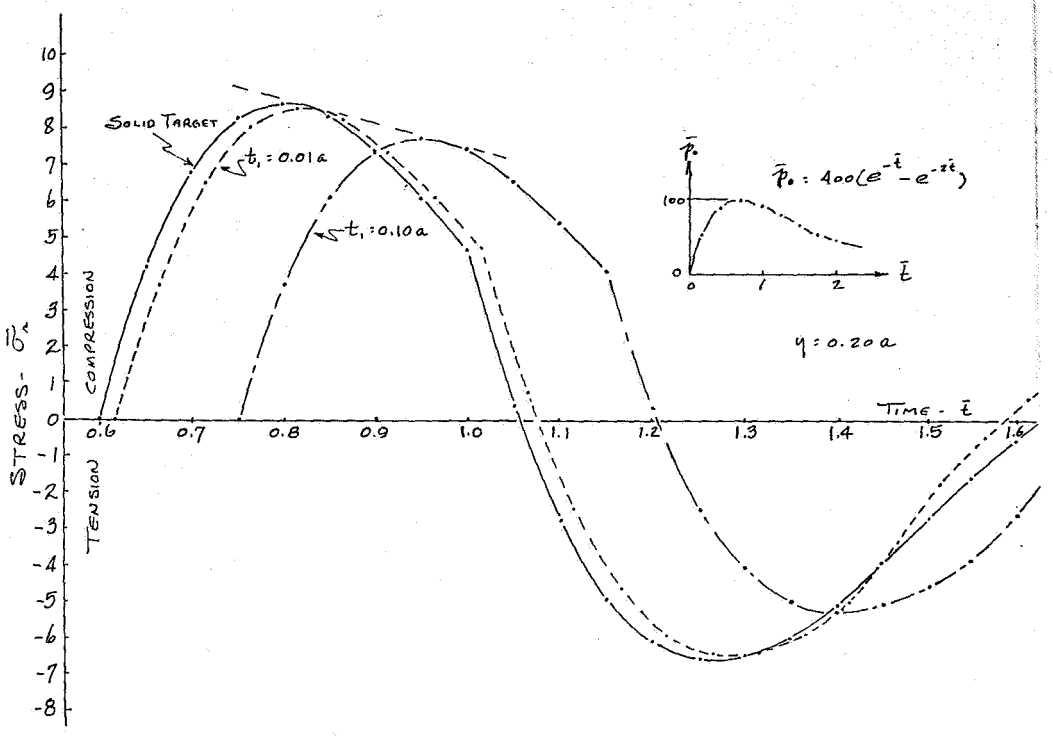

Figure 25. STRESS-TIME - LAMINATION THICKNESS RELATIONS

$[p_o = 400(e^{-t} - e^{-2t})]$

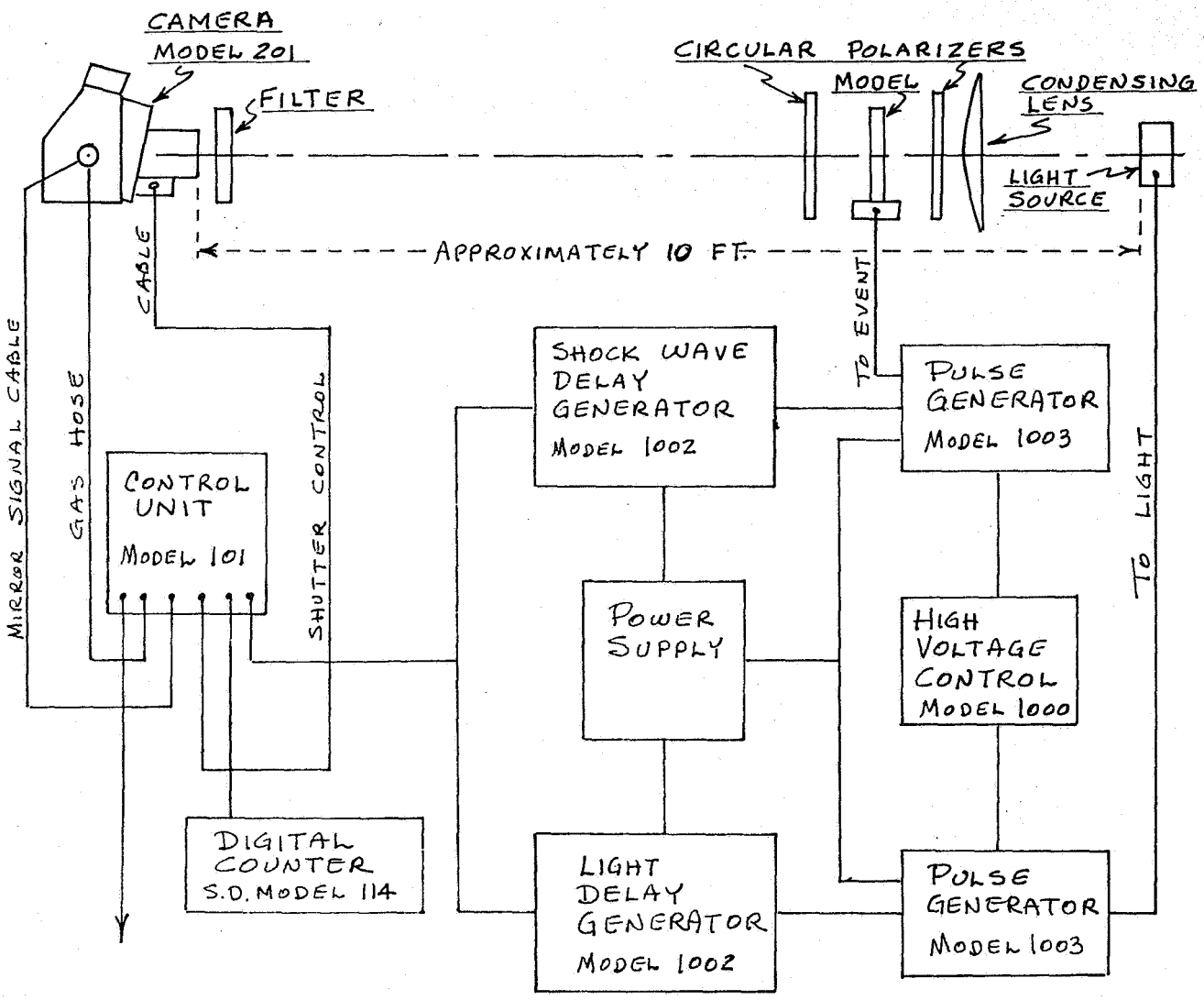

Figure 26. POLARISCOPE, CAMERA, AND CONTROLS

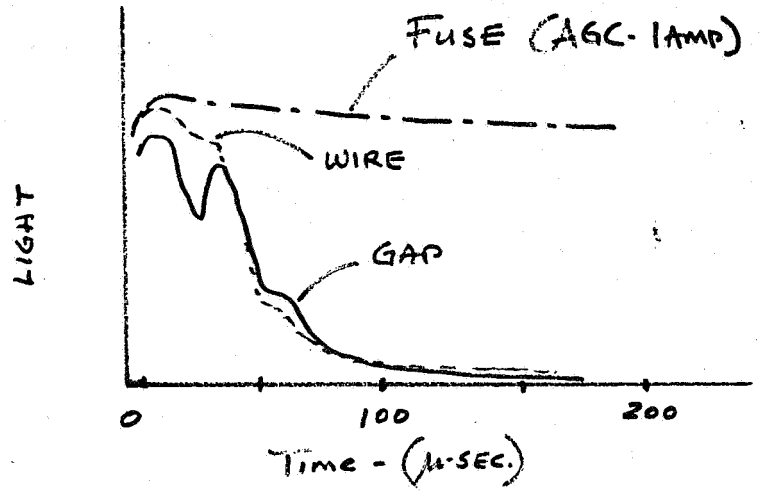

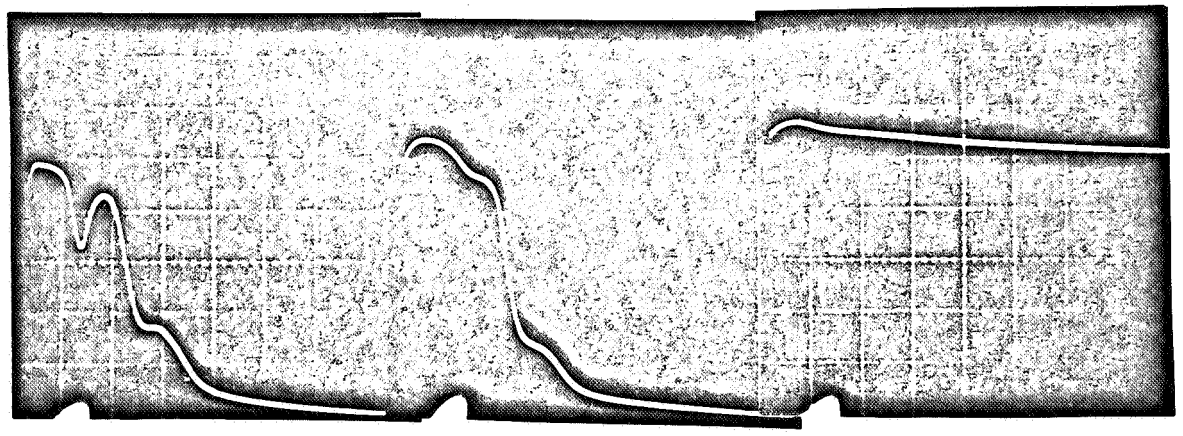

Figure 27. LIGHT CHARACTERISTICS

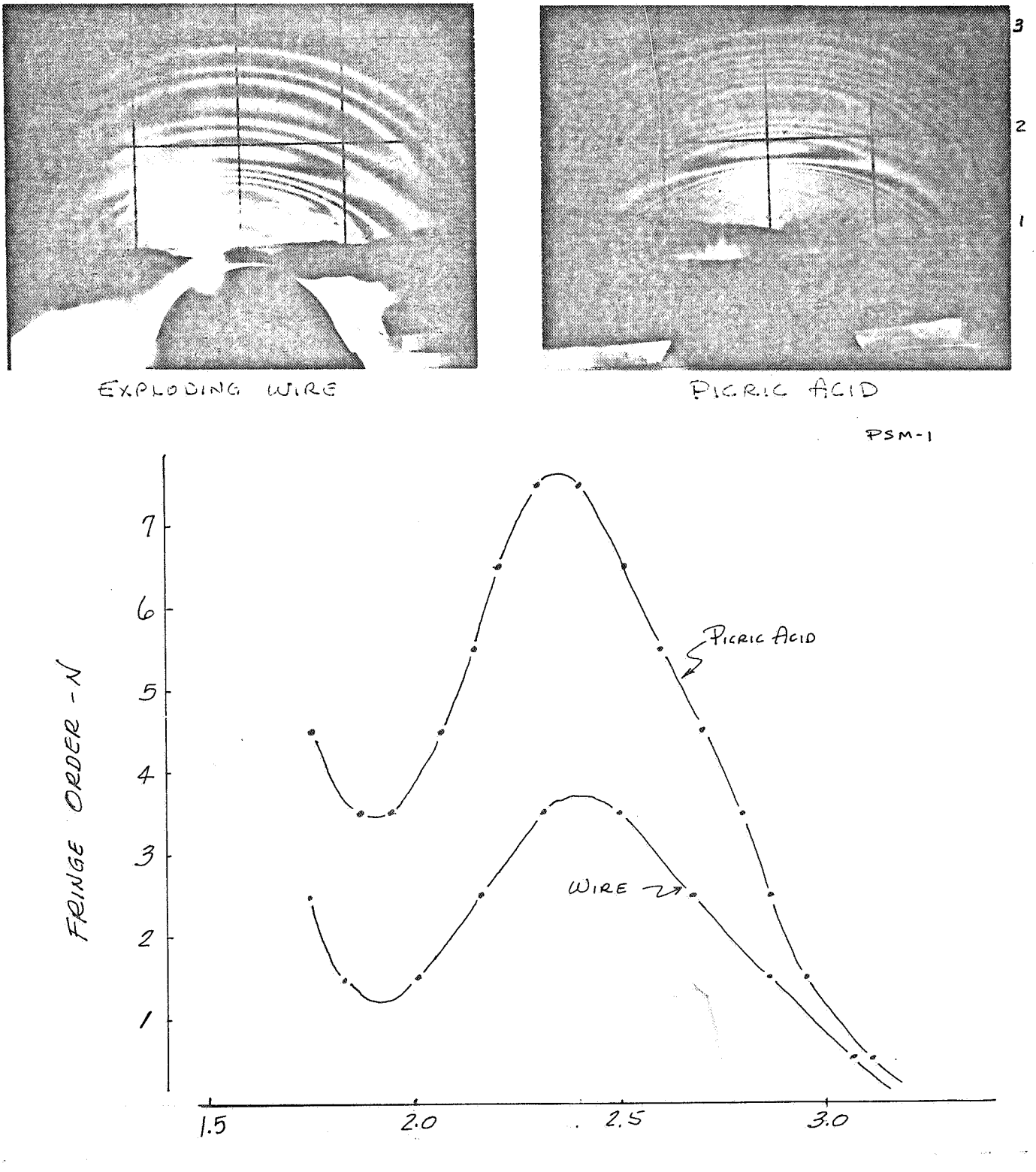

Figure 28. EFFECT OF ENERGY SOURCE UPON STRESS WAVES

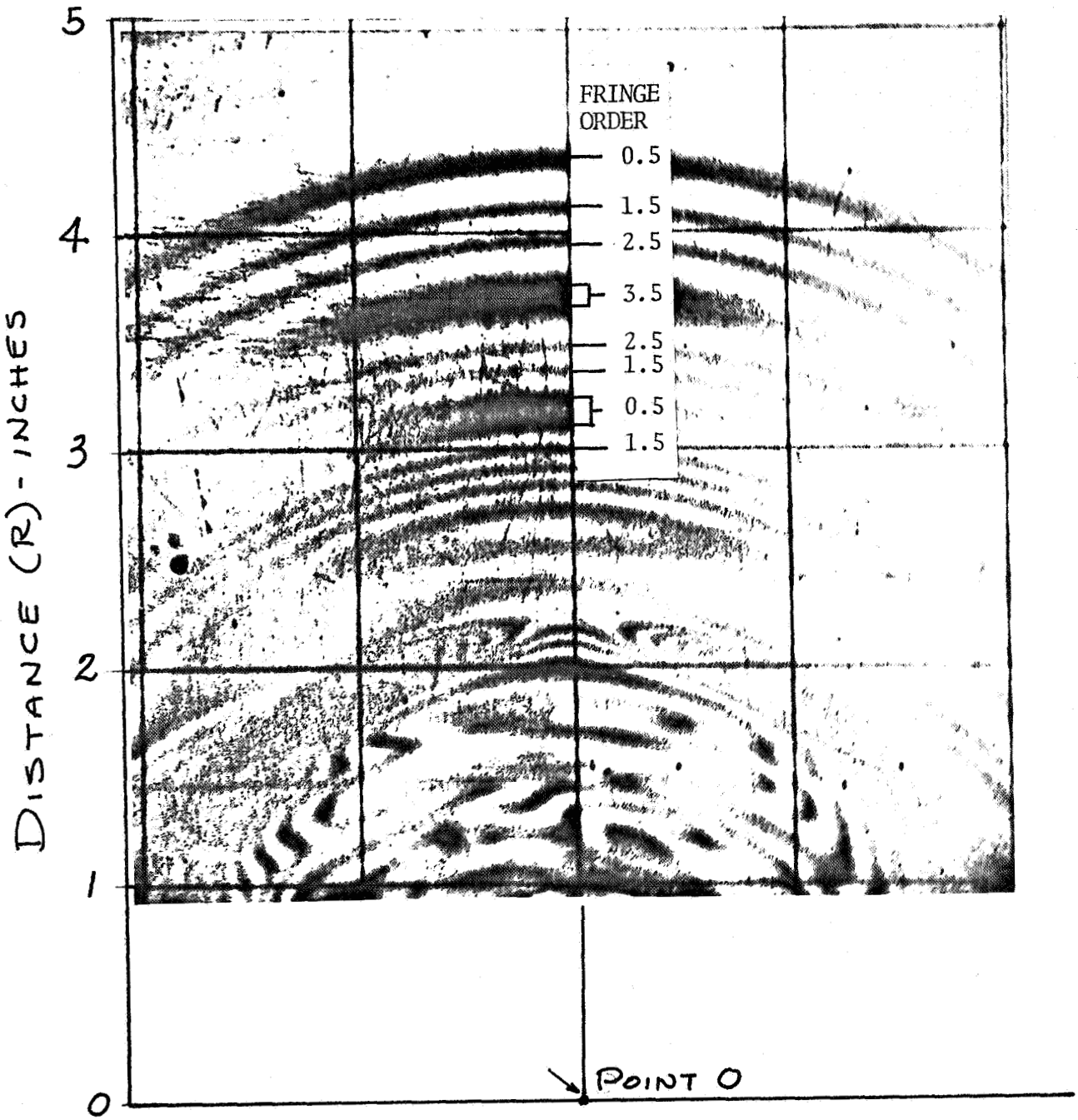

Figure 29. ILLUSTRATION OF FRINGE ORDER

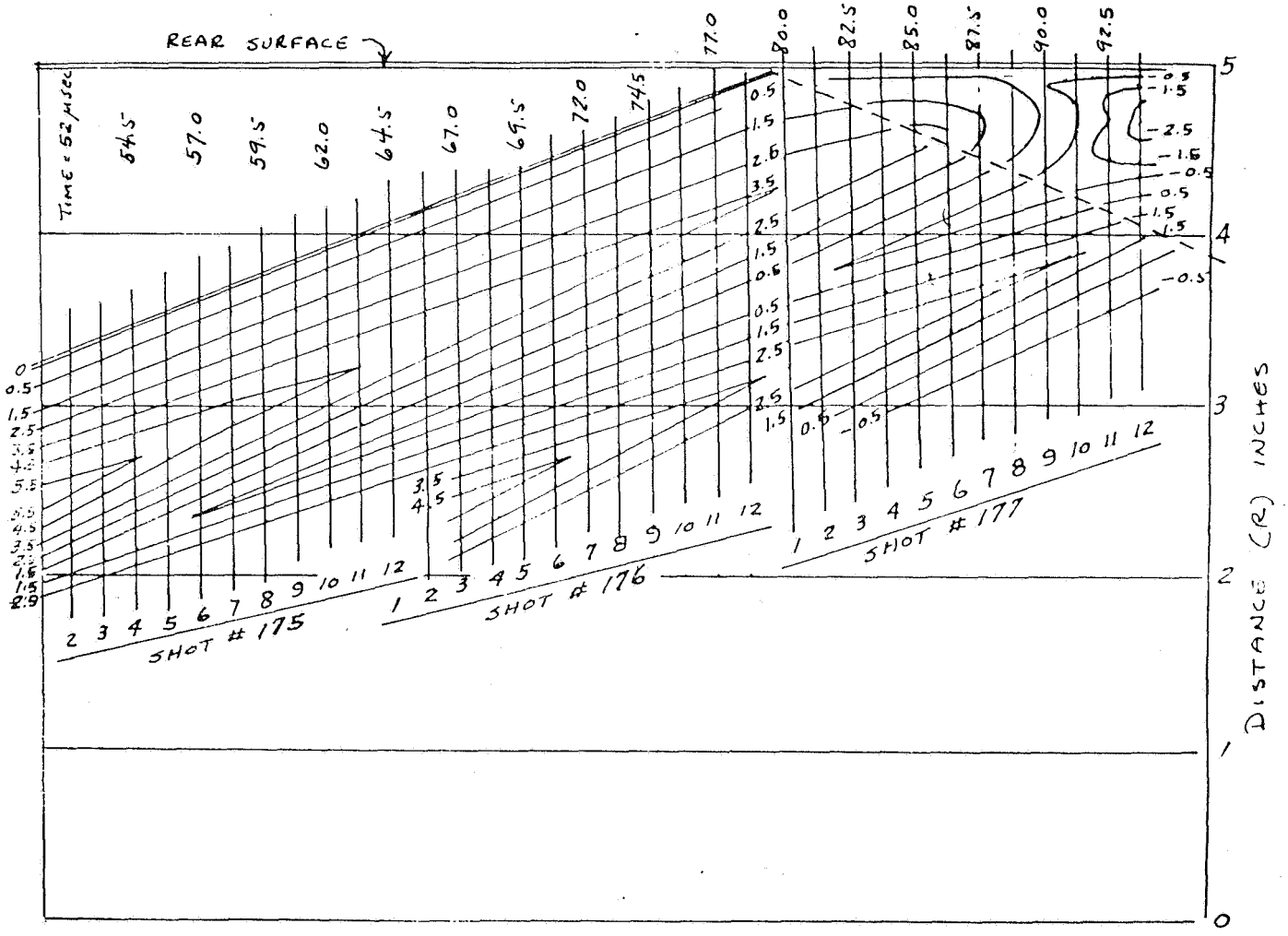

Figure 30. FRINGE LOCATIONS AT VARIOUS TIMES

Shot No. 175, Frame NO. 2

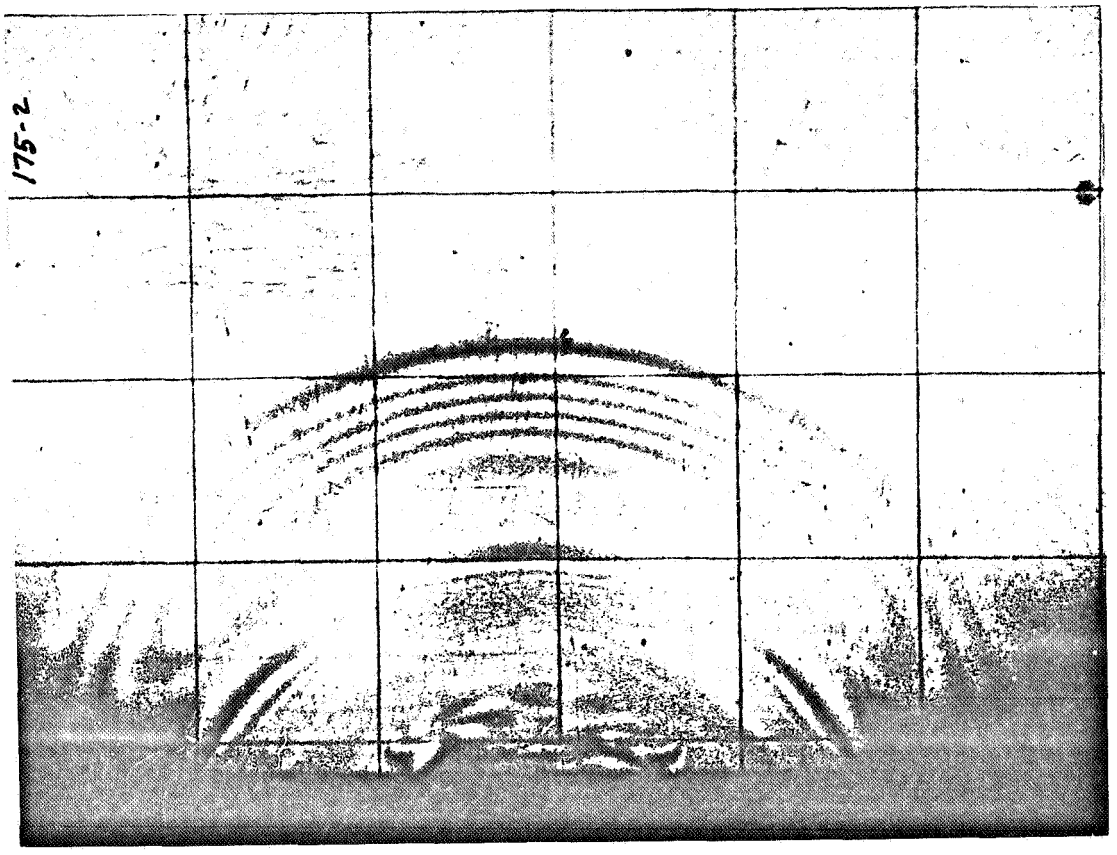

	N	R	UR	ET	ER	SIGMA R	SIGMA THETA
1	0.000	3.290	0.000	0.000	0.000	0.000	0.000
2	.500	3.200	-.124	-.038	-2.798	-3.163	-1.163
3	1.500	3.050	-.952	-.307	-8.587	-9.182	-3.182
4	2.500	2.940	-2.166	-.714	-14.514	-14.976	-4.976
5	3.500	2.830	-3.988	-1.348	-20.668	-20.406	-6.406
6	4.500	2.720	-6.417	-2.225	-27.065	-25.441	-7.441
7	5.500	2.580	-10.281	-3.688	-34.048	-29.533	-7.533
8	5.850	2.540	-11.534	-4.178	-36.470	-31.002	-7.602
9	5.500	2.480	-13.413	-4.927	-35.287	-27.536	-5.536
10	4.500	2.380	-16.173	-6.061	-30.901	-19.256	-1.256
11	3.500	2.280	-18.381	-7.006	-26.326	-11.279	2.720
12	2.500	2.200	-19.706	-7.596	-21.396	-3.876	6.123
13	1.500	2.130	-20.479	-7.952	-16.232	3.148	9.148
14	1.200	2.070	-20.926	-8.164	-14.788	5.427	10.227
15	1.500	2.020	-21.298	-8.347	-16.627	3.785	9.785

Figure 31. STRESS WAVE PHOTOGRAPHS AND COMPUTED RESULTS

Shot No. 175, Frame No. 4

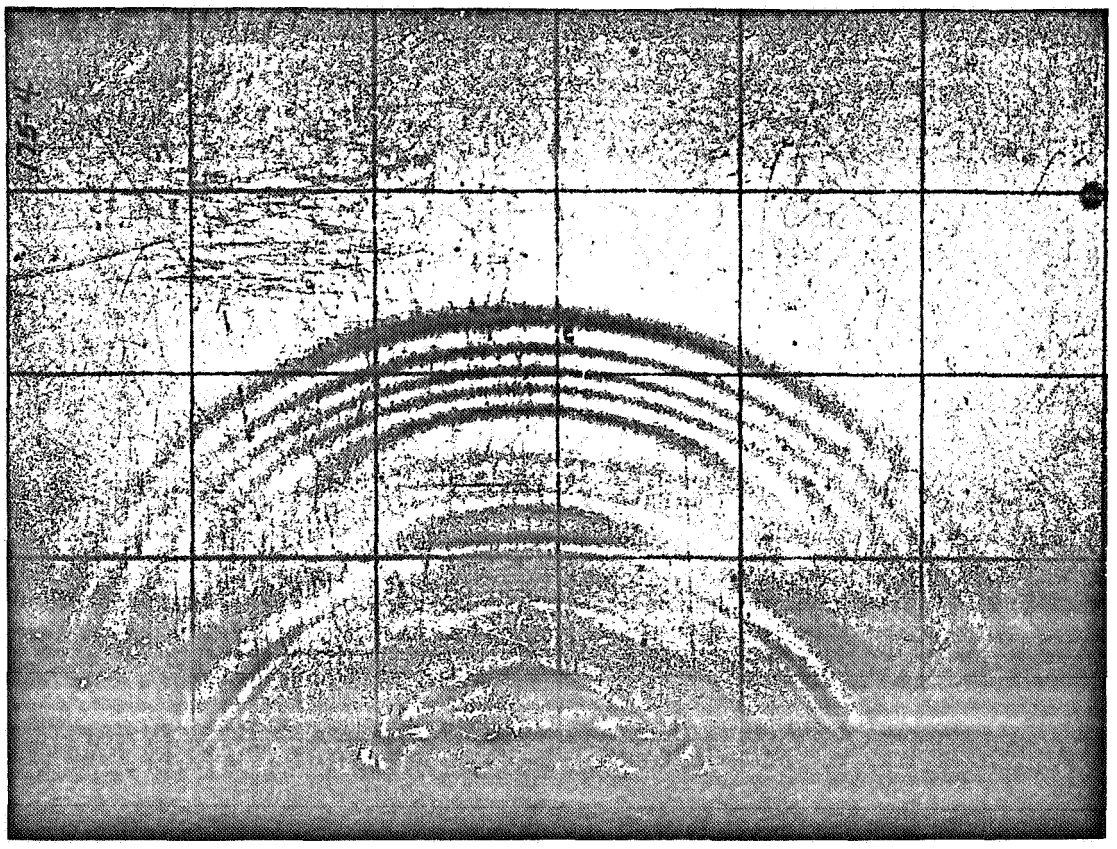

	N	R	UR	ET	ER	SIGMA R	SIGMA THETA
1	0.000	3.450	0.000	0.000	0.000	0.000	0.000
2	.500	3.360	-.124	-.036	-2.796	-3.166	-1.166
3	1.500	3.210	-.952	-.292	-8.572	-9.206	-3.206
4	2.500	3.080	-2.387	-.750	-14.550	-14.917	-4.917
5	3.500	2.950	-4.540	-1.467	-20.787	-20.213	-6.213
6	4.500	2.840	-6.969	-2.309	-27.149	-25.307	-7.307
7	5.500	2.700	-10.833	-3.708	-34.068	-29.502	-7.502
8	5.500	2.690	-11.136	-3.821	-34.181	-29.320	-7.320
9	4.500	2.580	-14.172	-4.971	-29.811	-21.013	-3.013
10	3.500	2.470	-16.601	-5.931	-25.251	-13.014	.985
11	2.500	2.390	-17.926	-6.474	-20.274	-5.685	4.314
12	1.500	2.300	-18.919	-6.896	-15.176	1.446	7.446
13	.800	2.210	-19.491	-7.148	-11.564	6.368	9.568
14	1.500	2.160	-19.808	-7.294	-15.574	2.087	8.087

Figure 31. CONTINUED

Shot No. 175, Frame No. 6

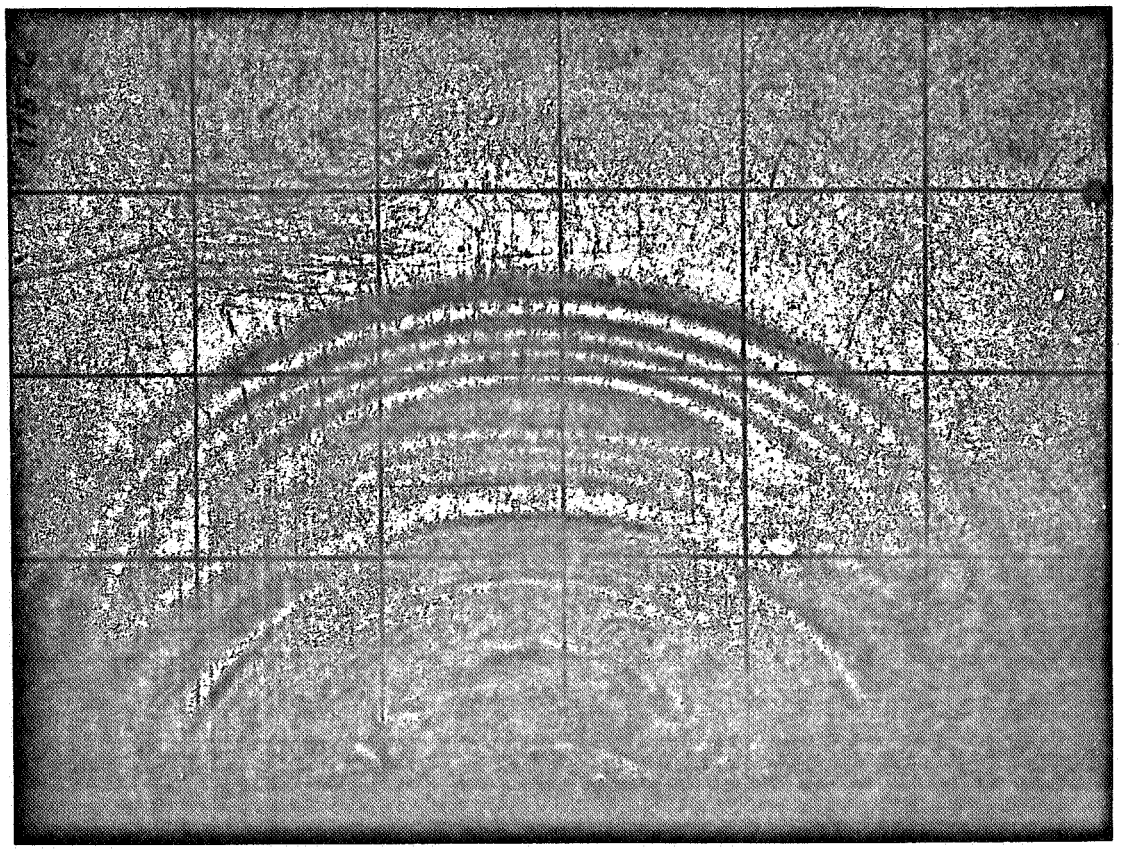

	N	R	UR	ET	ER	SIGMA R	SIGMA THETA
1	0.000	3.590	0.000	0.000	0.000	0.000	0.000
2	.500	3.510	-.110	-.031	-2.791	-3.175	-1.175
3	1.500	3.360	-.938	-.275	-8.555	-9.233	-3.233
4	2.500	3.220	-2.484	-.747	-14.547	-14.922	-4.922
5	3.500	3.090	-4.636	-1.432	-20.752	-20.269	-6.269
6	4.500	2.980	-7.065	-2.235	-27.075	-25.427	-7.427
7	5.150	2.880	-9.729	-3.145	-31.573	-28.152	-7.552
8	4.500	2.790	-12.126	-3.990	-28.830	-22.596	-4.596
9	3.500	2.670	-14.775	-4.958	-24.278	-14.582	-.582
10	2.500	2.570	-16.431	-5.588	-19.388	-7.114	2.885
11	1.500	2.470	-17.535	-6.024	-14.304	.040	6.040
12	.700	2.370	-18.142	-6.274	-10.138	5.603	8.403
13	1.500	2.290	-18.628	-6.483	-14.763	.780	6.780

Figure 31. CONTINUED

Shot No. 175, Frame No. 8

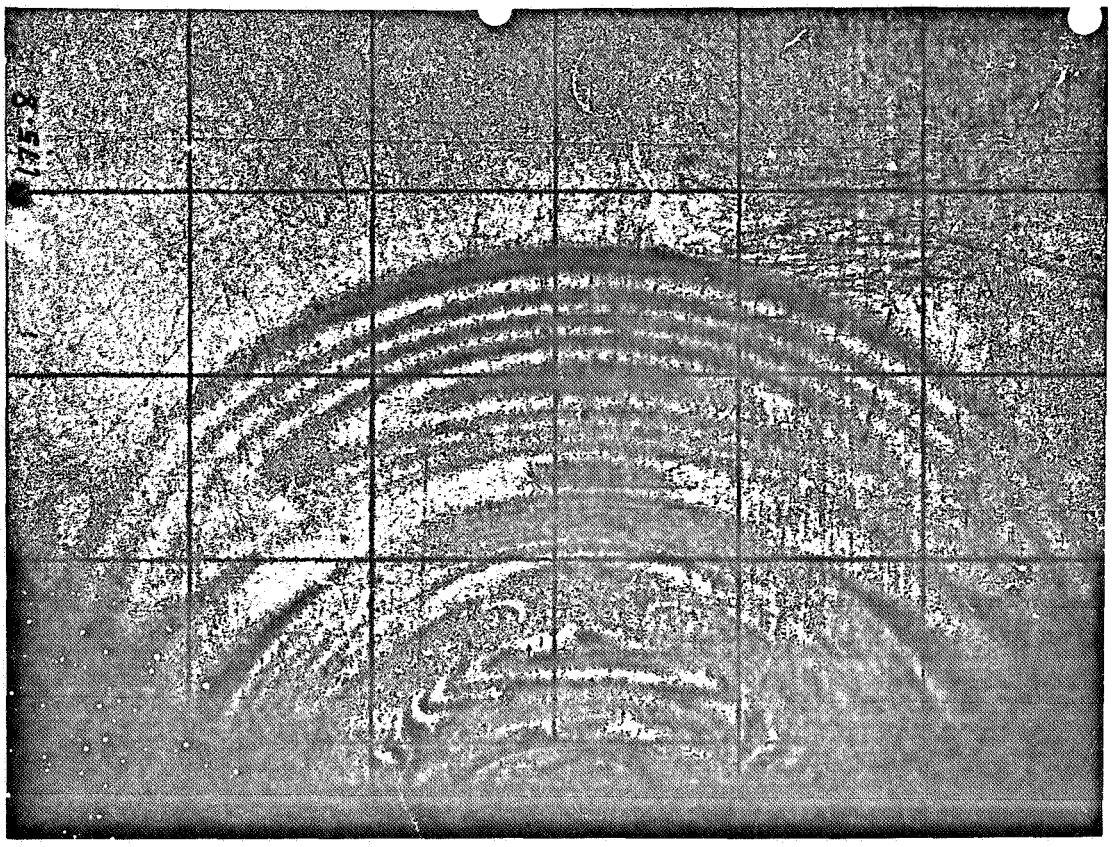

N	R	UR	ET	ER	SIGMA R	SIGMA THETA
1	0.000	3.750	0.000	0.000	0.000	0.000	0.000
2	.500	3.670	-.110	-.030	-2.790	-3.177	-1.177
3	1.500	3.510	-.993	-.278	-8.558	-9.227	-3.227
4	2.500	3.370	-2.539	-.730	-14.530	-14.950	-4.950
5	3.500	3.230	-4.857	-1.436	-20.756	-20.264	-6.264
6	4.500	3.090	-7.948	-2.417	-27.257	-25.133	-7.133
7	4.850	3.030	-9.497	-2.923	-29.695	-26.574	-7.174
8	4.500	2.980	-10.787	-3.353	-28.193	-23.624	-5.624
9	3.500	2.840	-13.878	-4.412	-23.732	-15.463	-1.463
10	2.500	2.750	-15.369	-4.944	-18.744	-8.153	1.846
11	1.500	2.640	-16.583	-5.393	-13.673	-.978	5.021
12	.500	2.550	-17.080	-5.582	-8.342	5.779	7.779
13	.500	2.510	-17.190	-5.626	-8.386	5.849	7.849

Figure 31. CONTINUED

Shot No. 175, Frame No. 10

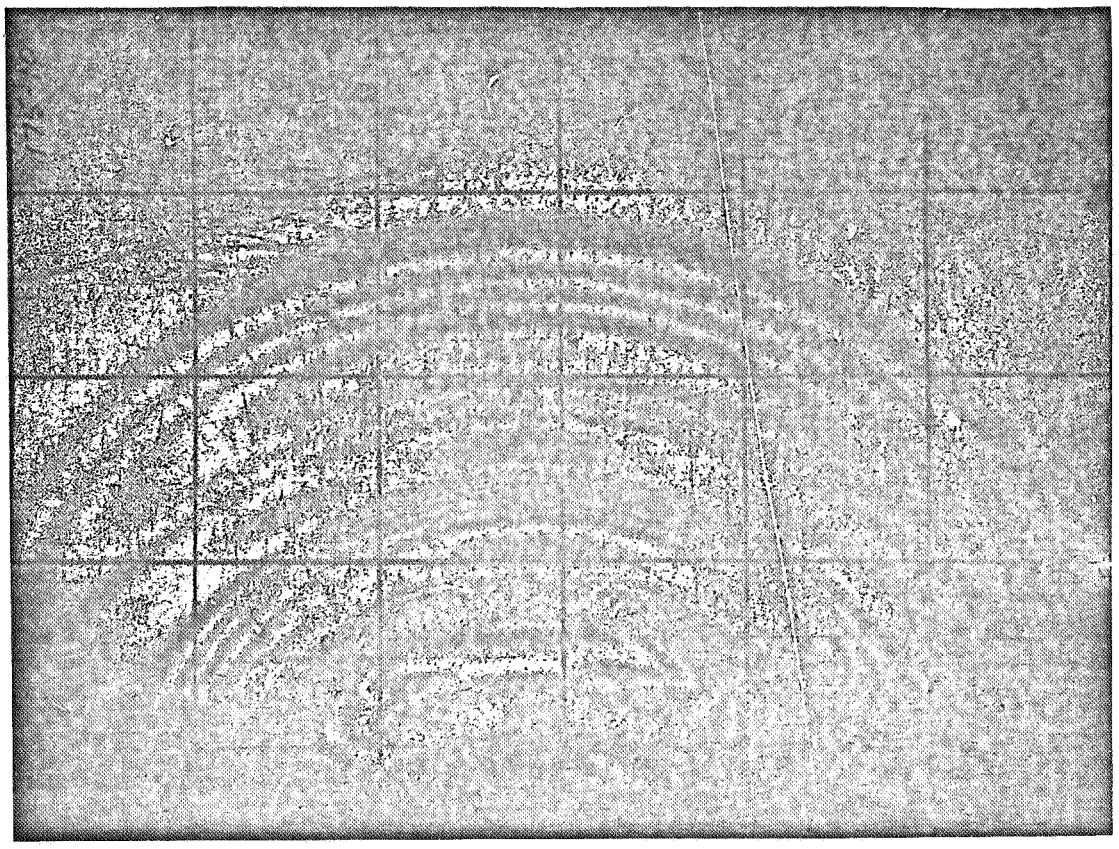

	N	R	UR	ET	ER	SIGMA R	SIGMA THETA
1	0.000	3.880	0.000	0.000	0.000	0.000	0.000
2	.500	3.810	-.096	-.025	-2.785	-3.184	-1.184
3	1.500	3.660	-.924	-.249	-8.529	-9.275	-3.275
4	2.500	3.510	-2.580	-.713	-14.513	-14.977	-4.977
5	3.500	3.360	-5.064	-1.440	-20.760	-20.258	-6.258
6	4.500	3.190	-8.818	-2.590	-27.430	-24.853	-6.853
7	4.650	3.170	-9.323	-2.749	-28.417	-25.565	-6.965
8	4.500	3.150	-9.828	-2.909	-27.749	-24.339	-6.339
9	3.500	3.010	-12.919	-3.910	-23.230	-16.273	-2.273
10	2.500	2.920	-14.409	-4.412	-18.212	-9.012	.987
11	1.500	2.810	-15.624	-4.834	-13.114	-1.880	4.119
12	.500	2.700	-16.231	-5.052	-7.812	4.923	6.923
13	.350	2.670	-16.301	-5.078	-7.010	5.933	7.333
14	.500	2.650	-16.348	-5.096	-7.856	4.993	6.993

Figure 31. CONTINUED

Shot No. 175, Frame No. 12

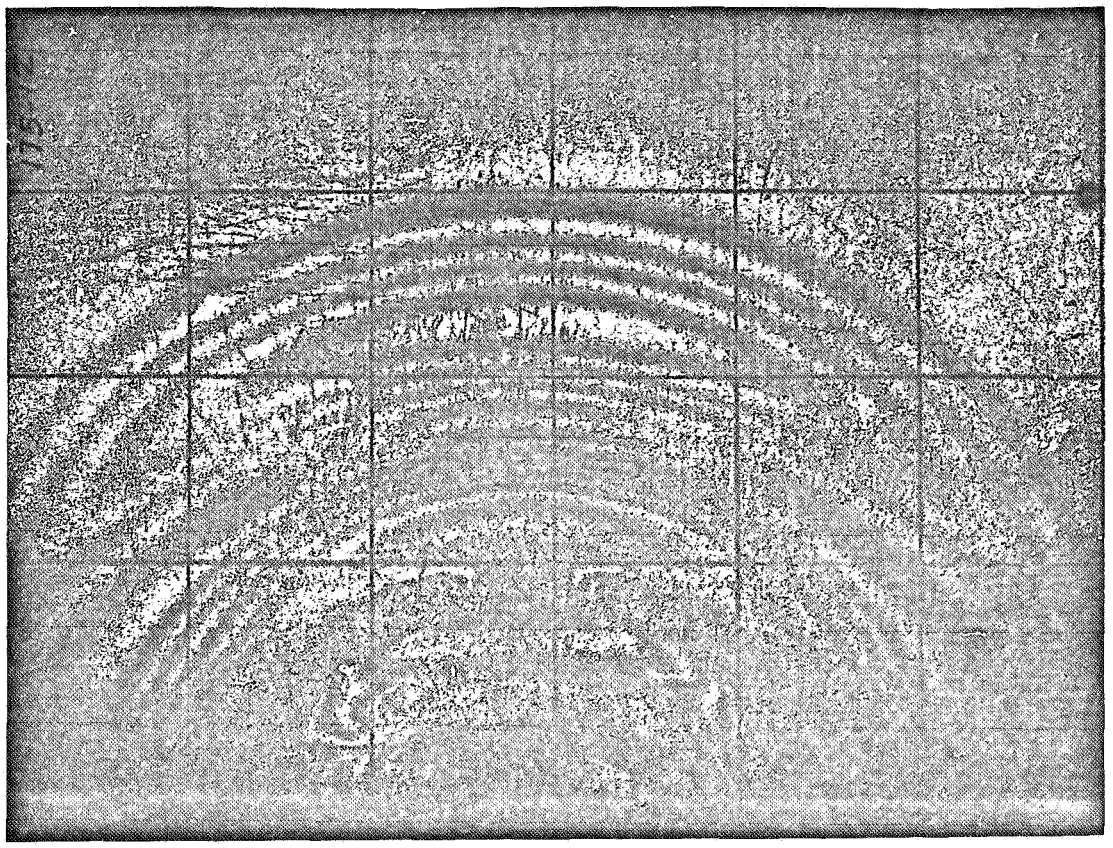

	N	R	UR	ET	ER	SIGMA R	SIGMA THETA
1	0.000	4.040	0.000	0.000	0.000	0.000	0.000
2	.500	3.970	-.096	-.024	-2.784	-3.186	-1.186
3	1.500	3.810	-.979	-.253	-8.533	-9.268	-3.268
4	2.500	3.660	-2.635	-.699	-14.499	-15.000	-5.000
5	3.500	3.500	-5.285	-1.442	-20.762	-20.253	-6.253
6	4.400	3.360	-8.337	-2.335	-26.623	-24.620	-7.020
7	3.500	3.200	-11.826	-3.396	-22.716	-17.102	-3.102
8	2.500	3.090	-13.648	-3.974	-17.774	-9.719	.280
9	1.500	2.980	-14.862	-4.372	-12.652	-2.624	3.375
10	.500	2.870	-15.469	-4.578	-7.338	4.158	6.158
11	.200	2.830	-15.547	-4.605	-5.709	6.137	6.937
12	.500	2.780	-15.643	-4.639	-7.399	4.258	6.258

Figure 31. CONTINUED

Shot No. 176, Frame No. 3

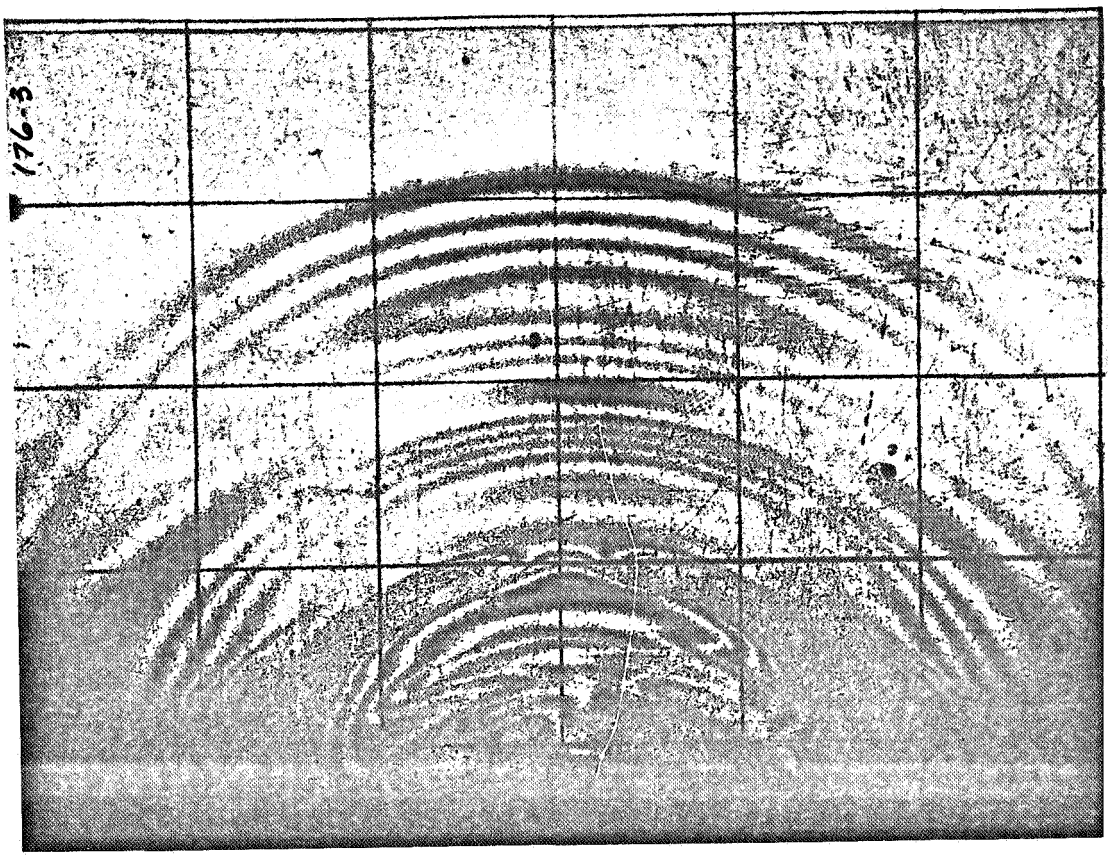

	N	R	UR	ET	ER	SIGMA R	SIGMA THETA
1	0.000	4.200	0.000	0.000	0.000	0.000	0.000
2	.500	4.130	-.096	-.023	-2.783	-3.188	-1.188
3	1.500	3.970	-.979	-.243	-8.523	-9.284	-3.284
4	2.500	3.800	-2.856	-.729	-14.529	-14.952	-4.952
5	3.500	3.640	-5.506	-1.444	-20.764	-20.250	-6.250
6	4.250	3.500	-8.500	-2.285	-25.745	-23.732	-6.732
7	3.500	3.390	-10.853	-2.967	-22.287	-17.794	-3.794
8	2.500	3.280	-12.675	-3.512	-17.312	-10.463	-.463
9	1.500	3.140	-14.220	-3.991	-12.271	-3.239	2.760
10	.500	3.020	-14.883	-4.204	-6.964	3.555	5.555
11	.200	2.970	-14.979	-4.236	-5.340	5.543	6.343
12	.500	2.920	-15.076	-4.269	-7.029	3.660	5.660

Figure 31. *CONTINUED*

Shot No. 176, Frame No. 5

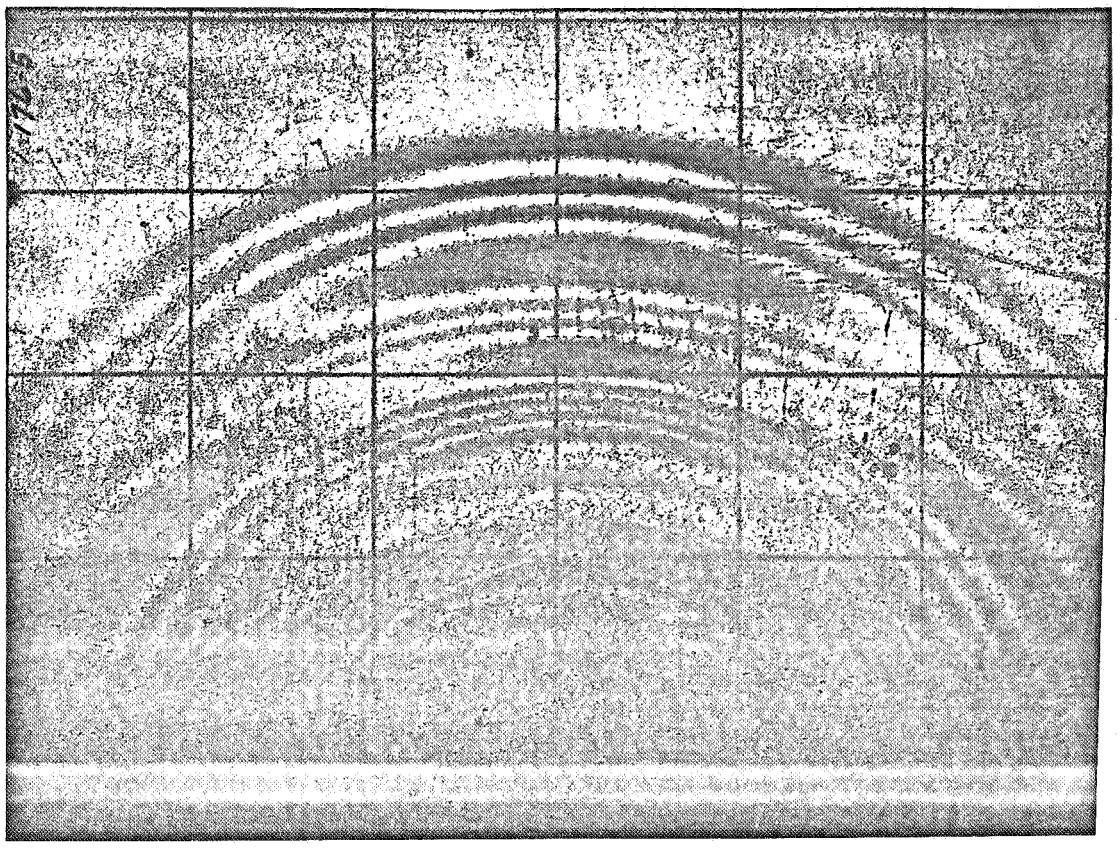

	N	R	UR	ET	ER	SIGMA R	SIGMA THETA
1	0.000	4.350	0.000	0.000	0.000	0.000	0.000
2	.500	4.280	-.096	-.022	-2.782	-3.189	-1.189
3	1.500	4.120	-.979	-.234	-8.514	-9.298	-3.298
4	2.500	3.940	-2.967	-.731	-14.531	-14.949	-4.949
5	3.500	3.770	-5.782	-1.464	-20.784	-20.218	-6.218
6	4.050	3.670	-7.866	-2.025	-24.381	-22.862	-6.662
7	3.500	3.560	-10.158	-2.658	-21.978	-18.292	-4.292
8	2.500	3.420	-12.476	-3.321	-17.121	-10.772	-.772
9	1.500	3.300	-13.801	-3.713	-11.993	-3.687	2.312
10	.500	3.170	-14.518	-3.933	-6.693	3.118	5.118
11	.100	3.120	-14.601	-3.959	-4.511	5.741	6.141
12	.500	3.070	-14.684	-3.986	-6.746	3.203	5.203

Figure 31. CONTINUED

Shot No. 176, Frame No. 7

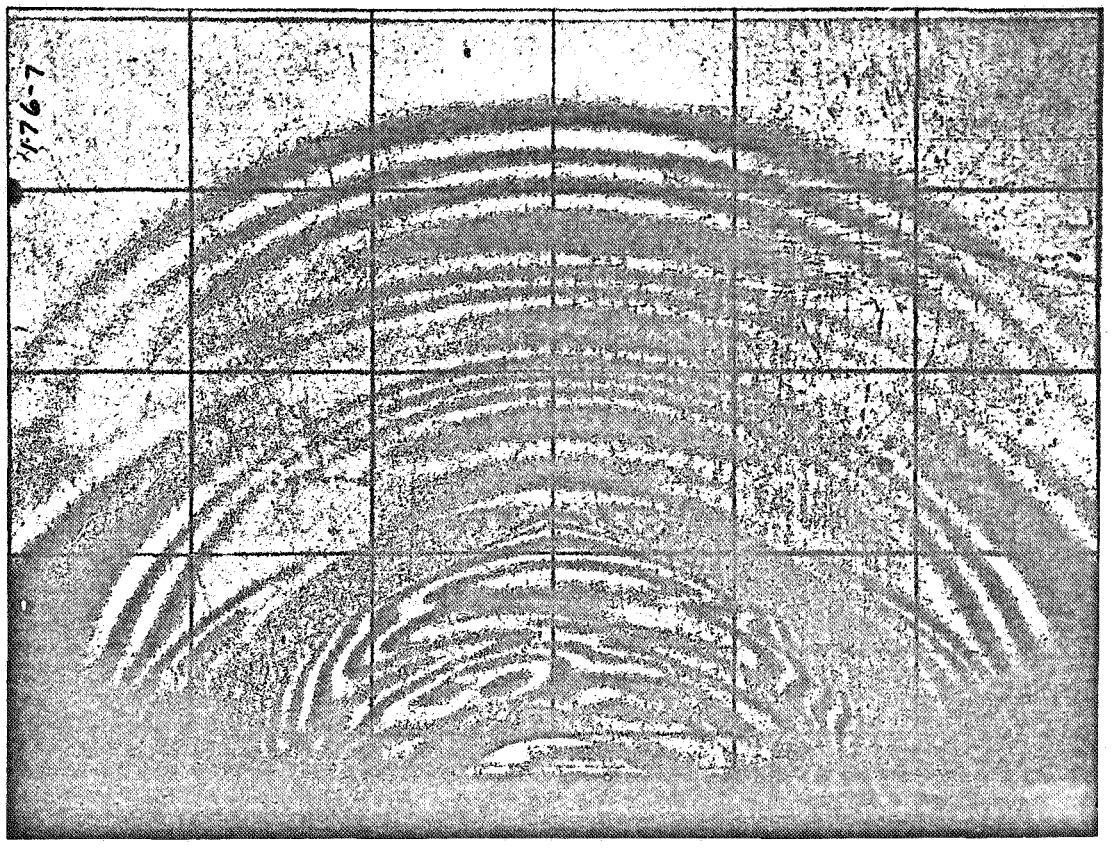

	N	R	UR	ET	ER	SIGMA R	SIGMA THETA
1	0.000	4.520	0.000	0.000	0.000	0.000	0.000
2	.500	4.440	-.110	-.024	-2.784	-3.185	-1.185
3	1.500	4.260	-1.104	-.255	-8.535	-9.264	-3.264
4	2.500	4.080	-3.091	-.735	-14.535	-14.943	-4.943
5	3.500	3.910	-5.906	-1.442	-20.762	-20.253	-6.253
6	3.900	3.830	-7.540	-1.865	-23.393	-22.153	-6.553
7	3.500	3.740	-9.378	-2.350	-21.670	-18.789	-4.789
8	2.500	3.610	-11.531	-2.934	-16.734	-11.395	-1.395
9	1.500	3.470	-13.076	-3.369	-11.649	-4.243	1.756
10	.500	3.350	-13.739	-3.561	-6.321	2.519	4.519
11	0.000	3.280	-13.835	-3.590	-3.590	5.791	5.791
12	.500	3.210	-13.932	-3.620	-6.380	2.614	4.614

Figure 31. CONTINUED

Shot No. 176, Frame No. 9

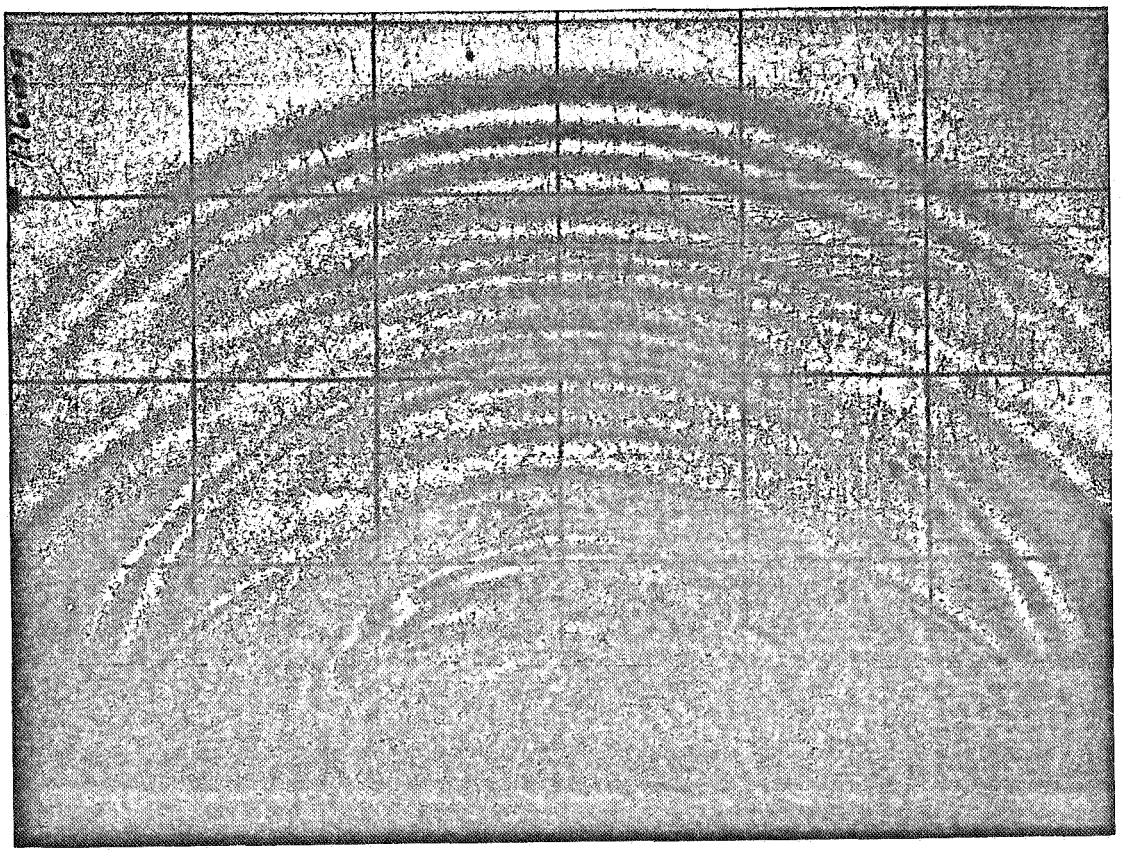

	N	R	UR	ET	ER	SIGMA R	SIGMA THETA
1	0.000	4.670	0.000	0.000	0.000	0.000	0.000
2	.500	4.590	-.110	-.024	-2.784	-3.187	-1.187
3	1.500	4.420	-1.048	-.234	-8.514	-9.299	-3.299
4	2.500	4.220	-3.256	-.748	-14.548	-14.921	-4.921
5	3.500	4.050	-6.072	-1.432	-20.752	-20.270	-6.270
6	3.700	4.000	-7.065	-1.679	-22.103	-21.162	-6.362
7	3.500	3.930	-8.456	-2.029	-21.349	-19.306	-5.306
8	2.500	3.770	-11.106	-2.715	-16.515	-11.748	-1.748
9	1.500	3.620	-12.762	-3.162	-11.442	-4.577	1.422
10	.500	3.520	-13.314	-3.315	-6.075	2.121	4.121
11	-.050	3.430	-13.426	-3.347	-3.071	5.721	5.521
12	.500	3.350	-13.525	-3.377	-6.137	2.221	4.221

Figure 31. CONTINUED

Shot No. 176, Frame No. 11

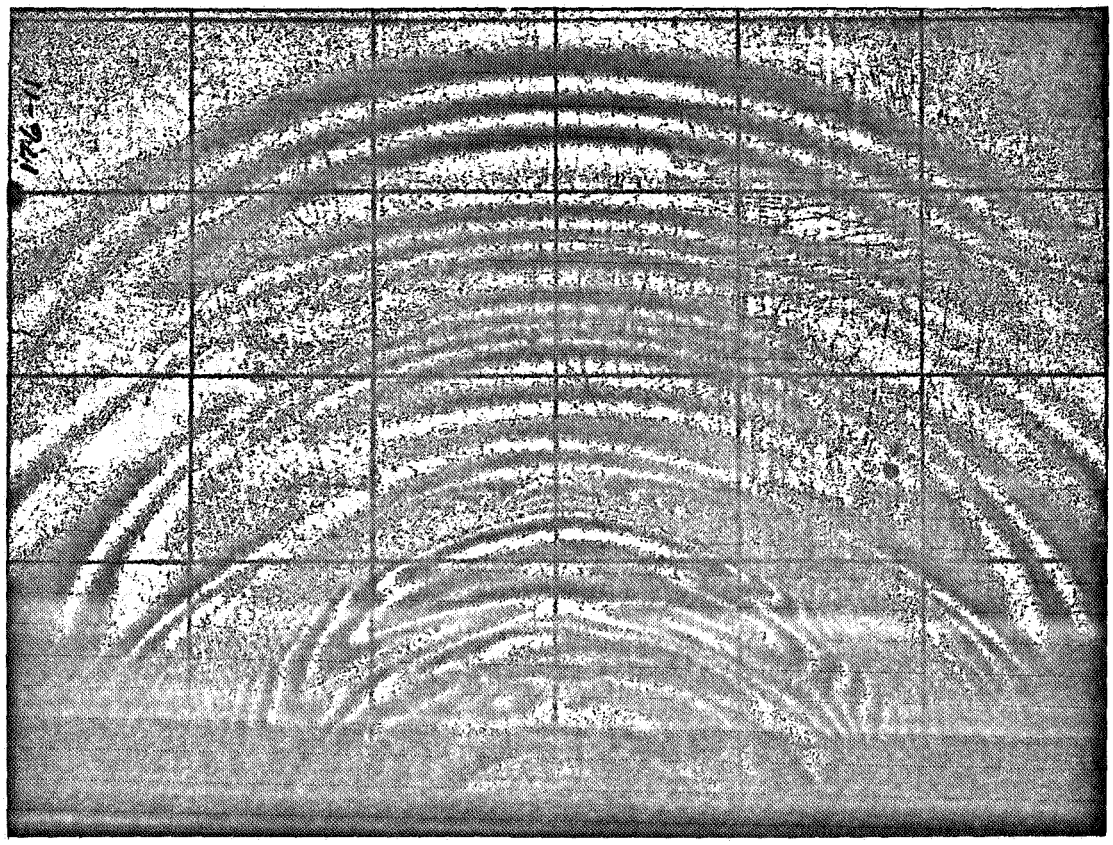

N	R	UR	ET	ER	SIGMA R	SIGMA THETA
1	0.000	4.830	0.000	0.000	0.000	0.000	0.000
2	.500	4.740	-.124	-.026	-2.786	-3.183	-1.183
3	1.500	4.560	-1.117	-.242	-8.522	-9.287	-3.287
4	2.500	4.370	-3.215	-.714	-14.514	-14.976	-4.976
5	3.500	4.190	-6.196	-1.413	-20.733	-20.300	-6.300
6	3.550	4.160	-6.779	-1.553	-21.149	-20.397	-6.197
7	3.500	4.120	-7.558	-1.741	-21.061	-19.771	-5.771
8	2.500	3.950	-10.373	-2.437	-16.237	-12.198	-2.198
9	1.500	3.800	-12.029	-2.862	-11.142	-5.060	.939
10	.500	3.670	-12.747	-3.053	-5.813	1.698	3.698
11	-.100	3.570	-12.857	-3.082	-2.530	5.617	5.217
12	.500	3.470	-12.967	-3.114	-5.874	1.798	3.798

ELAPSED TIME FOR JOB WAS 0009 MIN 14 SEC/ DATE 08-12-68

Figure 31. CONTINUED

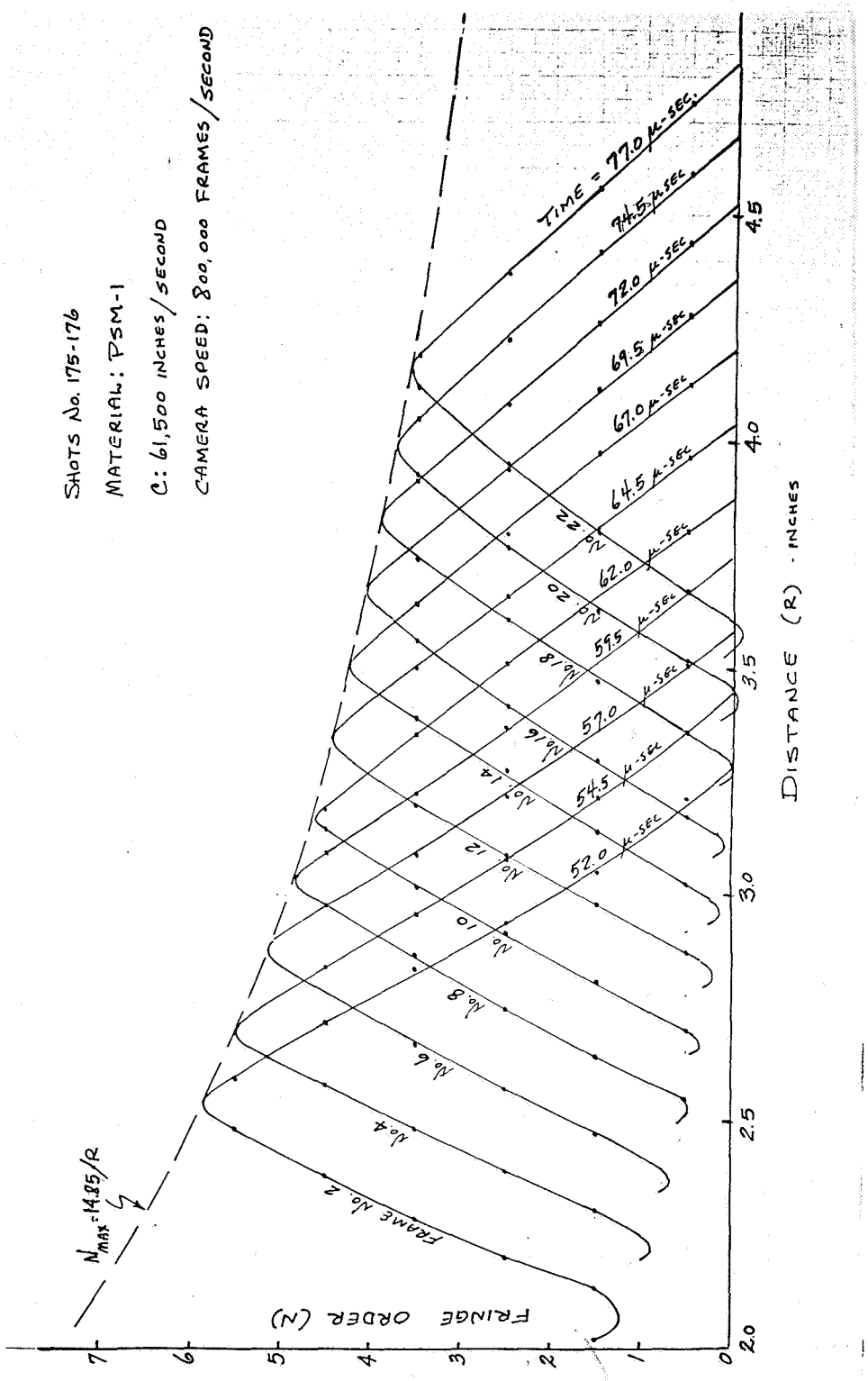

Figure 32. FRINGE NUMBER-DISTANCE-TIME RELATIONS

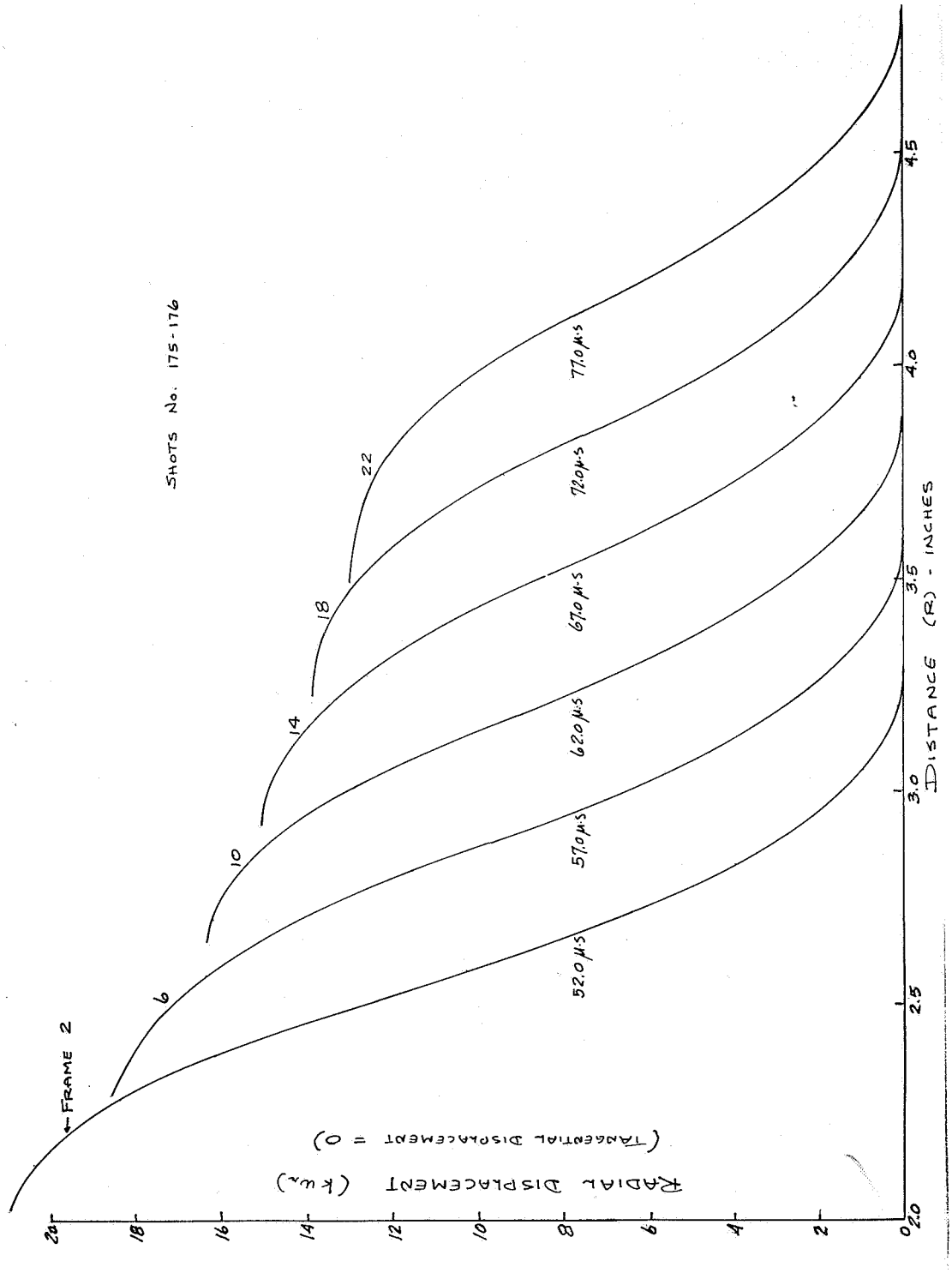

Figure 33. DISPLACEMENT-DISTANCE-TIME RELATIONS

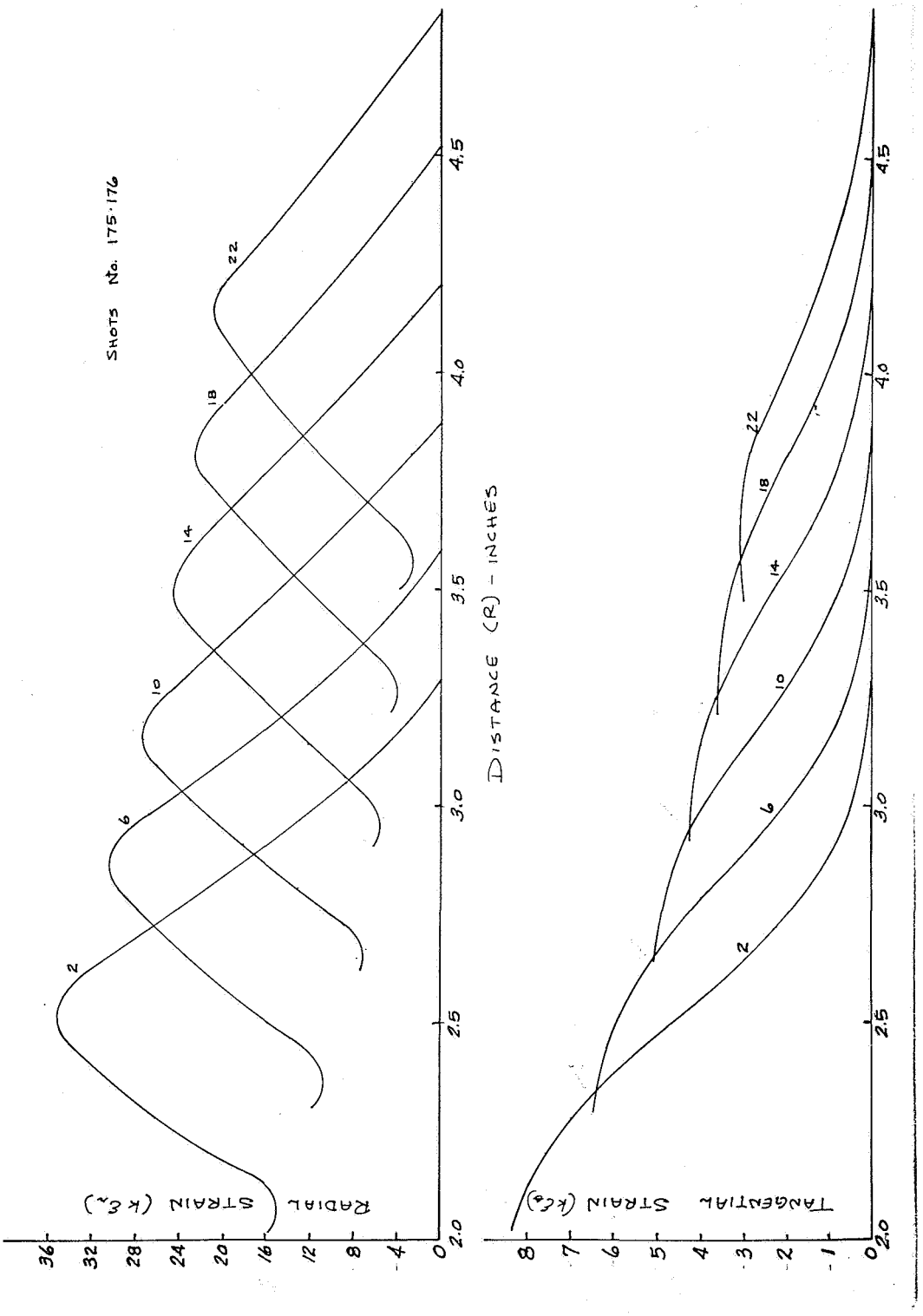

Figure 34. STRAIN-DISTANCE-TIME RELATIONS

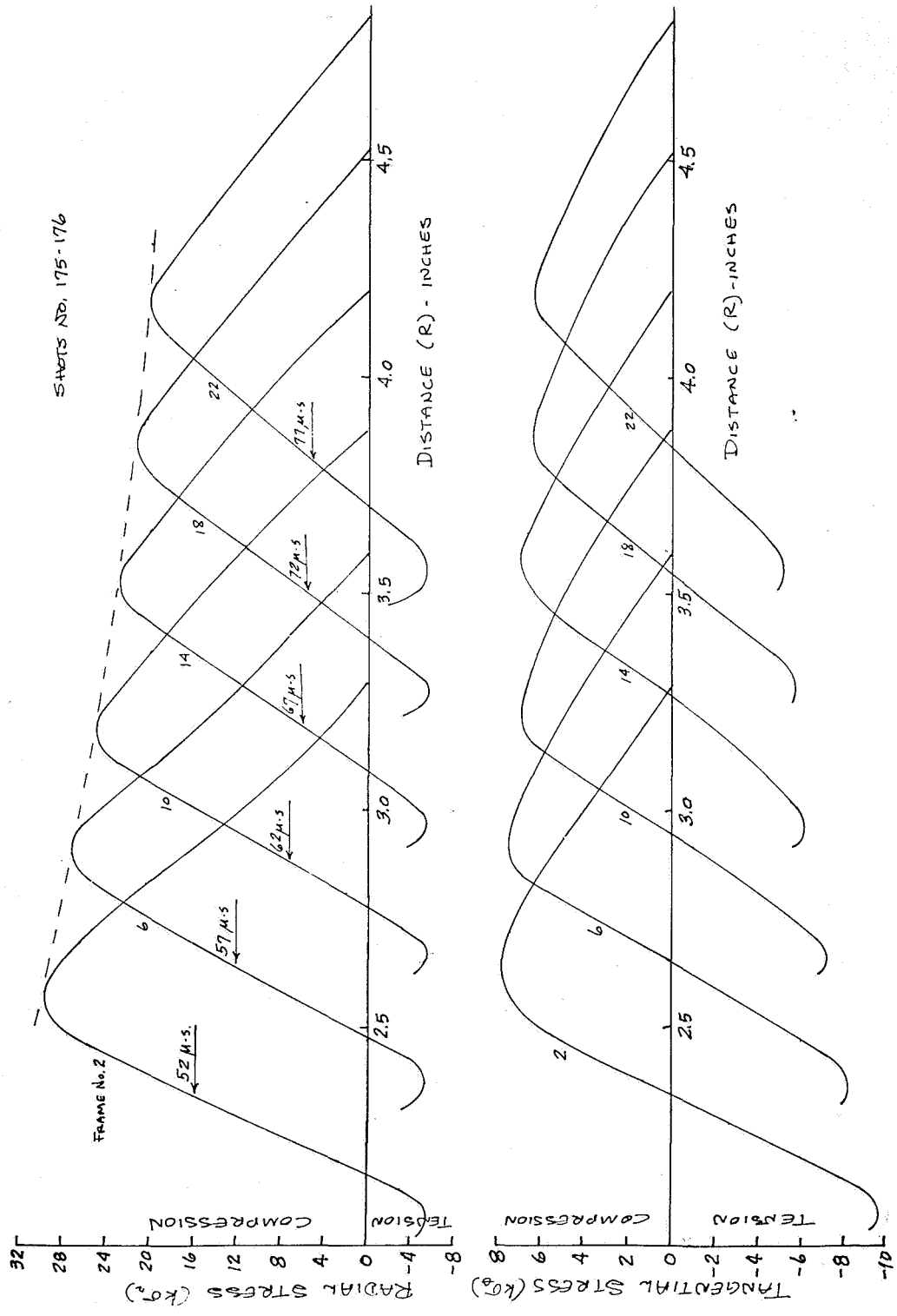

Figure 35. STRESS-DISTANCE-TIME RELATIONS

Shot No. 177, Frame No. 2

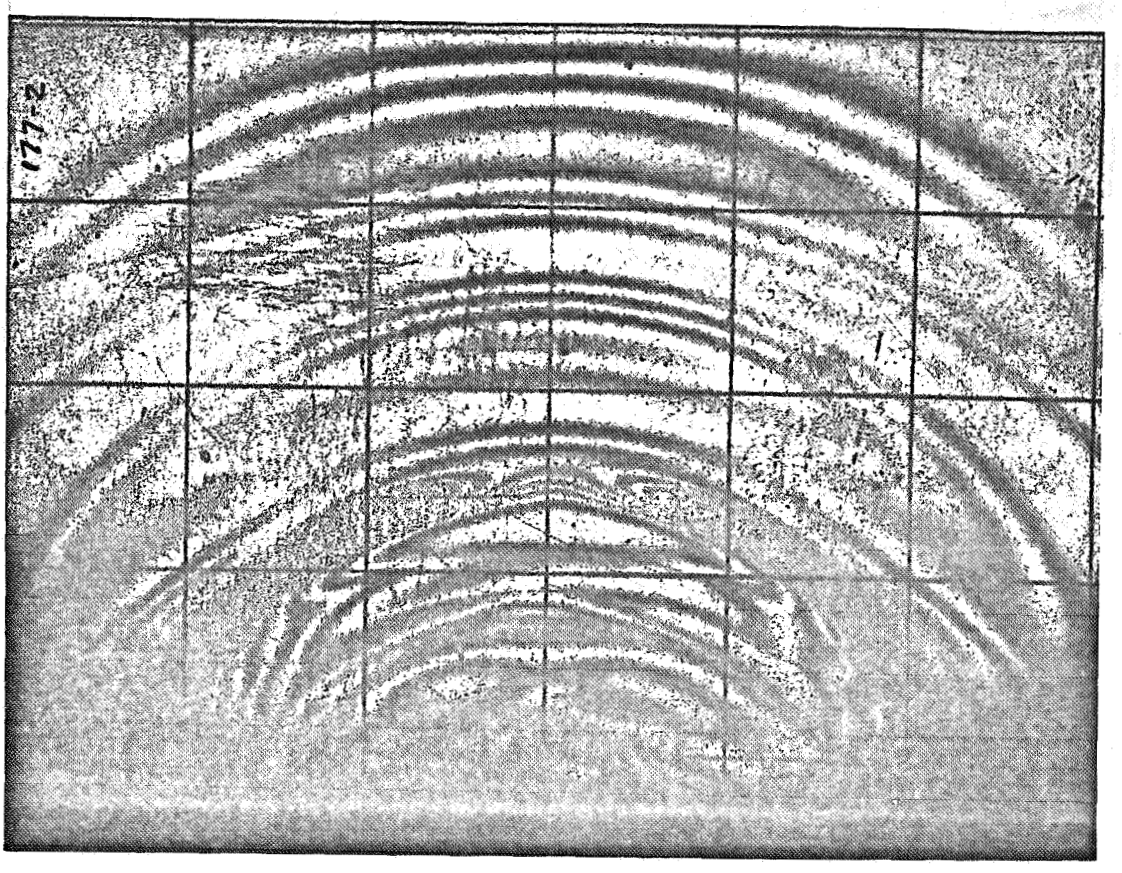

	N	R	UR	ET	ER	SIGMA R	SIGMA THETA
1	0.000	5.000	0.000	0.000	0.000	0.000	0.000
2	.500	4.930	-.096	-.019	-2.779	-3.194	-1.194
3	1.500	4.730	-1.200	-.250	-8.530	-9.273	-3.273
4	2.500	4.530	-3.408	-.730	-14.530	-14.951	-4.951
5	3.000	4.360	-5.989	-1.312	-17.872	-17.238	-5.238
6	2.500	4.210	-8.266	-1.842	-15.642	-13.156	-3.156
7	1.500	4.030	-10.253	-2.322	-10.602	-5.931	.068
8	.500	3.890	-11.026	-2.516	-5.276	.832	2.832
9	.200	3.750	-11.296	-2.586	-3.690	2.881	3.681

Figure 36. REFLECTED STRESS WAVE PHOTOGRAPHS AND COMPUTED RESULTS

Shot No. 177, Frame No. 4

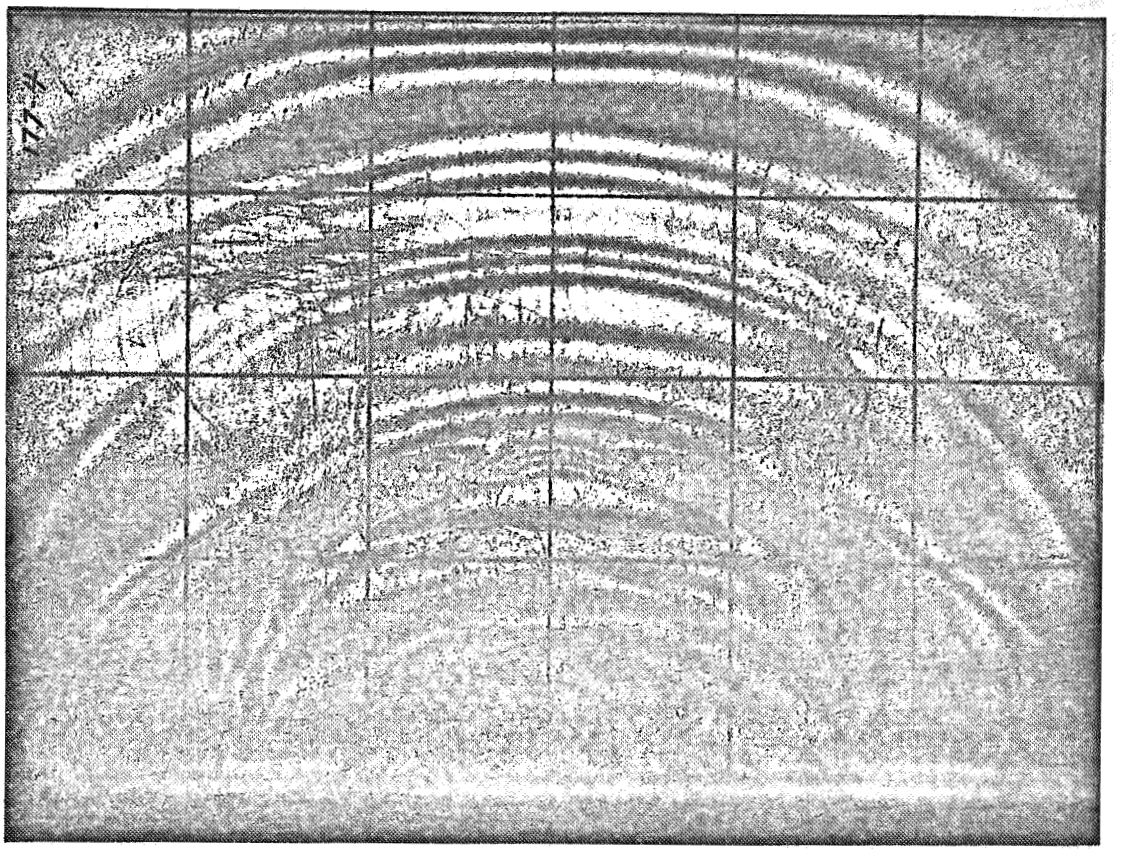

	N	R	UR	ET	ER	SIGMA R	SIGMA THETA
1	0.000	5.000	0.000	0.000	0.000	0.000	0.000
2	.500	4.930	-.096	-.019	-2.779	-3.194	-1.194
3	1.500	4.790	-.869	-.179	-8.459	-9.387	-3.387
4	2.500	4.610	-2.856	-.604	-14.404	-15.153	-5.153
5	2.750	4.500	-4.450	-.954	-16.134	-16.201	-5.201
6	2.500	4.390	-6.044	-1.313	-15.113	-14.010	-4.010
7	1.500	4.230	-7.810	-1.721	-10.001	-6.900	-.900
8	.500	4.070	-8.694	-1.932	-4.692	-.109	1.890
9	-.250	3.920	-8.797	-1.956	-.576	4.768	3.768

Figure 36. CONTINUED

Shot No. 177, Frame No. 6

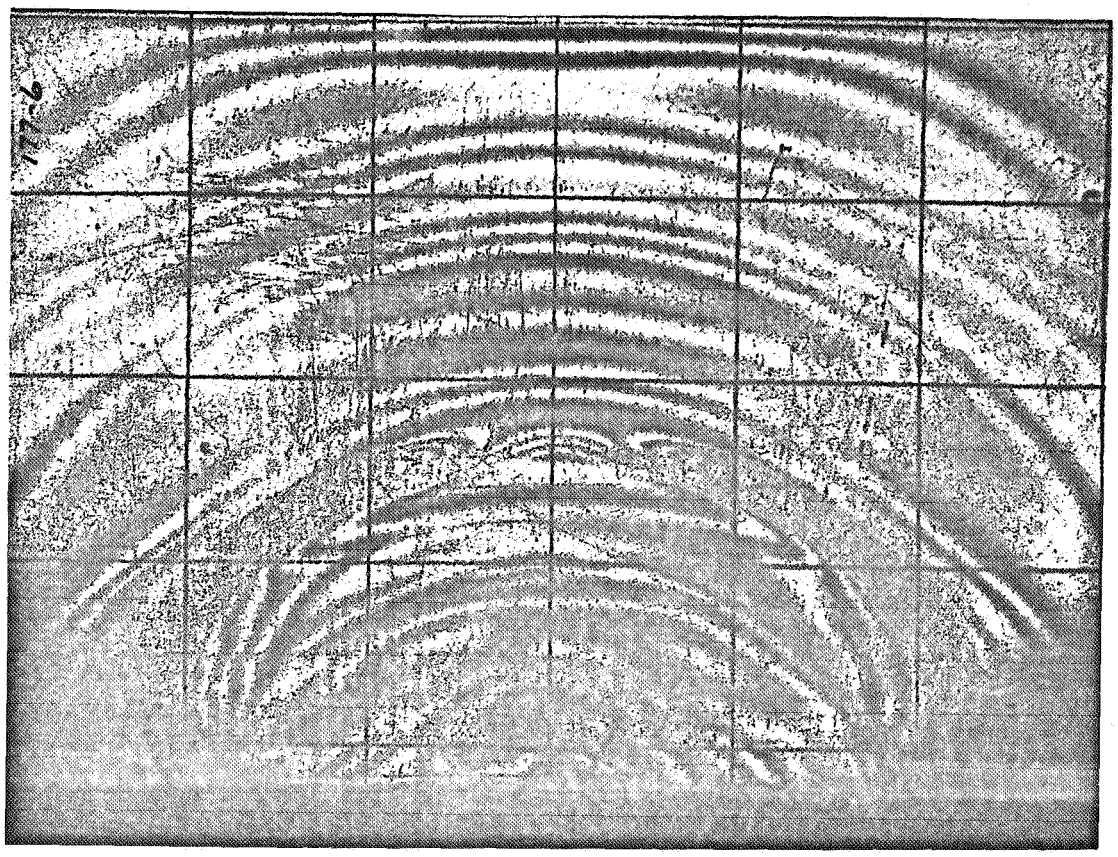

	N	R	UR	ET	ER	SIGMA R	SIGMA THETA
1	0.000	5.000	0.000	0.000	0.000	0.000	0.000
2	.500	4.920	-.110	-.022	-2.782	-3.189	-1.189
3	1.500	4.780	-.883	-.182	-8.462	-9.382	-3.382
4	2.500	4.610	-2.760	-.584	-14.384	-15.186	-5.186
5	1.500	4.400	-5.078	-1.096	-9.376	-7.908	-1.908
6	.500	4.250	-5.906	-1.286	-4.046	-1.150	.849
7	0.000	4.170	-6.016	-1.312	-1.312	2.116	2.116
8	-.500	4.060	-5.865	-1.274	1.485	5.282	3.282
9	-.500	4.010	-5.727	-1.240	1.519	5.227	3.227
10	0.000	3.920	-5.602	-1.209	-1.209	1.951	1.951

Figure 36. CONTINUED

Shot No. 177, Frame No. 8

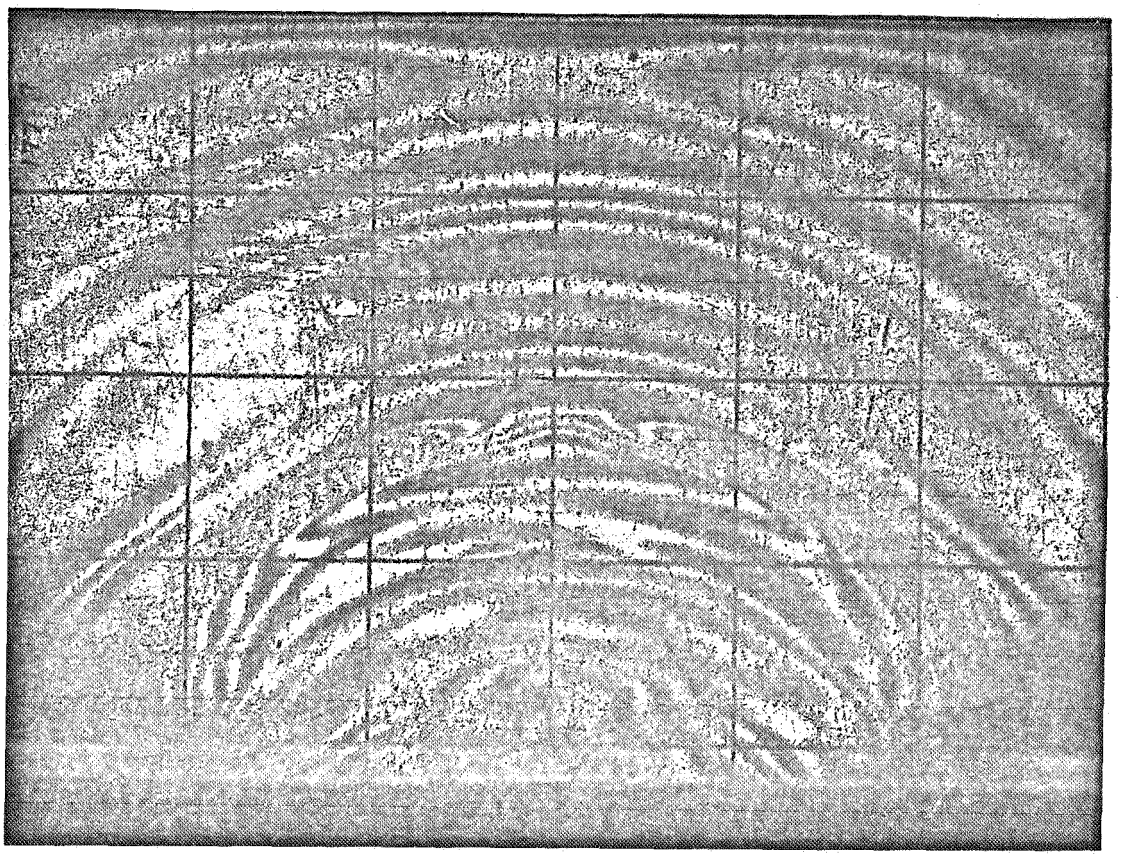

	N	R	UR	ET	ER	SIGMA R	SIGMA THETA
1	0.000	5.000	0.000	0.000	0.000	0.000	0.000
2	.500	4.910	-.124	-.025	-2.785	-3.185	-1.185
3	1.250	4.700	-1.138	-.238	-7.138	-7.679	-2.679
4	.500	4.470	-2.249	-.478	-3.238	-2.454	-.454
5	0.000	4.380	-2.373	-.506	-.506	.816	.816
6	-.500	4.270	-2.221	-.470	2.289	3.984	1.984
7	-.500	4.140	-1.863	-.385	2.374	3.847	1.847
8	0.000	4.060	-1.752	-.358	-.358	.578	.578

Figure 36. CONTINUED

Shot No. 177, Frame No. 9

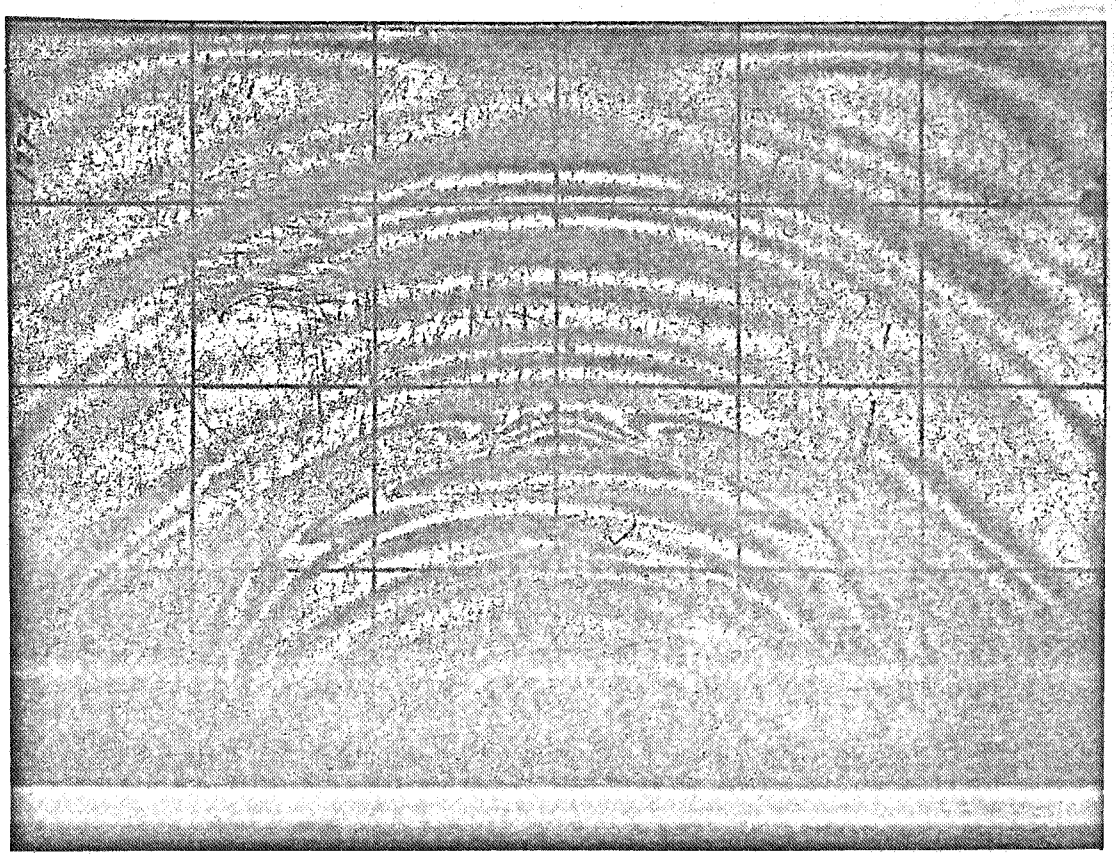

	N	R	UR	ET	ER	SIGMA R	SIGMA THETA
1	0.000	5.000	0.000	0.000	0.000	0.000	0.000
2	.300	4.800	-.165	-.034	-1.690	-1.879	-.679
3	.300	4.700	-.331	-.069	-1.725	-1.823	-.623
4	0.000	4.580	-.430	-.090	-.090	.145	.145
5	-.500	4.400	-.182	-.034	2.725	3.280	1.280
6	-.650	4.300	.135	.039	3.627	4.130	1.530
7	-.500	4.210	.420	.106	2.866	3.054	1.054
8	0.000	4.130	.531	.132	.132	-.213	-.213
9	.500	4.050	.420	.105	-2.654	-3.395	-1.395
10	1.500	3.950	-.131	-.033	-8.313	-9.622	-3.622
11	2.500	3.800	-1.787	-.463	-14.263	-15.381	-5.381

Figure 36. CONTINUED

Shot No. 177, Frame No. 10

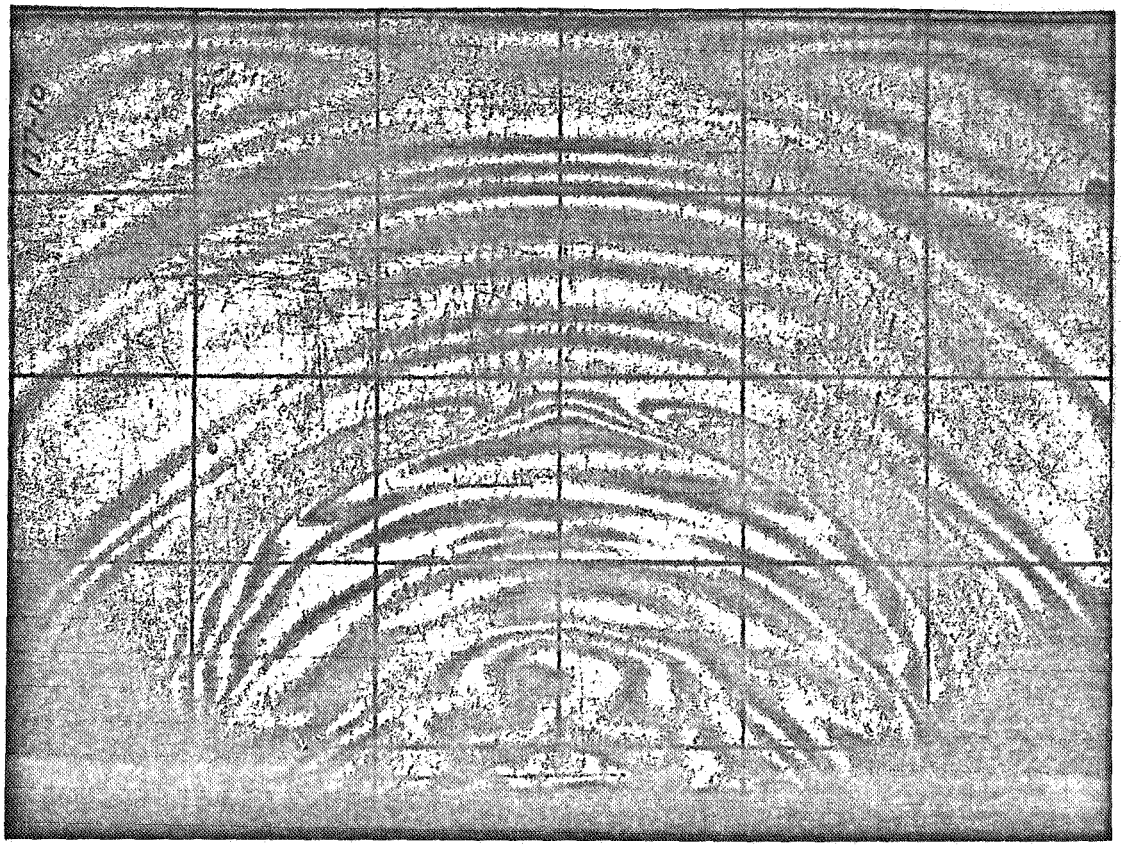

N	R	UR	ET	ER	SIGMA R	SIGMA THETA
1	0.000	5.000	0.000	0.000	0.000	0.000	0.000
2	-.500	4.930	.096	.019	2.779	3.194	1.194
3	-.600	4.880	.248	.050	3.362	3.789	1.389
4	-.500	4.790	.521	.107	2.867	3.053	1.053
5	-.600	4.680	.855	.177	3.489	3.584	1.184
6	-.500	4.580	1.159	.243	3.003	2.833	.833
7	0.000	4.280	1.573	.333	.333	-.537	-.537
8	.500	4.130	1.366	.283	-2.476	-3.682	-1.682
9	1.500	4.000	.648	.105	-8.174	-9.847	-3.847
10	2.500	3.780	-1.780	-.523	-14.323	-15.284	-5.284

Figure 36. CONTINUED

Shot No. 177, Frame No. 11

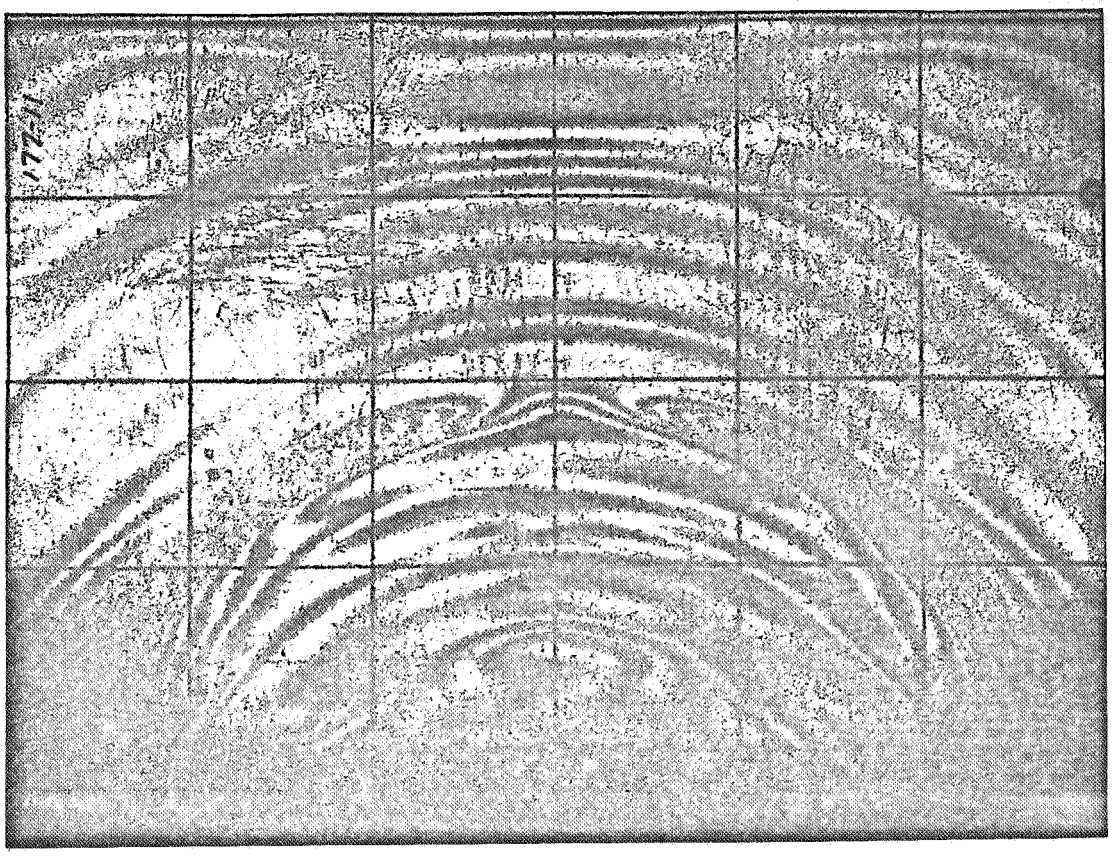

N	R	UR	ET	ER	SIGMA R	SIGMA THETA
1	0.000	5.000	0.000	0.000	0.000	0.000	0.000
2	-.500	4.940	.082	.016	2.776	3.198	1.198
3	-1.500	4.850	.579	.118	8.398	9.485	3.485
4	-1.400	4.750	1.380	.285	8.013	8.571	2.971
5	-1.500	4.680	1.940	.404	8.684	9.025	3.025
6	-1.650	4.580	2.809	.592	9.700	9.690	3.090
7	-1.500	4.470	3.766	.803	9.083	8.381	2.381
8	-.500	4.300	4.704	1.015	3.775	1.587	-.412
9	.500	4.170	4.704	1.014	-1.745	-4.861	-2.861
10	1.500	4.040	3.986	.837	-7.442	-11.028	-5.028
11	1.500	3.880	2.662	.503	-7.776	-10.489	-4.489

Figure 36. CONTINUED

Shot No. 177, Frame No. 12

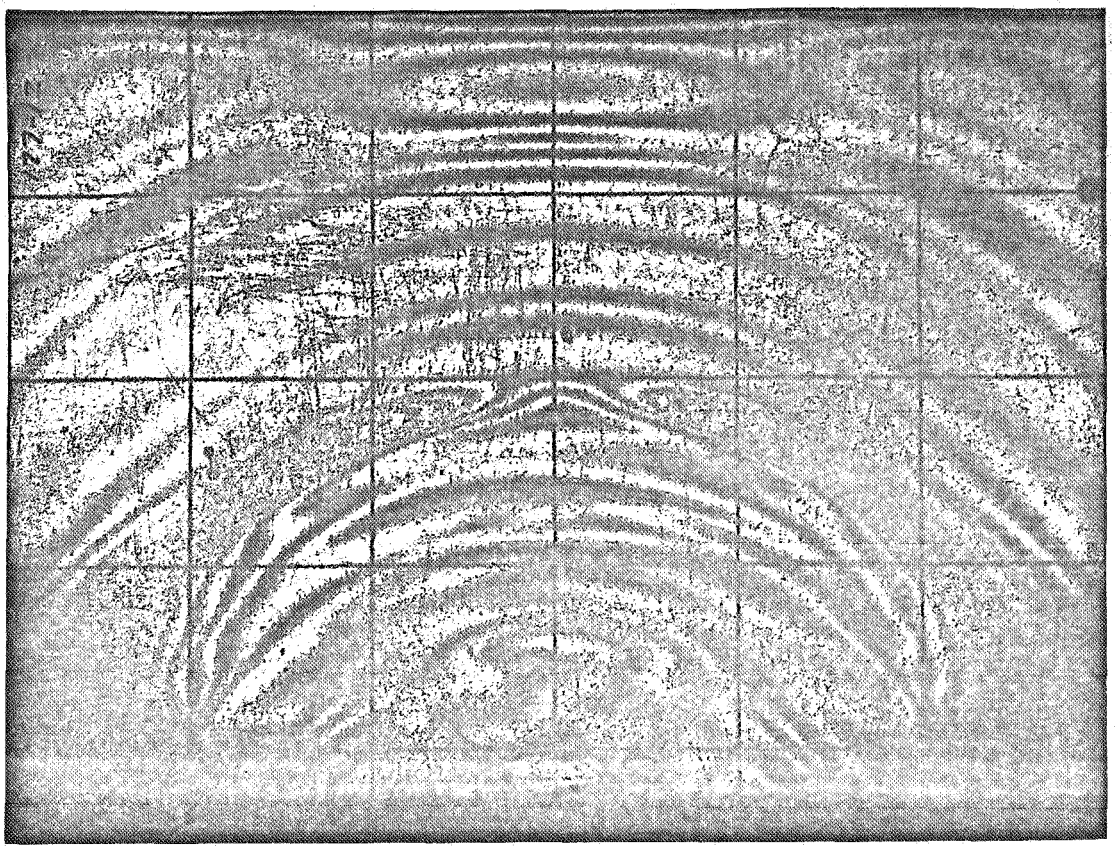

N	R	UR	ET	ER	SIGMA R	SIGMA THETA
1	0.000	5.000	0.000	0.000	0.000	0.000	0.000
2	-.500	4.970	.041	.008	2.768	3.212	1.212
3	-1.500	4.900	.427	.086	8.366	9.537	3.537
4	-2.500	4.810	1.421	.292	14.092	15.657	5.657
5	-2.800	4.700	3.030	.630	16.086	17.047	5.847
6	-2.500	4.590	4.639	.976	14.776	14.553	4.553
7	-1.500	4.450	6.185	1.317	9.597	7.552	1.552
8	-.500	4.350	6.737	1.442	4.202	.899	-1.100
9	.500	4.230	6.737	1.441	-1.318	-5.550	-3.550
10	1.500	4.120	6.129	1.294	-6.985	-11.765	-5.765
11	1.500	3.990	5.053	1.029	-7.250	-11.337	-5.337
12	.500	3.830	4.170	.805	-1.954	-4.525	-2.525

Figure 36. CONTINUED

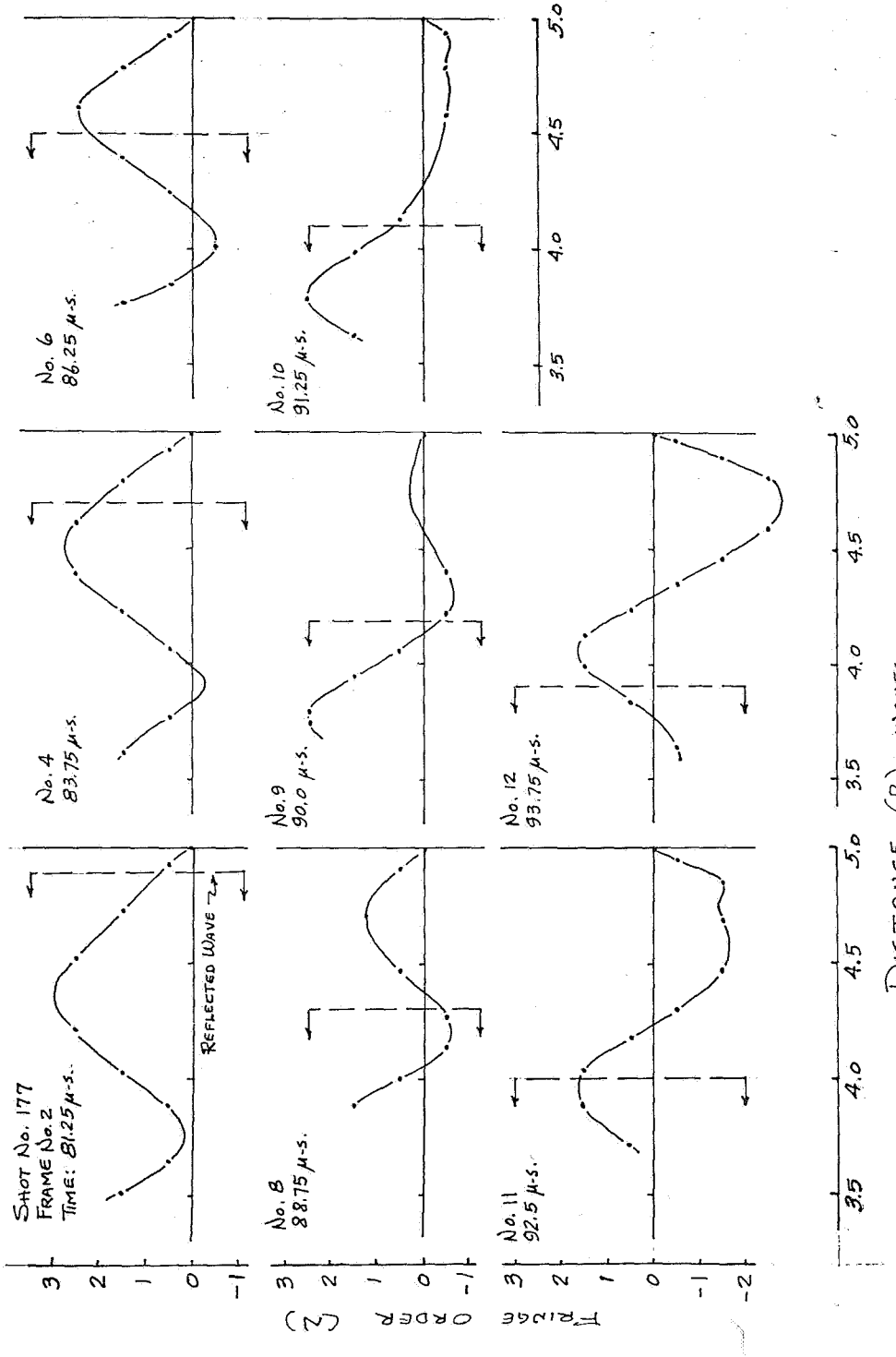

Figure 37. FRINGE NUMBER-DISTANCE-TIME RELATIONS (REFLECTED WAVES)

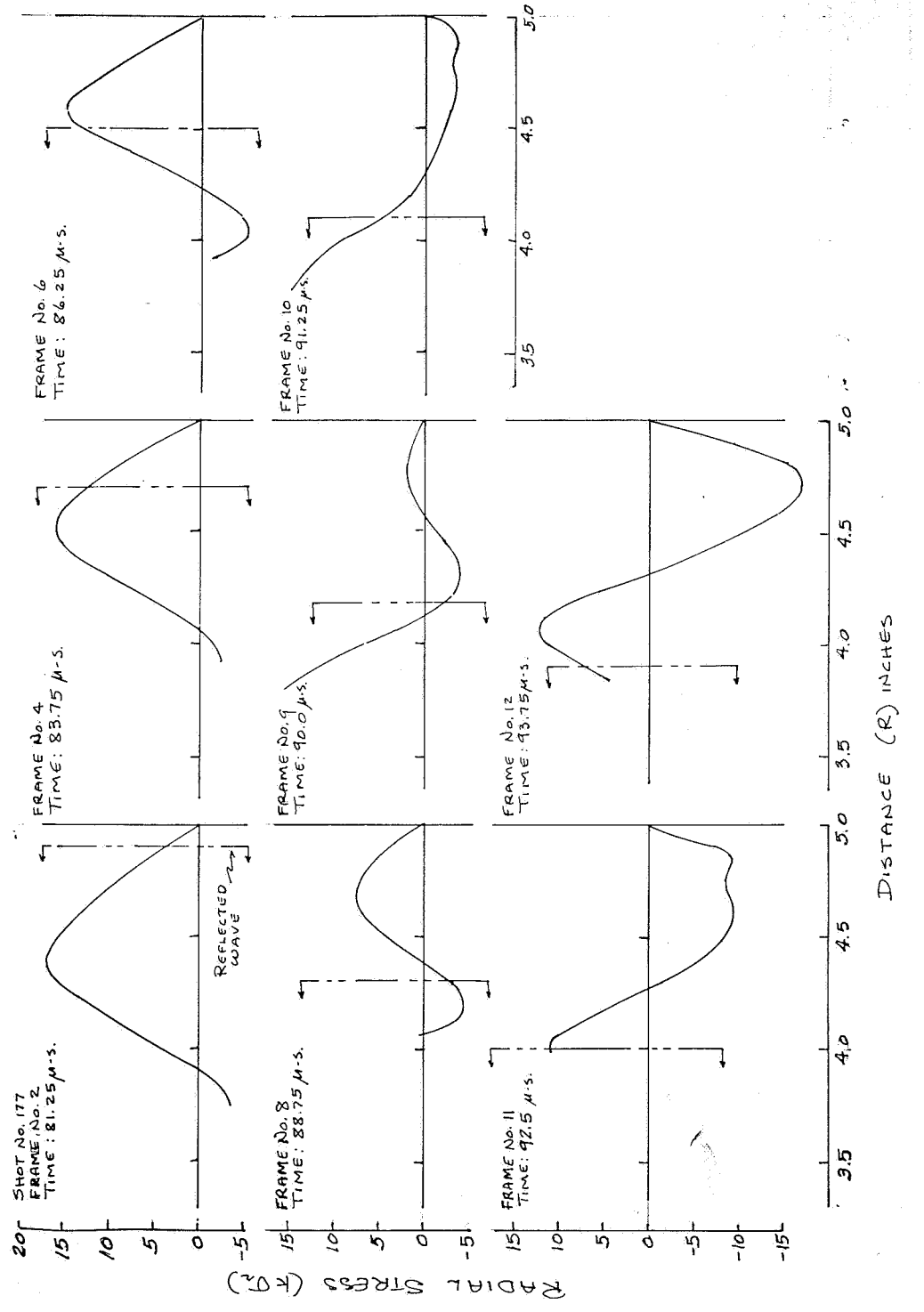

Figure 38. STRESS-DISTANCE-TIME RELATIONS (REFLECTED WAVES)

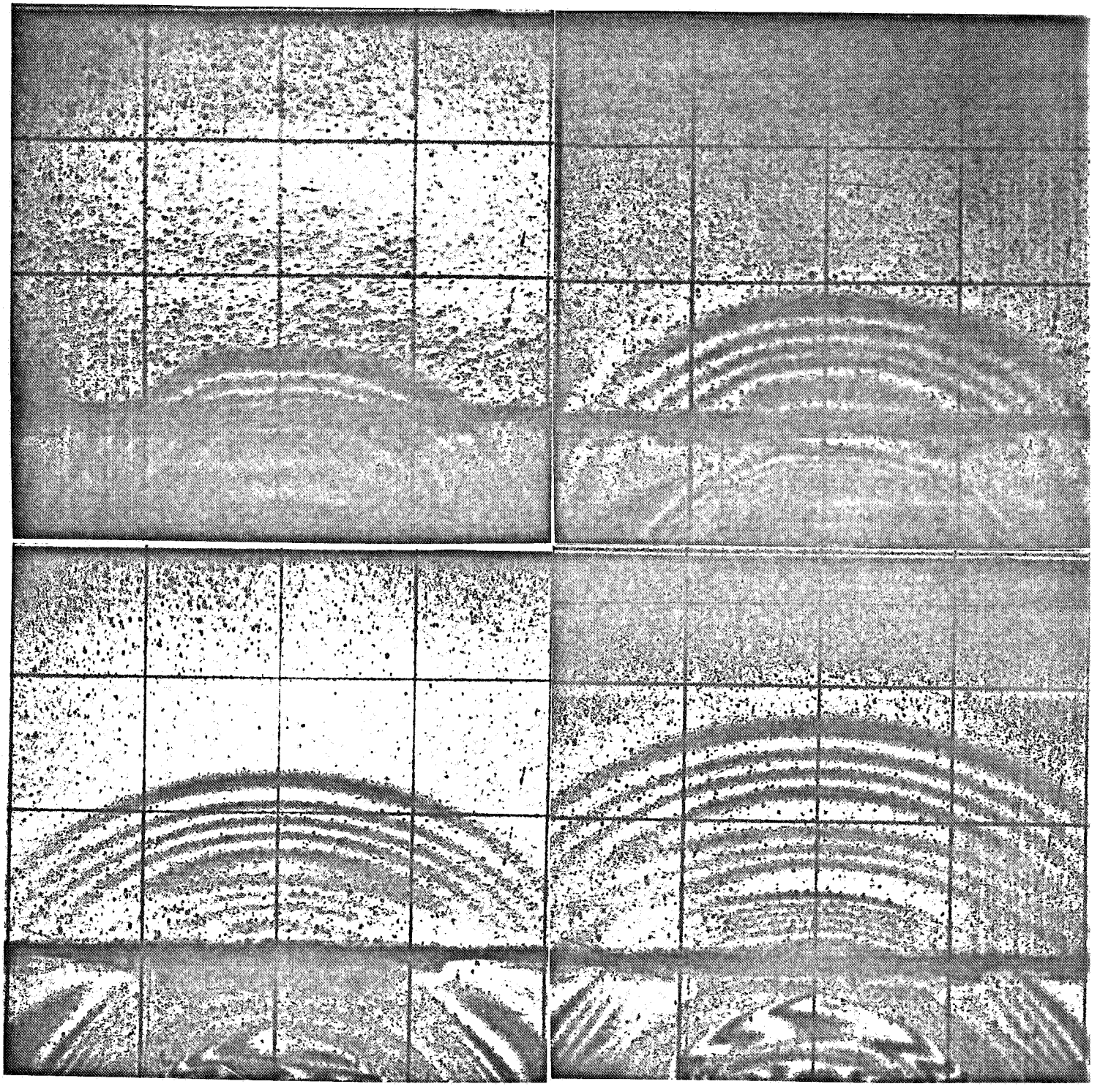

Figure 39. PASSAGE OF STRESS WAVE THROUGH A CEMENTED JOINT

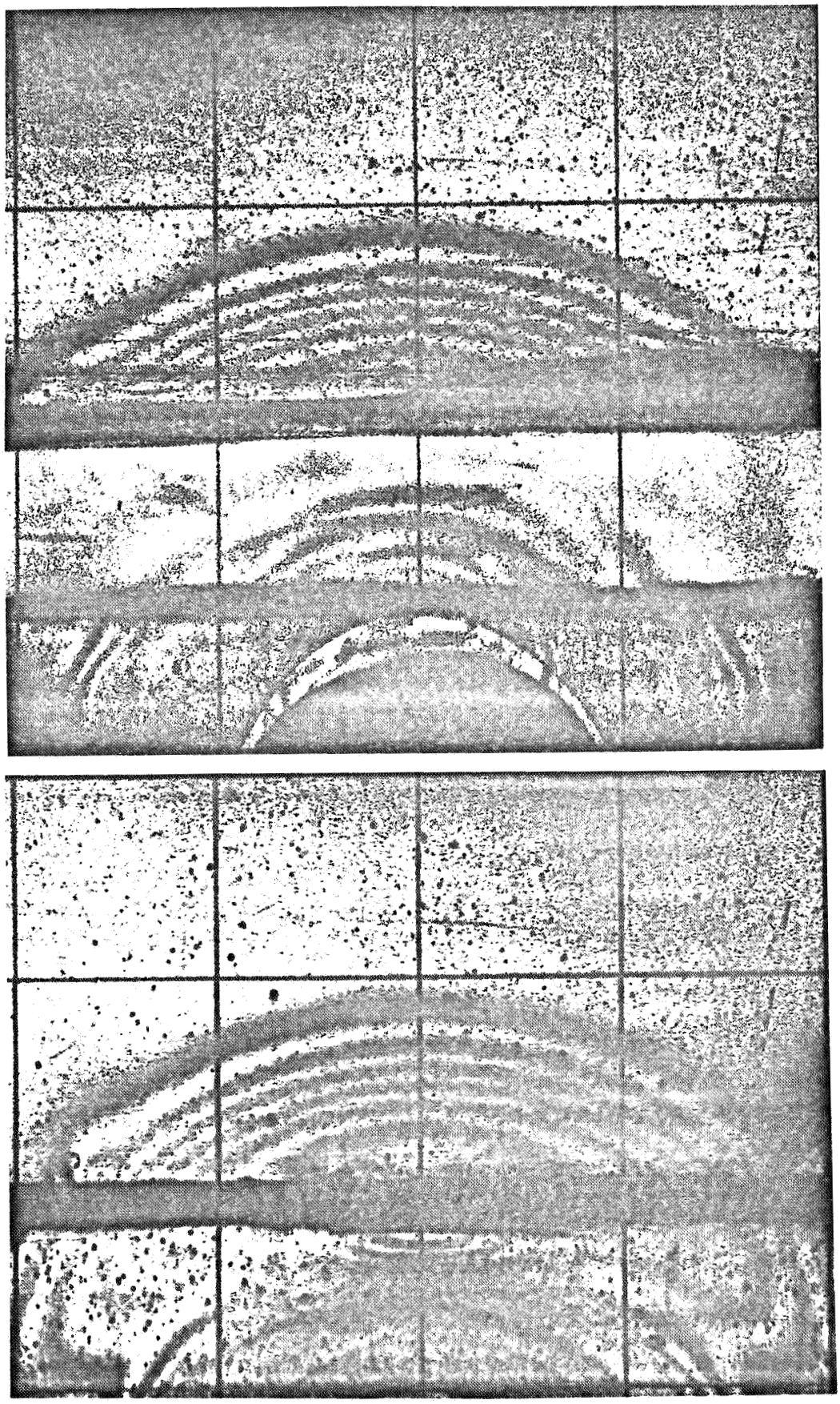

Figure 40. PASSAGE OF STRESS WAVES THROUGH CR-39 LAMINATIONS

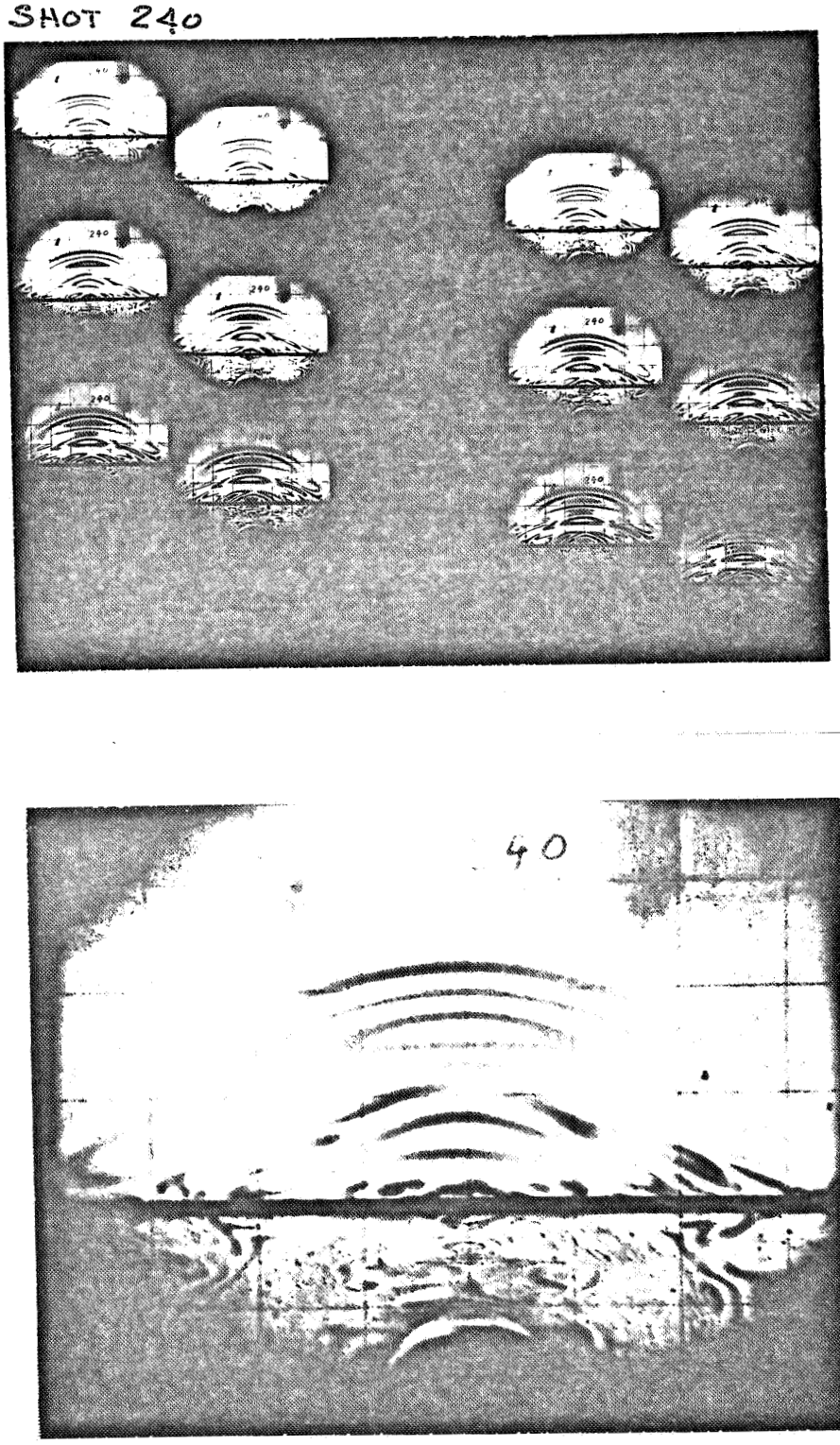

Figure 41. STRESS WAVES THROUGH 1/8-INCH ALUMINUM LAMINATE

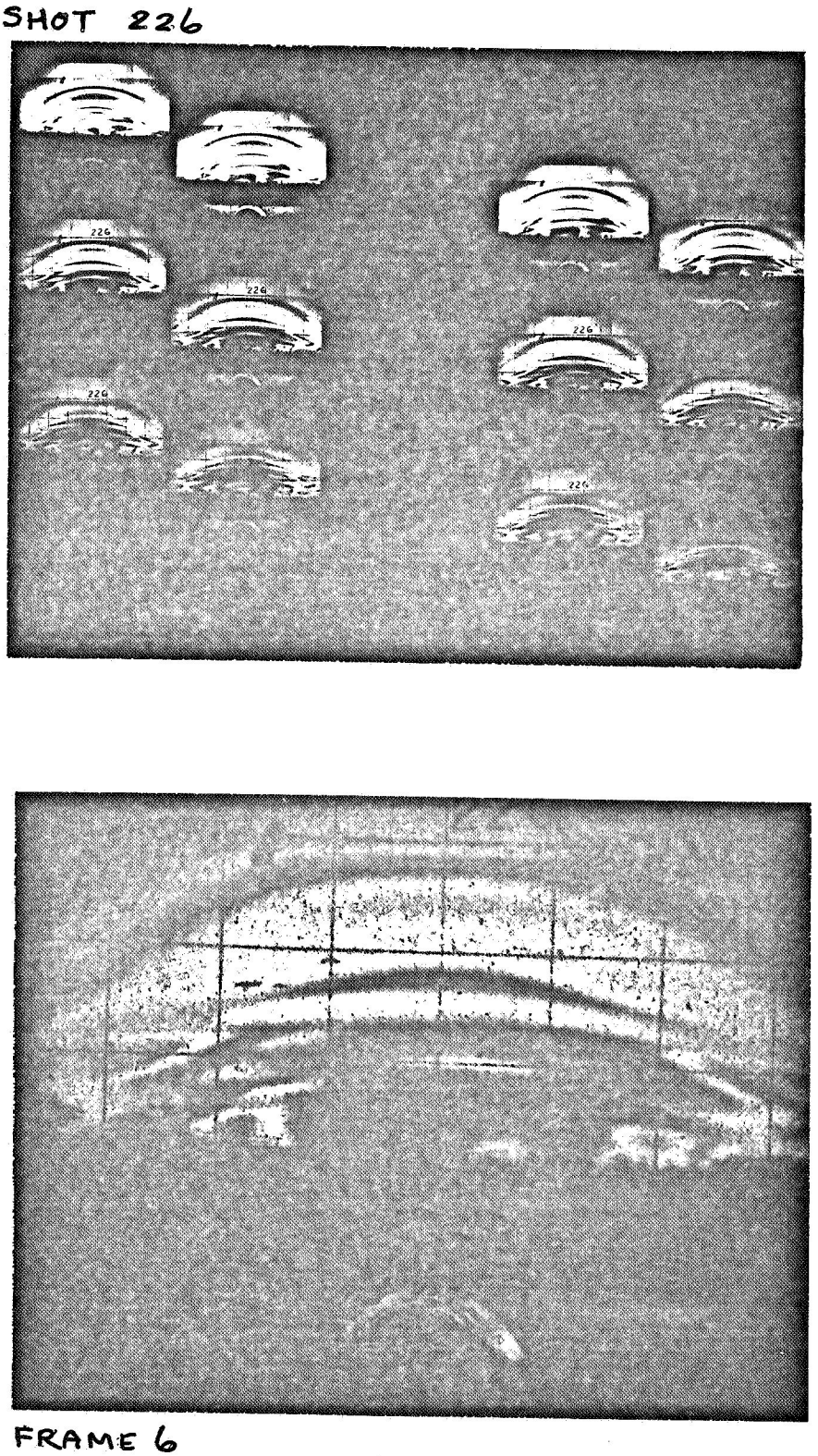

Figure 42. STRESS WAVES THROUGH 1.0-INCH ALUMINUM LAMINATE

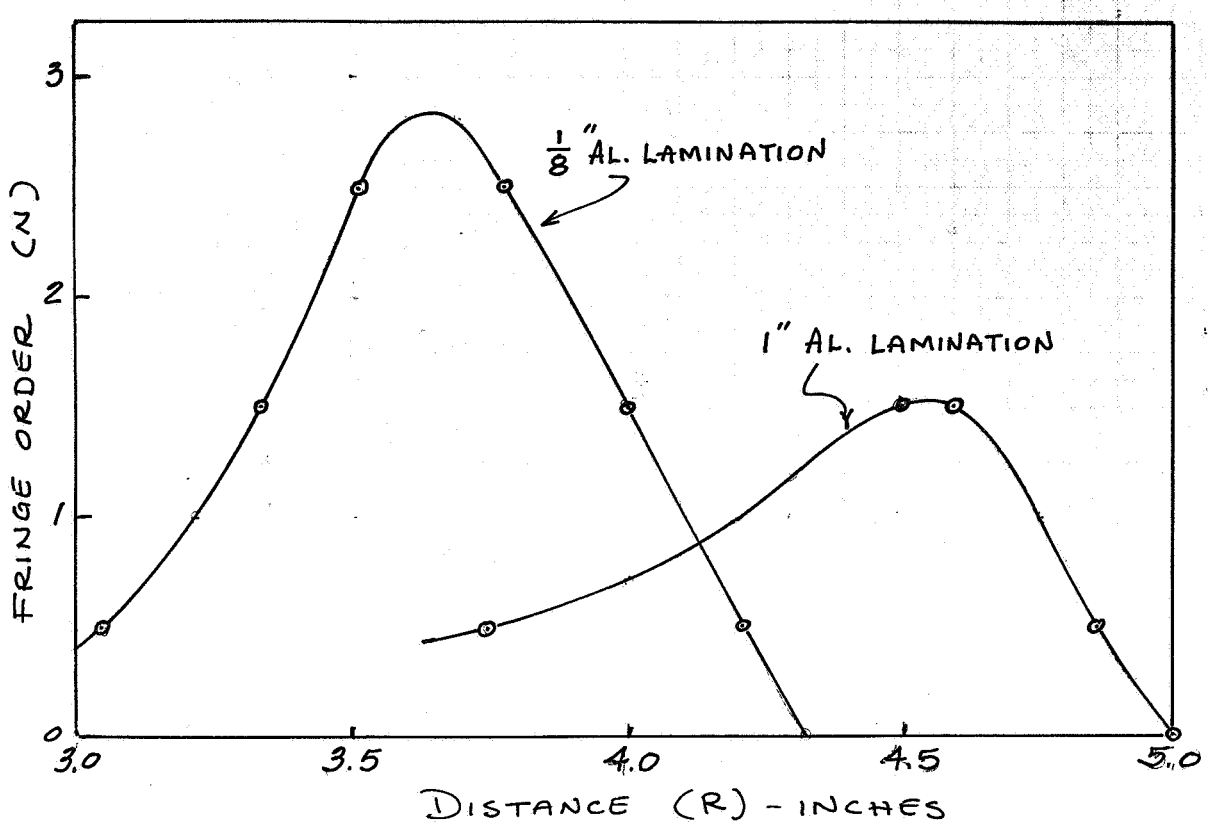

1/8 INCH LAMINATE

	N	R	UR	ET	ER	SIGMA R	SIGMA THETA
1	0.000	4.330	0.000	0.000	0.000	0.000	0.000
2	.500	4.210	-.165	-.039	-2.799	-3.162	-1.162
3	1.500	4.000	-1.324	-.325	-8.605	-9.152	-3.152
4	2.500	3.780	-3.753	-.954	-14.754	-14.589	-4.589
5	2.850	3.700	-4.934	-1.270	-17.002	-16.337	-4.937
6	2.850	3.600	-6.508	-1.702	-17.434	-15.641	-4.241
7	2.500	3.510	-7.837	-2.075	-15.875	-12.781	-2.781
8	1.500	3.330	-9.824	-2.653	-10.933	-5.398	.601
9	1.000	3.220	-10.583	-2.884	-8.404	-1.799	2.200
10	.500	3.050	-11.287	-3.106	-5.866	1.785	3.785

1 INCH LAMINATE

	N	R	UR	ET	ER	SIGMA R	SIGMA THETA
1	0.000	5.000	0.000	0.000	0.000	0.000	0.000
2	.500	4.860	-.193	-.039	-2.799	-3.161	-1.161
3	1.000	4.760	-.607	-.126	-5.646	-6.248	-2.248
4	1.500	4.600	-1.711	-.362	-8.642	-9.092	-3.092
5	1.500	4.500	-2.539	-.544	-8.824	-8.798	-2.798
6	1.200	4.300	-4.029	-.882	-7.506	-6.317	-1.517
7	1.000	4.200	-4.636	-1.025	-6.545	-4.797	-.797
8	.700	4.000	-5.575	-1.253	-5.117	-2.494	.305
9	.500	3.750	-6.403	-1.466	-4.226	-.860	1.139

Figure 43. FRINGE ORDER AND COMPUTED RESULTS - ALUMINUM LAMINATES

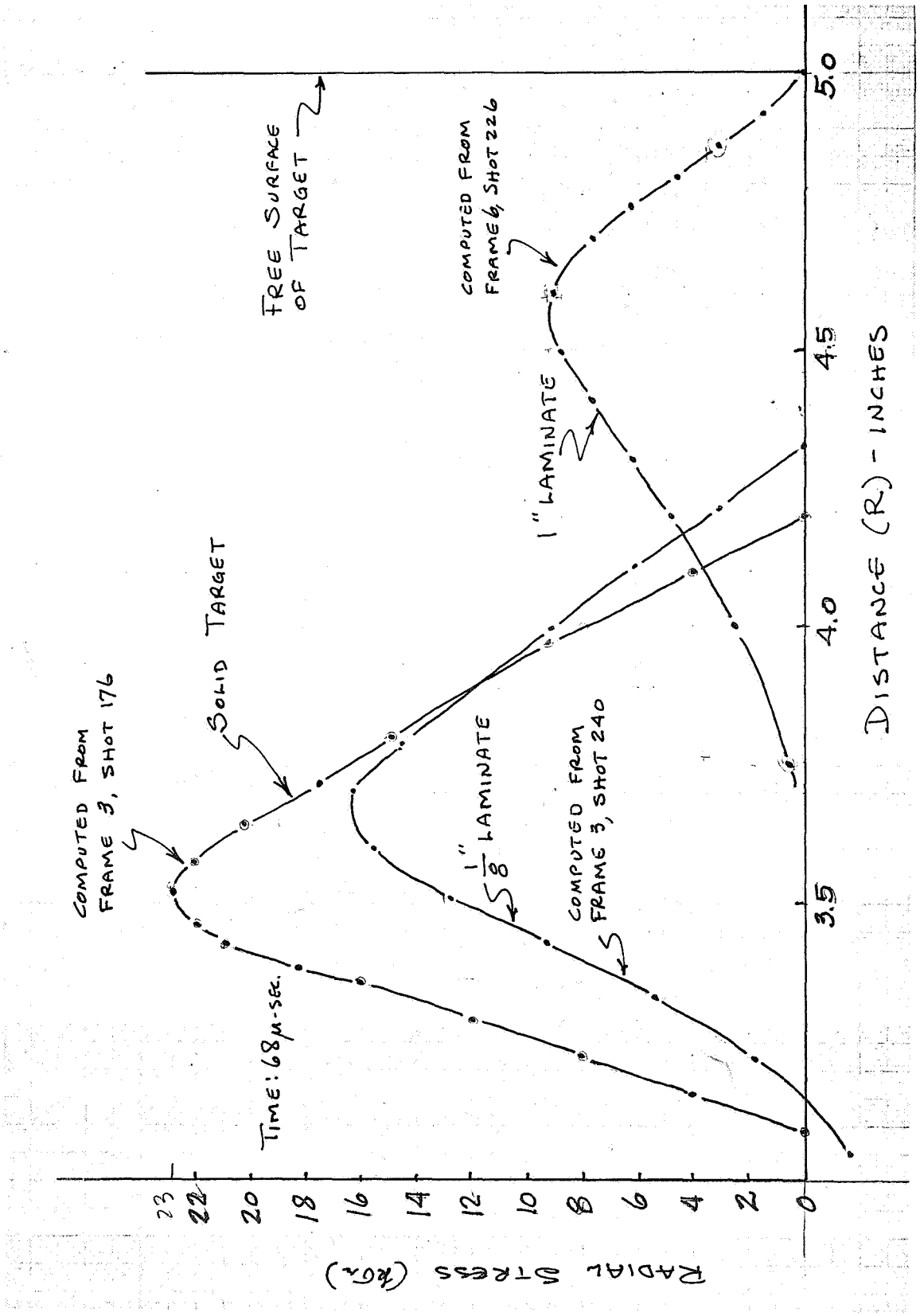

Figure 44. COMPARISON OF STRESSES IN HOMOGENEOUS AND LAMINATED TARGETS

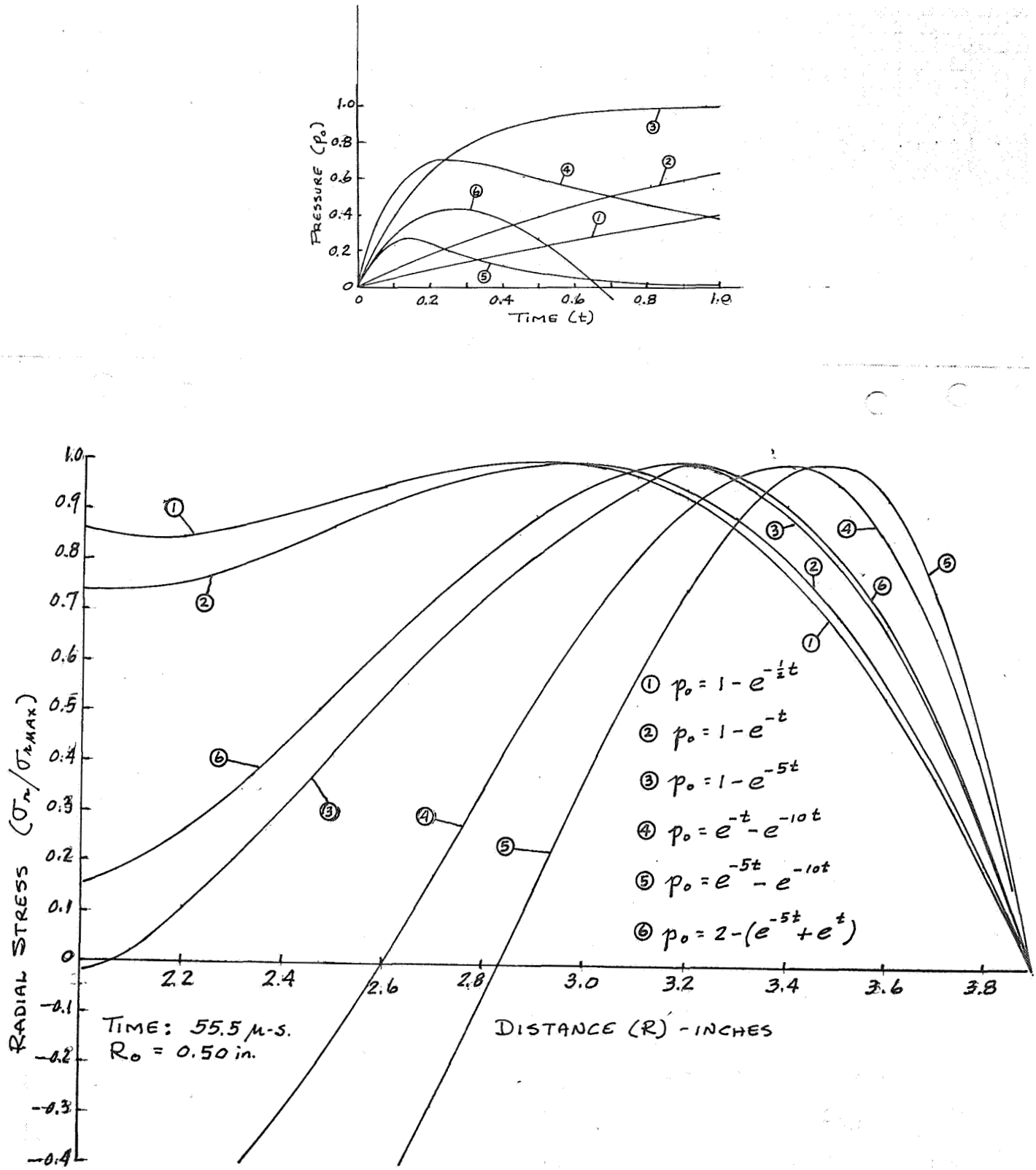

Figure 45. EFFECT OF FORCING FUNCTION UPON WAVE PROFILE (R_o=0.50)

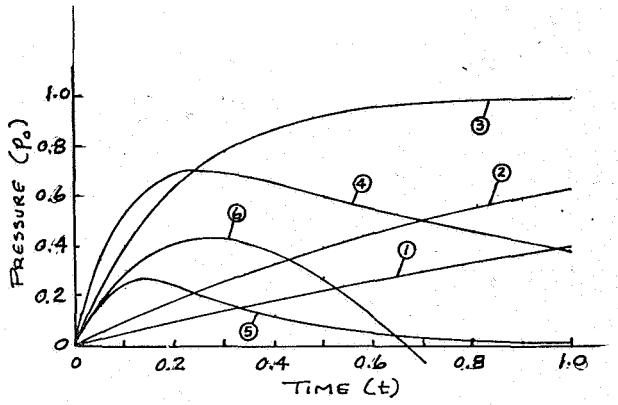

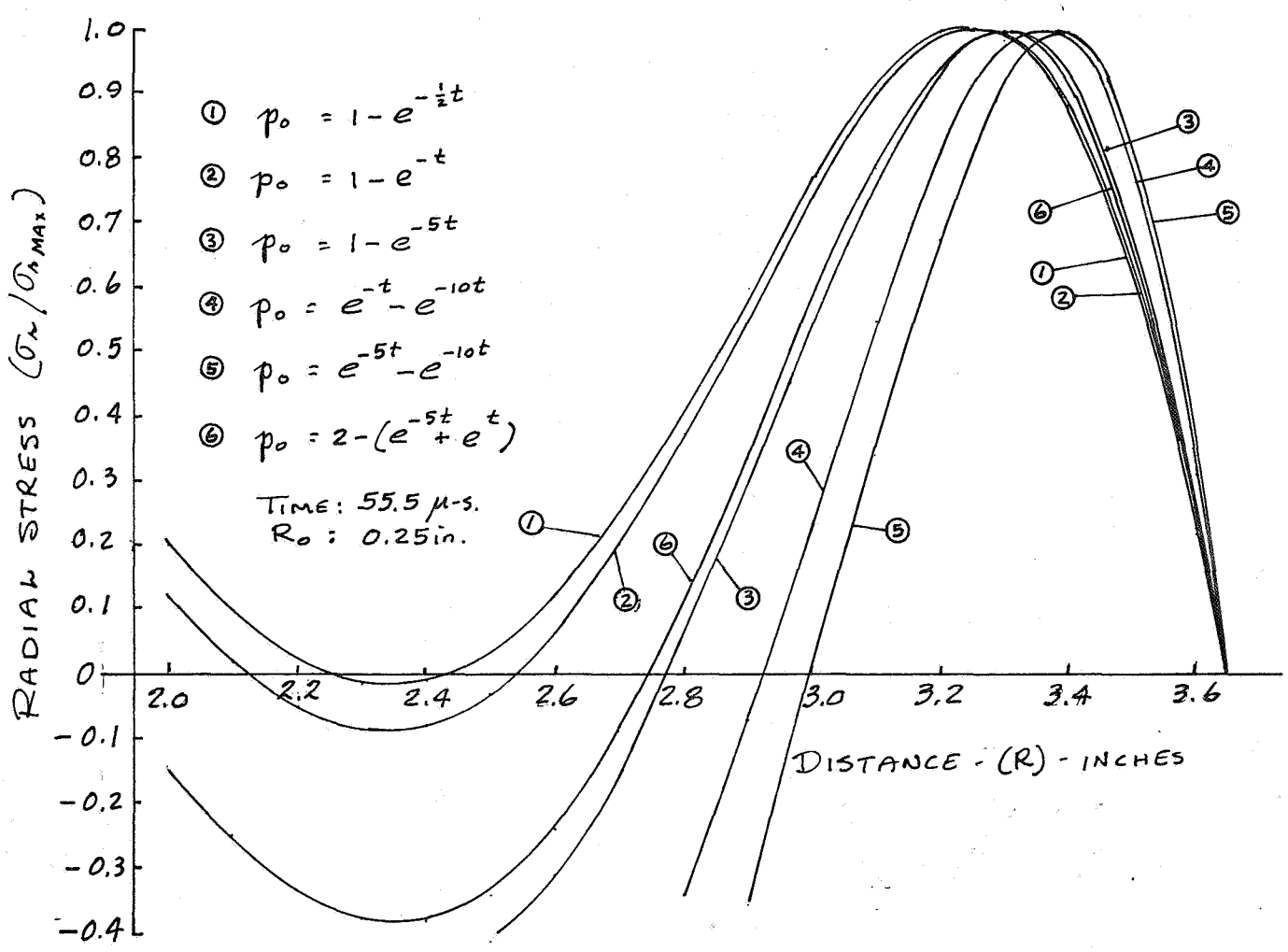

Figure 46. EFFECT OF FORCING FUNCTION UPON WAVE PROFILE (R_O=0.25)

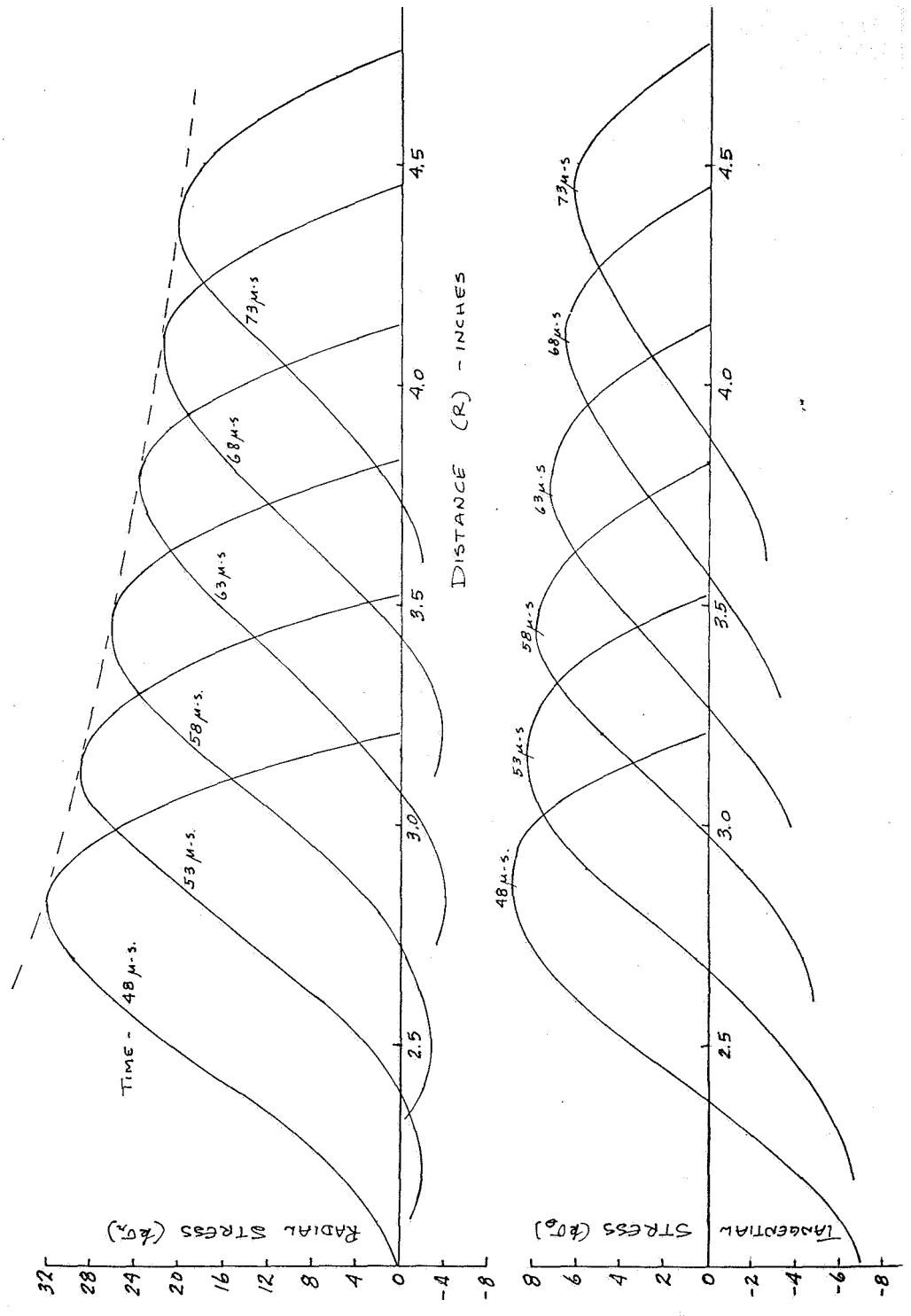

Figure 47. THEORETICAL STRESS-DISTANCE-TIME RELATIONS

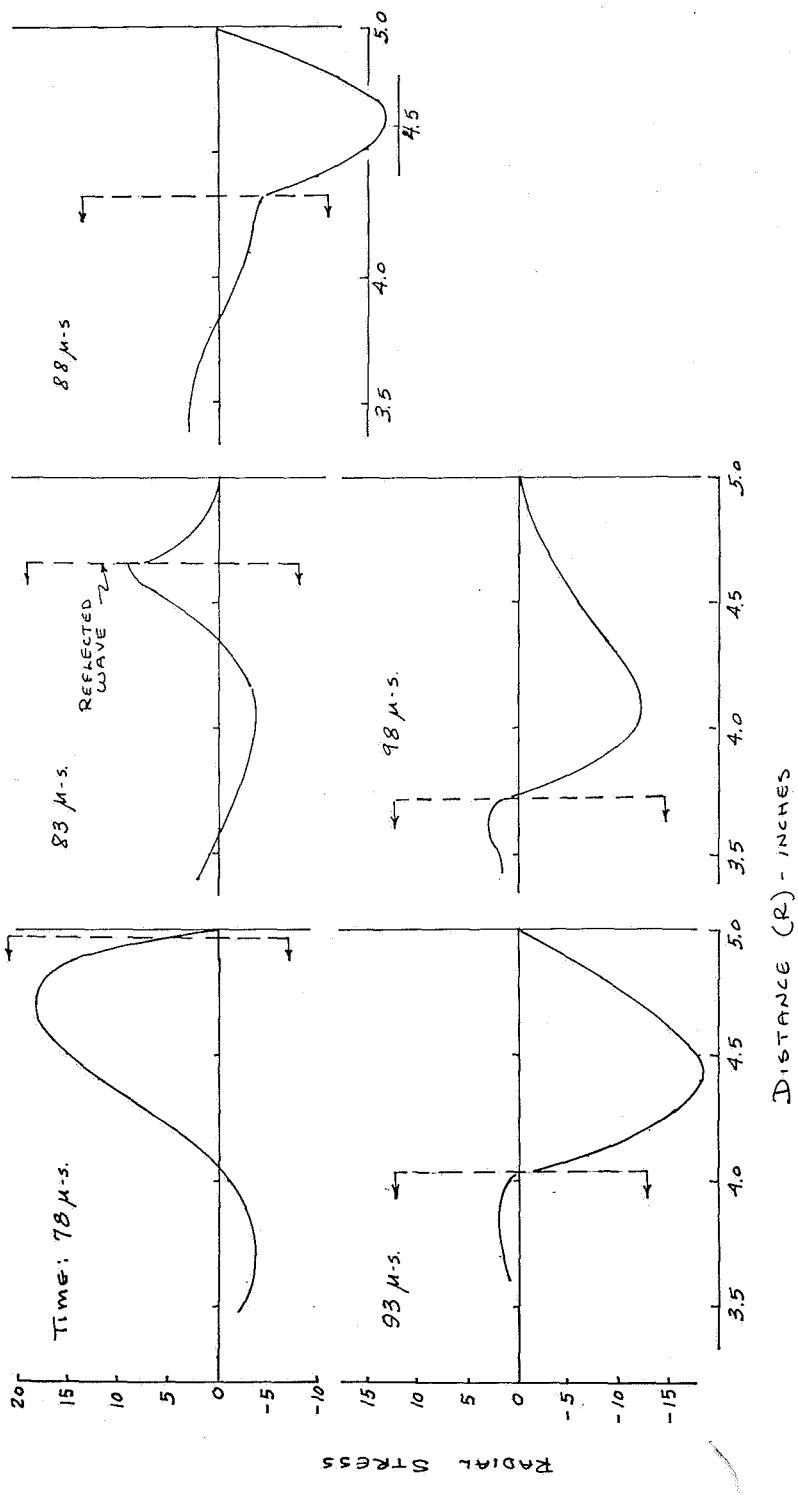

Figure 48. THEORETICAL STRESS-DISTANCE-TIME RELATIONS (REFLECTED WAVES)

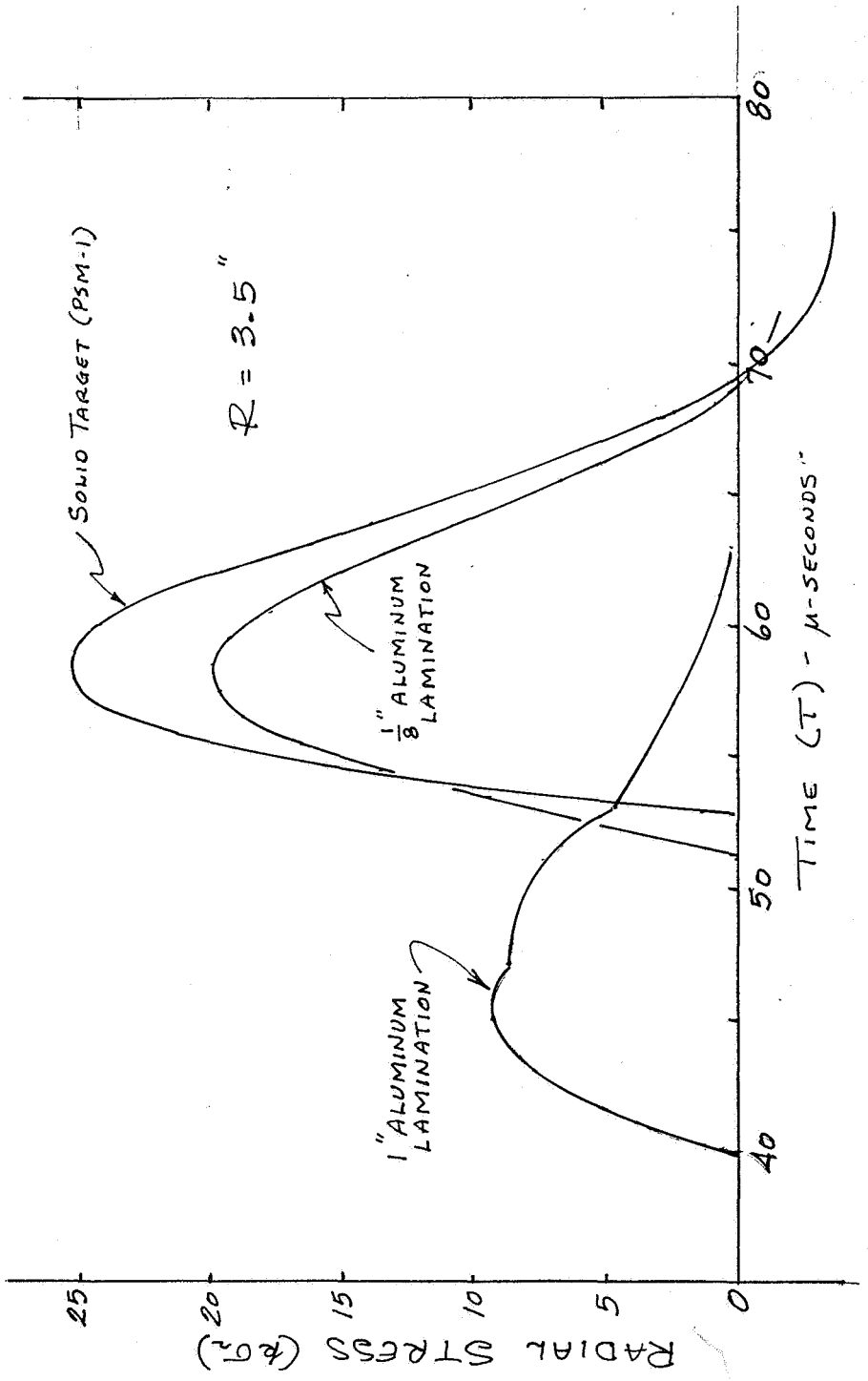

Figure 49. THEORETICAL STRESS-TIME RELATIONS FOR ALUMINUM LAMINATES

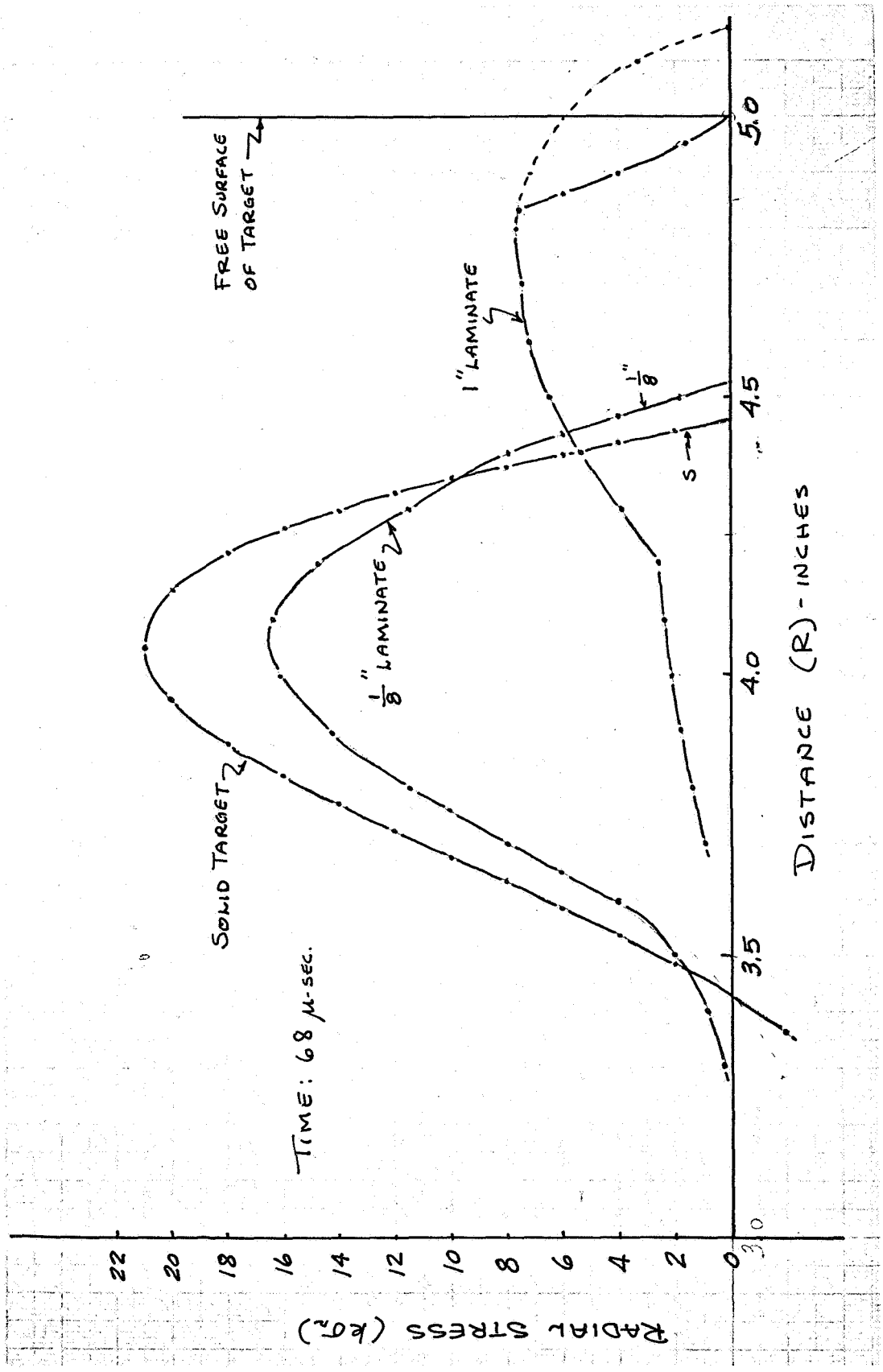

Figure 50. COMPARISON OF THEORETICAL STRESSES IN HOMOGENEOUS AND LAMINATED MATERIAL

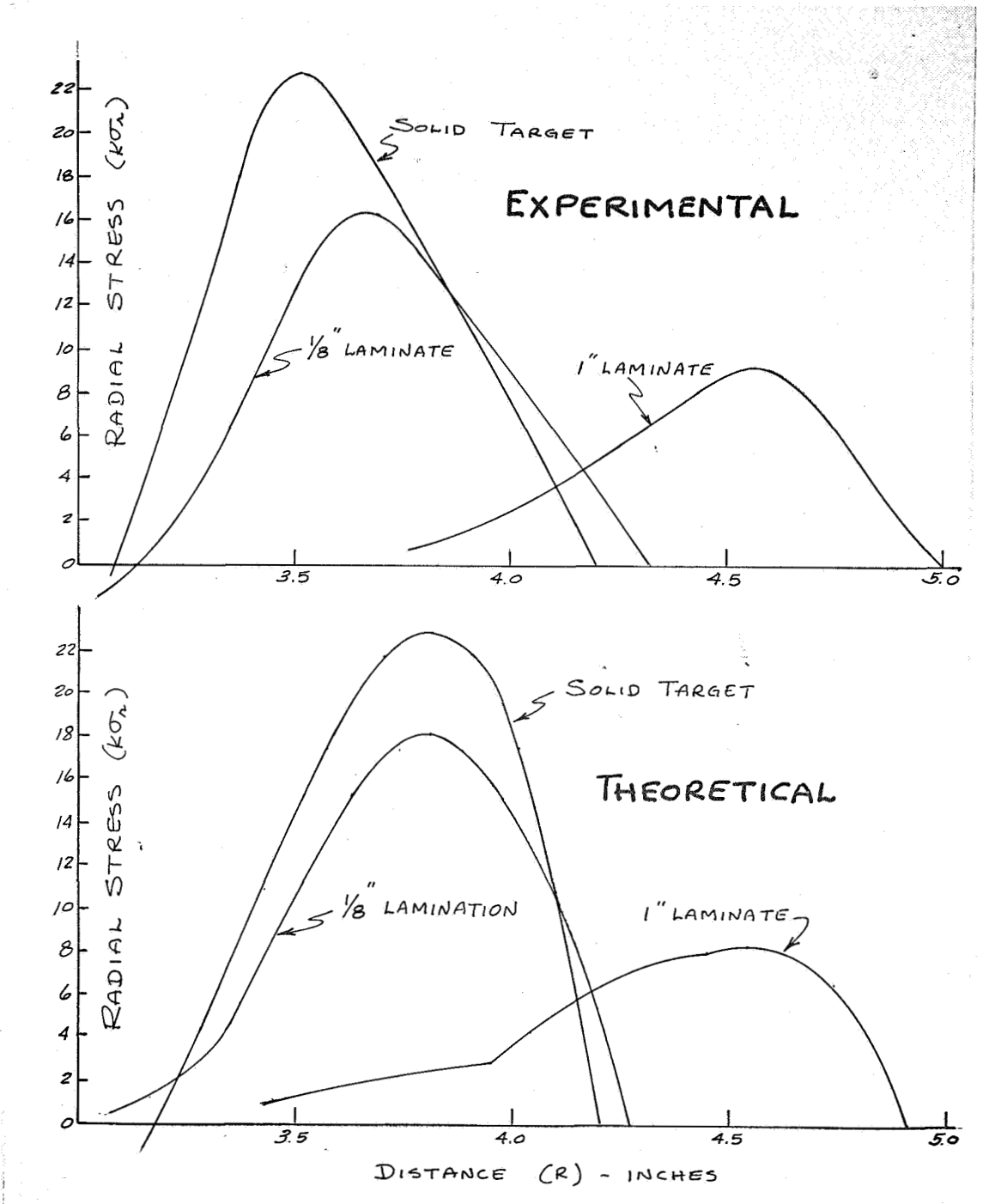

Figure 51. COMPARISON OF EXPERIMENTAL AND THEORETICAL RESULTS